Functional analysis of the conserved mitochondrial protein Mco76

DISSERTATION ZUR ERLANGUNG DES DOKTORGRADES DER NATURWISSENSCHAFTENDOCTOR RERUM NATURALIUM (DR. RER. NAT.) AN DER FAKULTÄT FÜR BIOLOGIE DER LUDWIG-MAXIMILIANS-UNIVERSITÄT MÜNCHEN

vorgelegt von

Siavash Khosravi

Aus Tehran, Iran

Jahr 2021

Diese Dissertation wurde

unter der Leitung von

Prof. Dr. Walter Neupert, Dr. Max Harner, and Prof. Dr. Barbara Conradt

im Bereich Zellbiologie – Anatomie III

des Biomedizinischen Centrums

der Ludwig-Maximilians-Universität München angefertigt

Erstgutachter: Prof. Conradt

Zweitgutachter: Prof. Osman

Tag der Abgabe: 16.12.2021

Tag der mündlichen Prüfung: 12.05.2022

EIDESSTATTLICHE RKLÄRUNG

Ich versichere hier mit an Eides statt, dass meine Dissertation selbständig und ohne unerlaubte Hilfsmittel angefertigt worden ist.

Die vorliegende Dissertation wurde weder ganz, noch teilweise bei einer anderen Prüfungs kommission vorgelegt.

Ich habe noch zu keinem früheren Zeitpunkt versucht, eine Dissertation einzureichen oder an einer Doktorprüfung teilzunehmen.

München, 23.08.2022

SIAVASH KHOSRAVI

„ Somewhere, something incredible is waiting to be known.”

Carl Sagan

Table of content

Summary

Mitochondria execute a multitude of functions in the cell. To maintain their form and function, they need to form a complex membrane system composed of the mitochondrial outer membrane and the mitochondrial inner membrane. Contact sites between mitochondria and other organelles or between the inner mitochondrial membrane (IM) and the outer mitochondrial membrane (OM) are crucial for biogenesis and maintaining the mitochondrial membrane systems. These contacts sites are protein complexes that facilitate the transport of phospholipids and metabolites from other organelles to mitochondria and between mitochondrial membranes. Phospholipids reached to the mitochondria will be further directed to the proper submitochondrial localization, where they will be used for downstream processes. Mco76 is a member of the UbiB protein family containing an ACDK-like kinase (ATPase) domain. Interestingly, Mco76 is conserved throughout the evolution from yeast to human. The study presented here describes a functional analysis of Mco76 by studying its genetic interactions and biochemical interactions. In addition, it provides new insights into the function of Mco76 in the transfer of lipids between the IM and the OM.

In this study, evidence was provided that Mco76 is present in the IM of mitochondria while its C-terminus is located in the mitochondrial intermembrane space (IMS). An immunoprecipitation assay was deployed to investigate biochemical interactions of Mco76. For the first time, Por1, Om14, and Om45 from the OM were identified as the protein interactors of Mco76. Hence, it was concluded that a novel contact site between the mitochondrial inner and outer membranes was discovered, providing potential hints into the function of Mco76. The genetic interactions of *MCO76* were investigated to understand the role of Mco76 and the contact site formed by its interactions. Deleting of *MCO76* from cells in which the CL pathway is impaired leads to a growth phenotype indicating *MCO76* plays a role in phospholipid homoeostasis. Although available literature suggests that Mco76 is involved in the import of CoQ from mitochondria, genetic interactions of *MCO76* suggest that *MCO76* and the contact site formed by its interactions have broader functions in the cell. This idea was further supported by showing that the deletion of *MCO76* reduces phosphatidic acid (PA) in mitochondria.

In addition, it was shown that overexpression of *MCO76* impairs mitochondrial architecture and alters mitochondrial morphology. Therefore, it was concluded that the defined levels of Mco76 are essential for mitochondrial architecture and morphology. Furthermore, it was shown that deletion of *MCP2* rescues the growth defect of cells lacking Mco76 and Ups1. This further indicates that an equilibrium between the Mco76

and Mcp2 is necessary when the mitochondrial phospholipid composition is disturbed. This idea is consistent with the model proposed by Kemmerer that Mcp2 and Mco76 function reciprocally in importing and exporting CoQ from mitochondria.

Overall, the study here established that Mco76 forms a contact site between the mitochondrial inner and outer membranes by interacting with Por1, om14, and Por1. Based on these findings, a model was proposed in which Mco76 facilitates the transfer of CoQ and phospholipids between the IM and the OM.

Zusammenfassung

Mitochondrien erfüllen eine Vielzahl von Funktionen in der Zelle. Um ihre Form und Funktion aufrechtzuerhalten, müssen sie ein komplexes Membransystem bilden, das aus der äußeren Mitochondrienmembran und der inneren Mitochondrienmembran besteht. Kontaktstellen zwischen Mitochondrien und anderen Organellen oder zwischen der inneren Mitochondrienmembran (IM) und der äußeren Mitochondrienmembran (OM) sind entscheidend für die Biogenese und die Aufrechterhaltung der mitochondrialen Membransysteme. Diese Kontaktstellen sind Proteinkomplexe, die den Transport von Phospholipiden und Metaboliten von anderen Organellen zu den Mitochondrien und zwischen den mitochondrialen Membranen erleichtern. Phospholipide, die in die Mitochondrien gelangen, werden an die richtige submitochondriale Lokalisation weitergeleitet, wo sie für nachgeschaltete Prozesse verwendet werden. Mco76 ist ein Mitglied der UbiB-Proteinfamilie, das eine ACDK-ähnliche Kinasedomäne (ATPase) enthält. Interessanterweise ist Mco76 in der Evolution von der Hefe bis zum Menschen konserviert. Die hier vorgestellte Studie beschreibt eine funktionelle Analyse von Mco76 durch Untersuchung seiner genetischen und biochemischen Interaktionen. Darüber hinaus liefert sie neue Erkenntnisse über die Funktion von Mco76 beim Transfer von Lipiden zwischen dem IM und dem OM.

In dieser Studie wurde nachgewiesen, dass Mco76 im IM der Mitochondrien vorhanden ist, während sich sein C-Terminus im mitochondrialen Intermembranraum (IMS) befindet. Ein Immunpräzipitationstest wurde eingesetzt, um die biochemischen Interaktionen von Mco76 zu untersuchen. Zum ersten Mal wurden Por1, Om14 und Om45 aus dem OM als Proteininteraktoren von Mco76 identifiziert. Daraus wurde geschlossen, dass eine neuartige Kontaktstelle zwischen der inneren und der äußeren Mitochondrienmembran entdeckt wurde, die potenzielle Hinweise auf die Funktion von Mco76 liefert. Die genetischen Interaktionen von MCO76 wurden untersucht, um die Rolle von Mco76 und die durch seine Interaktionen gebildete Kontaktstelle zu verstehen. Die Deletion von MCO76 aus Zellen, in denen der CL-Weg gestört ist, führt zu einem Wachstumsphänotyp, was darauf hindeutet, dass MCO76 eine Rolle bei der Phospholipid-Homöostase spielt. Obwohl die verfügbare Literatur darauf hindeutet, dass MCO76 am Import von CoQ aus Mitochondrien beteiligt ist, deuten genetische Interaktionen von MCO76 darauf hin, dass MCO76 und die durch seine Interaktionen gebildete Kontaktstelle umfassendere Funktionen in der Zelle haben. Dieser Gedanke

wurde weiter unterstützt, indem gezeigt wurde, dass die Deletion von MCO76 die Phosphatidsäure (PA) in den Mitochondrien reduziert.

Darüber hinaus wurde gezeigt, dass eine Überexpression von MCO76 die mitochondriale Architektur beeinträchtigt und die mitochondriale Morphologie verändert. Daraus wurde gefolgert, dass die definierten Mengen von Mco76 für die mitochondriale Architektur und Morphologie wesentlich sind. Darüber hinaus wurde gezeigt, dass die Deletion von MCP2 den Wachstumsdefekt von Zellen, denen Mco76 und Ups1 fehlen, ausgleicht. Dies ist ein weiterer Hinweis darauf, dass ein Gleichgewicht zwischen Mco76 und Mcp2 erforderlich ist, wenn die mitochondriale Phospholipidzusammensetzung gestört ist. Dieser Gedanke steht im Einklang mit dem von Kemmerer vorgeschlagenen Modell, wonach Mcp2 und Mco76 beim Import und Export von CoQ aus den Mitochondrien wechselseitig funktionieren.

Insgesamt konnte in der vorliegenden Studie nachgewiesen werden, dass Mco76 durch Interaktion mit Por1, om14 und Por1 eine Kontaktstelle zwischen der inneren und der äußeren Mitochondrienmembran bildet. Auf der Grundlage dieser Ergebnisse wurde ein Modell vorgeschlagen, in dem Mco76 den Transfer von CoQ und Phospholipiden zwischen dem IM und dem OM erleichtert.

1. Introduction

1.1 Mitochondria

A distinct feature of eukaryotic cells is the compartmentalization of the cytoplasm into an intricate system of intracellular compartments. Intracellular compartments, known as organelles, allow cells to separate and enable processes with entirely distinct biochemical requirements. Nucleus and mitochondria differ from the other organelles since two bilayer membranes surround them. In 1927, Wallin explained the mitochondrial envelope with its double membranes by the theory of endosymbiosis as the origin of mitochondria (Wallin, 1927). According to this theory, mitochondria are derived from an α-proteobacteria-related ancestor incorporated by the host cell. This idea has been widely accepted only after the profound work of Lynn Margulis in 1971 (Margulis, 1971; Sagan, 1993). The presence of DNA and protein-synthesizing machinery in mitochondria are the most substantial evidence supporting the theory of endosymbiosis as the origin of mitochondria in eukaryotic cells (Martin, 2010).

Although mitochondria still harbor their genome, it is drastically smaller than the former bacterial genome due to the loss of redundant genes and horizontal gene transfer between endosymbiont and the host (Burger et al., 2003). The human mitochondrial genome consists of 37 genes, of which 13 encode for proteins, 22 encode for tRNAs, and 2 for rRNAs (Anderson et al., 1981). Whereas the mitochondrial genome of the yeast *S. cerevisiae* only encodes for 8 proteins, 24 tRNAs, and 2 rRNAs (Foury et al., 1998). Importantly, all mitochondrial encoded proteins are essential for the respiratory function of mitochondria. However, the mitochondrial proteome is composed of approximately 1000 proteins. Thus, the majority is encoded by the nuclear genome. Therefore, they are synthesized in the cytosol, and they have to be imported into mitochondria (Mokranjac and Neupert, 2009).

Since mitochondria show a complex structure made up of two bilayer membranes, sophisticated import mechanisms had to be developed by the cell to import proteins into mitochondria. There is intricate machinery located in the outer mitochondrial membrane (OM) and the inner mitochondrial membrane (IM) responsible for the import and sorting of mitochondrial proteins to their correct sub-mitochondrial localization (Mokranjac and Neupert, 2009). Importantly, proper protein import is essential for cell viability since mitochondria must perform their multitude of functions. Mitochondria have been considered merely as the powerhouse of cells, and they

retained the ATP production capacity of their ancestor (Gray, 1992). Nevertheless, this point of view has been changed due to copious evidence showing mitochondria play salient roles in different cellular processes, such as calcium homeostasis, programmed cell death, and signal transduction (Chandel, 2014; McBride et al., 2006; Perrone et al., 2020).

1.2 Mitochondrial dynamics

Historically, mitochondria have been viewed as rigid bean-shaped organelles until recent studies have shed new light on how dynamic the mitochondrial network is. Different studies indicate that mitochondria have distinct ultrastructure and morphology in different cell types and tissues (Bereiter-Hahn and Vöth, 1994). The morphology of mitochondria is delicately controlled by two opposing events, fusion and fission (Nunnari et al., 1997; Rapaport et al., 1998) (Figure 1.1). This concerted interplay of fusion and fission is also called mitochondrial dynamics. Reduction of fusion events leads to a highly fragmented mitochondrial network in the cell. Likewise, mitochondria form a tremendously hyper-fused network with abundant branches when fission is disturbed (Figure 1.1). Mitochondrial fusion and fission are pivotal in the inheritance of mitochondrial DNA and mitochondrial quality control (Nunnari et al., 1997). Mitochondrial inheritance relies on the division of mitochondrial fragments from the network and delivering them to the daughter cell. However, the precise role of mitochondrial division in terms of mitochondrial inheritance is not completely understood so far. Besides, it has been proposed that fission and fusion of mitochondria serve as the quality control assurance for separating damaged mitochondrial DNA from undamaged ones by mitochondrial fission (Youle and van der Bliek, 2012). Last but not least, mitochondrial fusion and fission are vital for mitochondrial ultrastructure (Harner et al., 2016; Kojima et al., 2019).

Mitochondrial fusion and fission are complex processes since mitochondria are surrounded by two membranes, the OM and the IM. Since the integrity of Inter Membrane Space (IMS) and matrix space have to be guaranteed, fusion and fission events have to be very well orchestrated. Very elaborate molecular machinery has been evolved to control fusion and fission of the OM and the IM (Detmer and Chan, 2007; Hoppins et al., 2007; Mozdy et al., 2000; Rapaport et al., 1998).

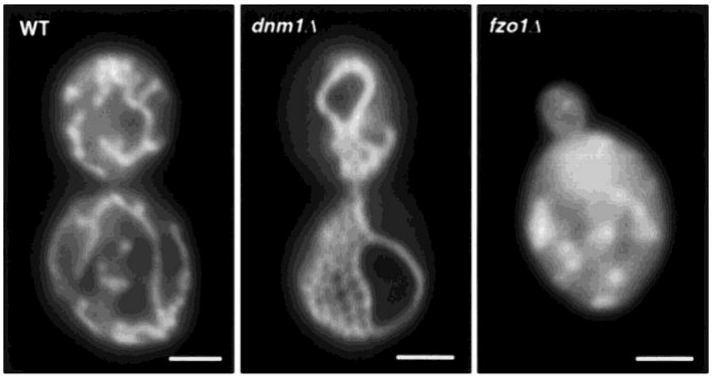

Figure 1.1 Mitochondrial morphology.

Fluorescence microscopy images of a *S. cerevisiae* wild-type strain, a *DNM1* deletion mutant and a *FZO1* deletion mutant. Matrix-directed GFP is used as the fluorescent dye. Modified from (Sesaki and Jensen, 1999). Scale bars 2µm.

Fission machinery comprises four proteins that orchestrate the mitochondrial division in yeast Dnm1, Fis1, Mdv1, and Caf4 (Hoppins et al., 2007; Labbé et al., 2014). Dnm1, a Dynamin-related GTPase, is mainly located in the cytosol and forms punctate structures at branch points of OM where the division events happen (Bleazard et al., 1999; Otsuga et al., 1998). Evidence has been provided that Dnm1 is essential for the division of the OM. First, deletion of *DNM1* leads to a hyper-fused mitochondrial network indicating that mitochondrial division is inhibited, but fusion still takes place (Otsuga et al., 1998). Second, Dnm1 forms a moderately curved filament in the GDP-bound state, the GTP-bound form of Dnm1 forms spiral structures (Ingerman et al., 2005). Strikingly, the size of these spiral structures matches perfectly with the diameter of mitochondria at sites of division. Additionally, it has been shown that mutations in the GTPase domain of Dnm1 abolish its ability to self-assemble and promote mitochondrial division (Ingerman et al., 2005). This indicates that the GTPase activity of Dnm1 is essential for mitochondrial division (Ingerman et al., 2005; Naylor et al., 2006). Fis1, another critical component of the fission machinery, is anchored in the OM. It has been shown that mitochondrial recruitment of Dnm1, Mdv1, and Caf4 have been compromised drastically in yeast cells lacking Fis1. Thus, Fis1 acts as the OM antenna for the division machinery (Griffin et al., 2005; Mozdy et al., 2000; Tieu and Nunnari, 2000). Significantly the process of mitochondrial fusion and fission (dynamics), as well as the key proteins, are conserved throughout evolution. Dnm1 and Fis1 have been conserved from yeast to mammals through evolution (Zhao et al., 2013). Dynamin-related protein 1 (DRP1), or dynamin-like protein 1 (DLP1), encoded by DNM1L, is the central molecular player that mediates mitochondrial fission in humans (Smirnova et al., 2001).

Mitochondrial fusion machinery is composed of several proteins. Fzo1, Ugo1, and Mgm1 are the most crucial proteins involved in OM and IM fusions. The paramount component of the mitochondrial fusion machinery is Fzo1 which has been identified first in *Drosophila melanogaster* (Hales and Fuller, 1997). Fzo1 is crucial for mitochondrial fusion events during cell growth and it is essential for long term maintenance of mitochondrial DNA (Hermann et al., 1998; Rapaport et al., 1998). The mammalian homologs of Fzo1 are called Mitofusin 1 and 2. Mitofusins are big GTPases containing two transmembrane domains that are integral in the OM. It has been shown that hydrolysis of GTP is essential for Fzo1 mediated membrane fission (Meeusen et al., 2004). Mammalian mitofusin forms oligomers in a GTP-dependent manner, and they can interact from opposing membranes (Ishihara et al., 2004; Koshiba et al., 2004). In yeast, another protein is involved in OM fusion, Ugo1 (Sesaki and Jensen, 2001). Ugo1 directly interacts with both Fzo1 and Mgm1, another component of mitochondria fusion machinery (Sesaki et al., 2003). Mgm1 is a dynamin related GTPase essential for the fusion of both mitochondrial membranes. It is present in two isoforms, a long isoform (l-Mgm1) and a short isoform (s-Mgm1). l-Mgm1 is anchored in the IM, while s-Mgm1 is a soluble IMS protein that is membrane associated (Herlan et al., 2003). s-Mgm1 is generated by proteolytic cleavage of the transmembrane domain by the rhomboid protease Pcp1 (Herlan et al., 2003). Strikingly, the presence of both l-Mgm1 and s-Mgm1 isoforms at a precise ratio is essential for mitochondrial fusion (Zick et al., 2009). The Membrane potential of IM is also required for the fusion of mitochondria (Meeusen et al., 2004). Therefore, an imbalance of s-Mgm1 and l-Mgm1 is often observed in unhealthy and not wholly functional mitochondria. hFis1, the functional orthologue of Fis1, interacts directly and indirectly with the mitochondrial fusion protein Opa1 (Zhao et al., 2013).

Concisely, mitochondria dynamics are crucial for the maintenance of mitochondrial form and function. Disruptions in these processes affect normal development, and they have been implicated in neurodegenerative diseases, such as Charcot-Marie-Tooth disease type 2A (CMT2A) and autosomal dominant optic atrophy (DOA). However, fusion of mitochondria is not only important for the dynamic of mitochondria, but also it is important for formation of mitochondrial ultrastructure (Harner et al., 2016).

1.3 Mitochondrial ultrastructure

Decades before studying mitochondrial morphology with fluorescence microscopes, their tremendously complex ultrastructure has been observed in electron micrographs (Palade, 1953; Rasmussen, 1995). Using electron microscopy, scientists observed that

two membranes encompass mitochondria, unlike most of the other organelles, the OM and IM (Palade, 1952). The IM consists of two functional compartments, the inner boundary membrane (IBM) and the crista membranes (CM) (Figure 1.2). The IBM is the area of the IM staying in close proximity to the OM. In contrast, cristae are invaginations into the interior of mitochondria. Crista junctions are narrow ring shape structures that connect cristae and the IBM. Another exciting characteristic of mitochondria is permanent contact sites between OM and IM (Hackenbrock, 1966, 1968). By this complex membrane system, mitochondria are divided into aqueous compartments (IMS), the intracristal space, and the matrix (Figure 1.2) (Daems and Wisse, 1966; Frey et al., 2002; Mannella et al., 2001; Perkins et al., 1997).

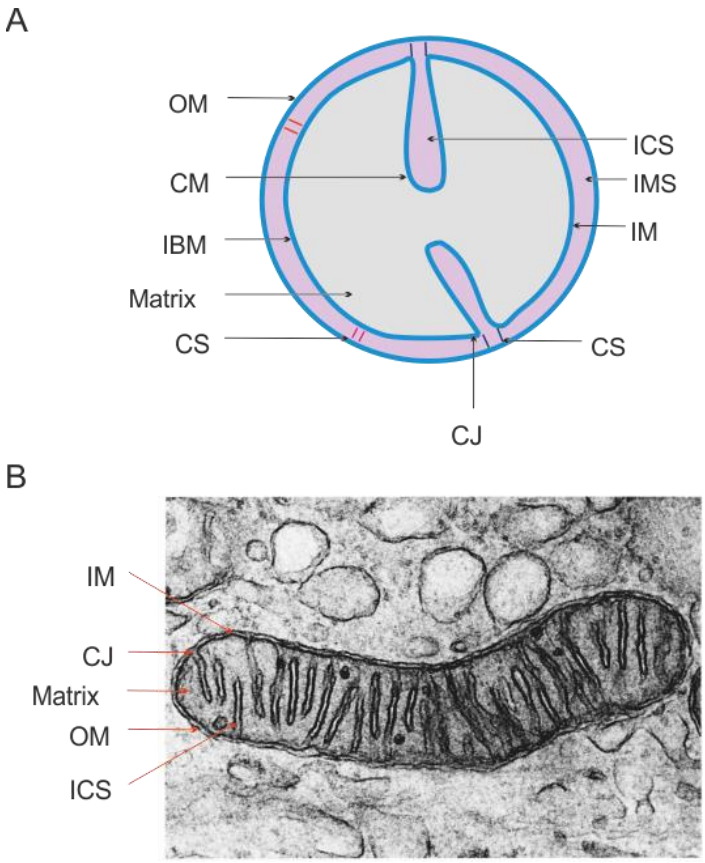

Figure 1.2 Architecture of mitochondria.

A. Schematic drawing of a wild type mitochondrion. OM, outer mitochondrial membrane; IM, inner mitochondrial membrane; IBM, inner boundary membrane; CM, crista membrane; CJ, crista junction; ICS, intracristae space; IMS, intermembrane space; different types of contact sites were indicated by red and black bars. Red and black bars indicate contact sites (CS).

B. Micrograph of mitochondrion from mouse epididymis. For abbreviations, see (A). From (Fawcet, 1981).

Although most mitochondria share these common features, electron microscopy images revealed that mitochondria of different cell types show extraordinarily versatile shapes in particular regarding the form of cristae. They can be tubular, lamellar, or even triangular in astrocytes (Figure 1.3) (Fawcett 1981). Lamellar cristae are predominantly present in tissue with high energy demand like skeletal muscle. Tubular cristae are mainly present in steroidogenic tissue. The diverse forms of cristae in cells with different functions indicate that mitochondria's structure and function are tightly connected. Cristae differ not only in a cell type specific but also developmental specific manner. For instance, in the adrenal cortex of fetal or neonatal rats, the form of cristae changes from the lamellar type to the tubular type during differentiation (Voutilainen and Kahri, 1979). In his groundbreaking paper of 1966, Charles Hackenbrock showed that mitochondria change their structure in response to ADP depletion (Hackenbrock, 1966). Furthermore, it has been observed that induction of apoptosis leads to changes in the IM shape, and matrix volume (Hackenbrock, 1966). Apparently, the mitochondrial ultrastructure can be adapted according to physiological conditions. These observations strengthen the hypothesis that IM and cristae are dynamic and change according to the physiology of cells.

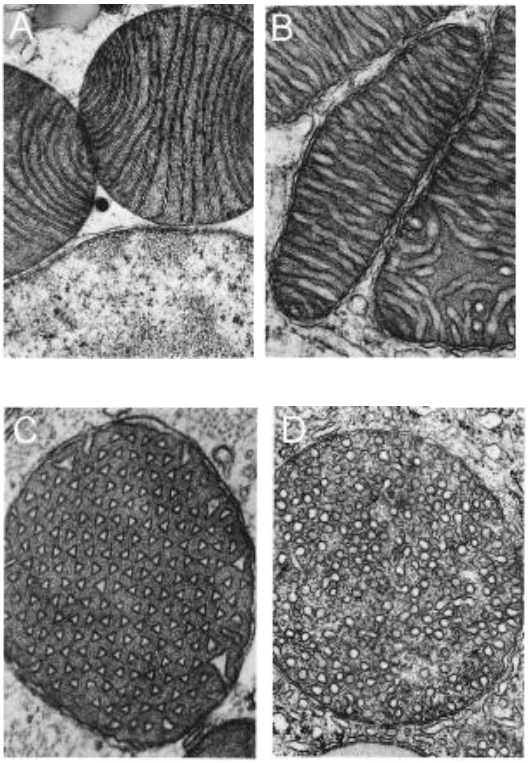

Figure 1.3 The versatility of mitochondrial architecture.

Electron microscopic images of mitochondria in (A) brown adipose cell from bat, (B) cell from hamster adrenal cortex, (C) astrocyte of hamster brain, (D) rat adrenal cortex. Modified from (Fawcet, 1981).

Astoundingly, abounding evidence indicates that the CM is functionally distinct from the IBM, and obviously, they have different protein compositions. Proteins needed for oxidative phosphorylation, such as electron transport chain complex and the F_1F_O ATP-synthase, are mainly located in cristae, and proteins of the import machinery TIM23 are mainly localized in the IBM (Gilkerson et al., 2003; Vogel et al., 2006). Further studies on the precise differential localization of proteins and their dynamics between IBM and the cristae membrane revealed that the TIM23 protein import machinery localizes to 60% in the IBM and 40% in the cristae membrane. However, when import machinery is activated by overexpression of GFP containing mitochondrial signal sequence (mGFP), 70% of Tim23 proteins were detected in the IBM due to enhanced import activity of mitochondria (Schülke et al., 1997; Vogel et al., 2006; Wurm and Jakobs, 2006). More recent evidence by single particle tracking (SPT) in living cells has also confirmed that proteins of electron transport chain complexes diffuse mainly in the cristae membrane and Tim23 protein diffuses predominantly in IBM (Appelhans and Busch, 2017).

Various studies have identified proteins that are responsible for the maintenance and generation of cristae. These are proteins essential for the dimerization of the F_1F_O ATP-synthase, the MICOS complex, and the mitochondrial fusion machinery (Cipolat et al., 2004; Davies et al., 2012; Harner et al., 2011; Jones and Fangman, 1992; Paumard et al., 2002b; Rabl et al., 2009). The F_1F_O ATP-synthase is a protein complex that consists of at least 17 different subunits and it catalyzes adenosine triphosphate formation (Rubinstein et al., 2003; Velours and Arselin, 2000). Significantly, these complexes form dimers with wedge-like arrangements involved in tthe formation of membrane curvature (Arnold et al., 1998). In this respect, the subunits Su *e* and Su *g* have to be emphasized since they are crucial for dimerization of the F_1F_OATP-synthase (Arnold et al., 1998). Likewise, Su *e* was one of the first genes reported to be critical for the ultrastructure of mitochondria. It has been observed that depletion of Su *e* leads to defective oligomerization of F_1F_O ATP- synthase and altered cristae morphology with onion-like structures in yeast (Paumard et al., 2002a).

The MICOS complex, identified by different groups simultaneously, is composed of six different subunits in yeast Mic10, Mic12, Mic19, Mic26, Mic27, and Mic60. Mic19 is a soluble protein in the IMS, whereas all other MICOS subunits are integrated into the IM. The most essential functions of the MICOS complex are the formation of contact sites (CS) and the formation of cristae junctions (CJs) (Harner et al., 2011; Hoppins et al., 2011; von der Malsburg et al., 2011). Deletion of core components of the MICOS

complex, *MIC60*, and *MIC10*, lead to the formation of internal membrane vesicles and the absence of CJs, suggesting their role in CJ formation (Alkhaja et al., 2012; Harner et al., 2011; Hoppins et al., 2011; von der Malsburg et al., 2011). Bohnert et al. observed that the oligomerization of Mic10 leads to the deformation of membranes. So, they suggested that Mic10 serves as a scaffold for the MICOS formation and cristae biogenesis. (Bohnert et al., 2015). Additionally, it has been observed that targeting Mic60 to the plasma membrane of prokaryotes leads to the formation of cristae-like invaginations. It indicates the possible role of Mic60 in the formation of cristae in mitochondria (Tarasenko et al., 2017). In addition, MICOS forms CS between the OM and the IM of mitochondria by interacting with proteins of the OM such as TOM complex (Bohnert et al., 2012; von der Malsburg et al., 2011; Zerbes et al., 2012), TOB/SAM (Bohnert et al., 2012; Darshi et al., 2011; Harner et al., 2011; Körner et al., 2012), Fzo1-Ugo1 (Harner et al., 2011) and the GTPase Miro (Modi et al., 2019). This plethora of interacting partners indicates additional functions of MICOS. In their seminal paper published in2016, Alton et al. provided evidence indicating that the MICOS complex plays a role in phospholipid homeostasis of mitochondria by forming contact sites. The phosphatidylserine decarboxylase, Psd1, is present in the IM and is able to decarboxylate PS not only in the IM but also on the OM. MICOS complex is essential in putting the two membranes in close proximity (Aaltonen et al., 2016). There are some indications that MICOS is involved in mitochondria protein import. Malsburg and co-workers have observed defects in mitochondrial protein import in cells lacking Mic60 (von der Malsburg et al., 2011). Although the exact contribution of MICOS in the mitochondrial protein import is not known so far, the interactions of Mic60 with several essential proteins of mitochondrial import machinery such as Tob55, Tim23, and Tom40 indicates that it might promote the import of proteins into mitochondria by spatially locating of TIM, TOM and TOB complexes in close proximity.

It has been observed that Mgm1, the fusion protein of IM, plays a vital role in cristae formation in addition to dimeric F_1F_O ATP-synthase and MICOS (Cipolat et al., 2004; Meeusen et al., 2006; Wong et al., 2000). Sesaki et al. showed that yeast cells lacking Mgm1 had enlarged mitochondria with aberrant cristae morphology (Sesaki et al., 2003; Song et al., 2009). However, deletion of *MGM1* was not linked to loss of cristae so far since it leads to loss of mitochondrial DNA and consequently loss of respiratory chain complex and dimeric F_1F_O ATP-synthase. Based on recent evidence, Harner et al. put forward a working model that might explain the role of Mgm1 in the process of crista formation. They have proposed a model in which two different mechanisms are responsible for the formation of lamellar cristae and tubular cristae (Harner et al., 2016). According to this model, the formation of lamellar cristae depends on the

mitochondrial IM fusion machinery. Mgm1 fuses two opposing membranes at sites where it interacts with the OM. Upon membrane fusion of Mgm1, the nascent crista is generated, and its high membrane curvature is stabilized by dimerization of F_1F_O ATP-synthase. MICOS is in this process only necessary for the termination of lamellar crista formation by stopping Mgm1 mediated fusion. However, the formation of tubular cristae is independent of mitochondrial fusion and initiated by the assembly of MICOS. The import of lipids and proteins is the driving force of tubular cristae formation. Like lamellar cristae, dimerization of F_1F_O ATP-synthase stabilizes the formed membrane curvature (Harner et al., 2016; Khosravi and Harner, 2020). In a more recent study, Kojima et al. provided additional evidence supporting this model. The authors observed that mitochondria lacking both Mgm1 and Mic60 do not show any IM structure, indicating that Mgm1 and Mic60 work in parallel mechanisms (Kojima et al., 2019). Surprisingly, depletion of Mgm1 and Mdm35, components of the mitochondrial lipid transport system, led to a strikingly similar phenotype. This indicates that tubular cristae formation depends not only on proteins and protein complexes but also on the import of phospholipids plays an important role in this process (Kojima et al., 2019).

1.4 Membrane phospholipids

Biological membranes consist of membrane proteins and lipids. Although membrane lipids contribute significantly to the function of organelles, they have not been studied as detailed as the corresponding proteins. In fact, different biological membranes have particular compositions of lipids. Biological membranes from yeast to humans are mainly composed of glycerophospholipids and to a minor extend of sterols and sphingolipids (in yeast ergosterol; in mammals cholesterol) (Zinser and Daum, 1995). Phospholipids are well-known for their ability to provide a matrix for embedding proteins and the other lipids exposing their polar head group to the surface and a polar acyl chain group to the interior of the bilayer (Dowhan, 1997). The building block of glycerophospholipids is phosphatidic acid (PA), composed of a glycerol backbone, two fatty acids, and a phosphate group. The phosphate group of PA can be substituted with various head groups, such as choline, ethanolamine, serine, inositol, or glycerol, to form different phospholipid species (Figure 1.4) (van Meer et al., 2008). The most abundant phospholipids in backer's yeast are phosphatidylcholine (PC) (Mannella et al., 2001) and phosphatidylethanolamine (PE) (Ejsing et al., 2009; Zinser and Daum, 1995). Cardiolipin (CL) is a distinct and unique phospholipid that can be found exclusively in mitochondria. It is composed of two phosphatidic acids, which are bound together with a glycerol backbone (Figure 1.4).

Phospholipids are divided into two distinct groups according to their overall shape structures depending on their head groups. The first group is made up of bilayer forming phospholipids like PC, phosphatidylserine (PS), and phosphatidylserine (PI) (Longtine et al., 1998; Mannella et al., 2001). They have an overall cylindrical shape since the area of the head group to the acyl chain group has a similar diameter in cross sections. The second group of phospholipids consists of non-bilayer forming phospholipids like phosphatidylethanolamine (PE), Cardiolipin (CL), and phosphatidic acid (PA). They have an overall canonical shape since in cross sections, the area of the head group is smaller than the area of the acyl chain group (Basu Ball et al., 2018; van den Brink-van der Laan et al., 2004).

Mitochondria of different cell types share four characteristics regarding their lipid composition: (1) sterol, and sphingolipids are only found at a low amount, (2) they have a low ratio of phospholipids to proteins (Longtine et al., 1998), (3) they have a high CL content and (4) PC, and PE are the major phospholipids (Horvath and Daum, 2013). There are minor variations in the relative phospholipid abundance of mitochondria that have been reported in different studies. Differences in growth conditions and purity of mitochondrial fractions used to measure phospholipids probably are the reason for observing slight variations in the relative phospholipid abundance. In mitochondria, PE and PC comprise approximately 30-40% of total phospholipids while CL and (PI) account for 10-15 % of phospholipids. PA and PS comprise approximately 5% of the total phospholipids (Horvath and Daum, 2013; Zinser and Daum, 1995). Intermediates of the CL biosynthesis pathway, phosphatidylglycerol (PG), phosphatidylglycerol phosphate (PGP), and CDP-Diacylglycerol (CDP-DAG) do not accumulate in wild type mitochondria under normal conditions.

Additionally, to the unique overall lipid composition of mitochondria, the IM differs from the OM. The mitochondrial IM has a lower phospholipid to proteins ratio than mitochondrial OM. Furthermore, the distribution of CL between IM and OM is asymmetrical. The majority of CL (75%) is present in the mitochondrial IM, while only a smaller fraction, 25%, localizes in the OM (de Kroon et al., 1997; Gebert et al., 2009; Zinser and Daum, 1995). This clearly indicates an important role of CL per se and phospholipids in general regarding mitochondrial functionality. The tendency of CL and PE to form negatively curved membranes makes them favorable for several mitochondrial processes like protein import, fusion, fission, oxidative phosphorylation, and maintaining the ultrastructure of mitochondria. In line with this, it has been observed that CL and PE can stabilize respiratory supercomplexes and F_1F_O ATP-synthase dimers, emphasizing their important role for oxidative phosphorylation

(Acehan et al., 2011; Böttinger et al., 2012). Furthermore it has been shown that CL stabilizes mitochondria translocators like the TIM23 and TOM complexes (Gebert et al., 2009; Malhotra et al., 2017). This also implies a role of CL in mitochondrial protein import. Besides, PA plays a vital role in mitochondrial morphology by its ability to stabilize curved membranes. It has been shown that Drp1, which is involved in mitochondrial fission, binds to the head group of phosphatidic acids (Adachi et al., 2016). This implies the critical role of PA in mitochondrial morphology. All these results together emphasis how essential these non-bilayer forming phospholipids are for the form and function of mitochondria.

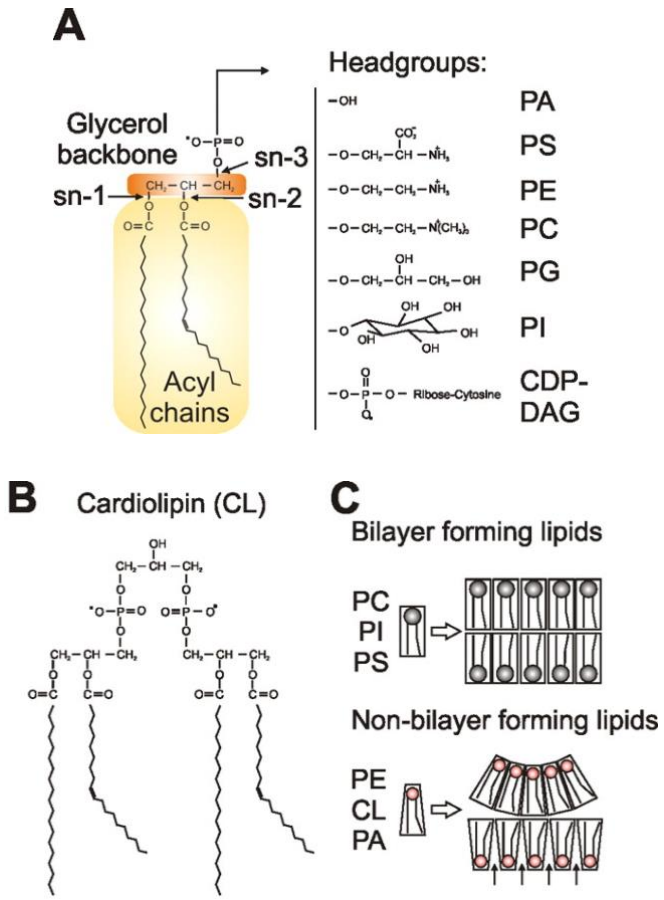

Figure 1.4 Phospholipids of mitochondria.

A) Structural elements of phospholipids. The main structural element of glycerophospholipids is the glycerol back bone. Acyl chains with different lengths and saturation are attached to the *sn-1* and *sn-2* hydroxyl groups. Versatile head groups with varying chemical properties can be attached to the sn-3 position of the glycerol backbone and form different classes of phospholipids.

B) CL is a unique phospholipid that consists of two PA moieties covalently linked to each other by a glycerol bridge.

C)Different shapes of bilayer and non-bilayer forming lipids. Non-bilayer forming lipids induce membrane curvature. Figures modified from (Osman et al., 2011).

1.5 Inter-organellar and intra-mitochondrial transport of phospholipids

Mitochondria cannot be made *de novo,* so mitochondria need to import and incorporate the lipids for membrane biogenesis and homeostasis from other organelles. Therefore, inter-organellar contact sites are essential for lipid transfer into mitochondria. However, since mitochondria are the primary site of PE synthesis, inter-organellar contact sites are equally crucial for transferring lipid out of mitochondria. So far, it has been suggested that contact sites between mitochondria and the endoplasmic reticulum (ER), the vacuole (in higher eukaryotes, the lysosomes), and lipid droplets are involved in transferring lipids into and out of mitochondria (Tamura et al., 2020; Zung and Schuldiner, 2020).

The ER-mitochondria encounter structure complex (ERMES) is the primary tethering protein complex forming contact sites between mitochondria and ER in yeast (Kornmann et al., 2009). The ERMES complex is composed of four subunits, i.e., Mmm1, Mdm12, Mdm10, Mdm34, and two regulatory proteins, i.e., Lam6 and Gem1 (Kornmann et al., 2009; Stroud et al., 2011; Zung and Schuldiner, 2020). ERMES has a multitude of functions, such as regulation of mitochondria fission and transfer of coenzyme Q precursors. Furthermore, evidence indicates that ERMES is directly involved in lipid transport (Kojima et al., 2019; Tamura et al., 2019a; Tamura et al., 2019b). For instance, deletion of *MDM12* in yeast cells leads to delay in converting PS to PE, as pulse-chase analyses have shown (Kornmann et al., 2009). It indicates that disruption of ERMES impairs phospholipid exchange between ER and mitochondria. Additionally, the crystal structure of Mdm12 has shown that it contains a hydrophobic pocket that could accommodate a phospholipid (Kawano et al., 2018). More importantly, it has been observed that the Mdm12-Mmm1 complex is able to transfer phospholipids *in vitro* (Kawano et al., 2018). By *in vitro* assay using isolated yeast membranes, Kojima et al. demonstrated that lack of the ERMES components impairs the phosphatidylserine transport from the ER to mitochondria (Kojima et al., 2016). These findings indicate that the ERMES complex has an essential role in inter-organellar lipid transfer (Figure 1.5).

Mitochondria form two different contact sites with the vacuole, vCLAMPs, and Vps13-Mcp11 contact sites. A vCLAMP is composed of a subunit of the HOPS complex, Vps39, a Rab GTPase, Ypt7, and Tom40 in the OM. Deletion of ERMES subunits led to

expansion of mitochondria-vacuole interface mediated by vCLAMP as GFP-Vps39 elucidated it(Elbaz-Alon et al., 2014; González Montoro et al., 2018; Hönscher et al., 2014). This finding shows that the interaction of mitochondria with the vacuole or the ER is tightly regulated. This conclusion is in line with the observation that simultaneous deletion of *VPS39* and a subunit of ERMES, like Mdm12, is lethal for the cell (Elbaz-Alon et al., 2014). Vps13 is another protein that mediates contacts between the vacuole and mitochondria through its interaction with Mcp1, a protein of the OM (González Montoro et al., 2018). Overexpression of *MCP1* partially rescues the growth defect from an impaired ERMES complex (Tan et al., 2013). This indicates that the interaction of Vps13 and Mcp1 might have a redundant role with the ERMES complex in phospholipid homeostasis of the mitochondria. Additionally, it has been suggested that Lam6 might have a role in forming a contact site between the mitochondria and the vacuole. Lam6 localized not only at mitochondria-ER contact sites but also at the mitochondria-vacuole and ER-vacuole contact sites. It has GRAM and VASt domains thought to mediate sterol transport at organellar contact sites (Elbaz-Alon et al., 2015; Gatta et al., 2015; Murley et al., 2017).

Mitochondria need to transport lipids between the IM and the OM to maintain their homeostasis. PS and PA are mainly produced in the ER, but as mentioned in the previous section, they are precursors for synthesizing PE and CL. However, enzymes that are involved in CL and PE biosynthesis are localized in the IM of mitochondria. Therefore, PA and PS must be transported first from the ER to the OM and then the OM to the IM. Ups1 and Ups2 are proteins that are localized in the IMS (Sesaki et al., 2006). It has been shown that the deletion of *UPS1* and *UPS2* leads to the reduction of CL and PE respectively (Connerth et al., 2012; Tamura et al., 2009). Interestingly, it has been observed that recombinantly purified Usp1-Mdm35 and Ups2-Mdm35 complexes are able to transfer PA and PS in vitro, respectively (Miyata et al., 2016). This indicates intra-mitochondrial transport of PA and PS from OM to IM through the IMS is mainly accomplished by the Ups1/Ups2-Mdm35 protein complex (Figure 1.5).

Nevertheless, deletion of *Usp1* does not entirely halt CL synthesis in the cells. This suggests that there must be some alternative pathways that transport PA from OM to IM. Miyata et al. have reported that the formation of CL in the absence of Ups1 is almost completely inhibited by deletion of *MDM31*, *MDM35*, and *FMP30* (Miyata et al., 2017). This suggests that Mdm35, Fmp30 and Mdm31 are crucial for the formation of CL independent of Ups1. Additionally, it has been shown that simultaneous deletion of *POR1* and *POR2* reduces CL content of cells to 10%. Interestingly, Por1, a protein of the OM, forms a CS between the OM and the IM by interacting with the mitochondrial IM proteins, Mdm31 and Mdm35. So, it has been put forward that this CS might serve

as a spot for transport of PA to the IM for CL biosynthesis (Miyata et al., 2018) (Fig 1.5). Although CL is synthesized in the mitochondrial IM, it is also present in the OM, where it is essential for the function of the TOM complex. This indicates that CL has to be transported across the IMS from the IM to the OM. However, it is still unknown how CL is transported from the IM to the OM.

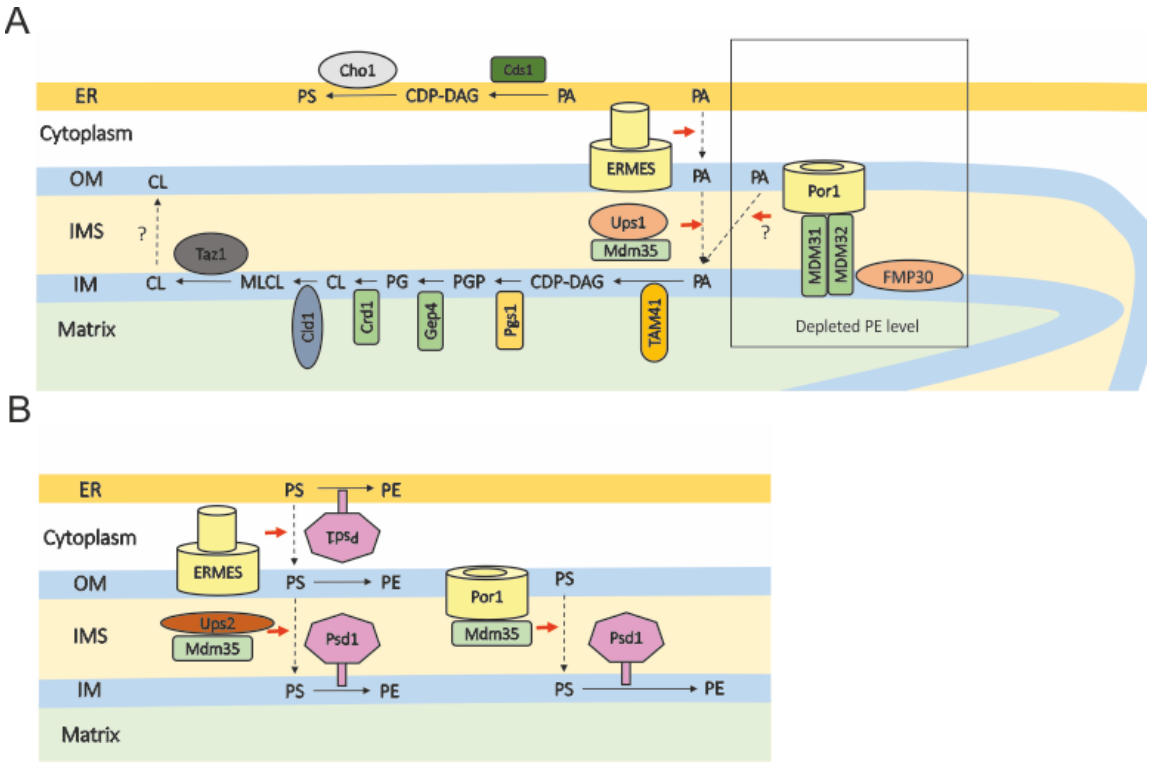

Figure 1.5 Transport of PA and PS from ER to mitochondria in yeast.

A) Current model for transport of PA from the ER to mitochondria and from the OM to the IM. Arrows with solid and dotted lines indicate phospholipid conversion and transport, respectively. Red arrows indicate direct involvement in lipid transfer. The decreased PE level (boxed area) might trigger the alternative CL synthetic pathway.

B) Current model for transport of PS from the ER to mitochondria and from the OM to the IM. Psd1 localization in the ER is carbon source dependent (Friedman et al., 2018). Arrows with solid and dotted lines indicate phospholipid conversion and transport, respectively. Red arrows indicate direct involvement in lipid transfer.

Psd1 does not only synthesize PE in mitochondria but also the Kennedy pathway and Psd2 in the ER contribute to PE synthesis in *S. cerevisiae* (Bürgermeister et al., 2004; Gulshan et al., 2010; Iadarola et al., 2020; Trotter and Voelker, 1995). Nevertheless, PE that Psd1 synthesizes in the IM compromises the majority of cellular PE and the excess of PE in the mitochondria will later be transferred to the ER (Achleitner et al., 1995; Kodaki and Yamashita, 1987; Shiao et al., 1998). It has been recently revealed that PS can be converted to PE on the IMS side of OM by Psd1, too (Figure 1.5) (Aaltonen et al., 2016). Interestingly, this is mediated by Mic60 dependent contact

sites between the IM and the OM, indicating the importance of inter-mitochondrial contact sites in mitochondrial phospholipid homeostasis. Synthesis of PE in the mitochondrial OM might facilitate the transport of PE from mitochondria to the ER via bypassing an extra step of transport from the IM to the OM. However, it is not known so far what mechanisms are precisely involved in this process. Surprisingly, it has been recently reported that Psd1 has a dual localization. Psd1 localizes in mitochondria and the ER in a metabolic dependent manner (Figure 1.5) (Friedman et al., 2018). ER localized Psd1, and mitochondrial localized Psd1 contribute to the synthesis of functionally distinct pools of PE, which serve the cell differentially (Friedman et al., 2018).

1.6 The UbiB protein family in yeast

Mcp2 proposed to have a role in mitochondrial lipid homeostasis, belongs to a protein group called the UbiB protein family, which comprises one-quarter of microbial protein kinase like super family (PKLs) (Kannan et al., 2007). The UbiB protein family members are present in archaea, bacteria, and eukaryotes. In eukaryotes, they are exclusively present in mitochondria and plastids (Kannan et al., 2007; Leonard et al., 1998). The most prominent member of the UbiB protein family in *Escherichia coli* is UbiB, and in *Providencia stuartii*, Aarf supports the biosynthesis of ubiquinone (Coenzyme Q/CoQ). CoQ is a lipid-soluble electron carrier well known for its role in energy metabolism, more specifically in the mitochondrial respiratory electron transport chain (Mitchell, 1975; Poon et al., 2000).

The yeast genome contains three UbiB family genes, *COQ8, MCP2,* and *MCO76. COQ8, MCP2,* and *MCO76* are conserved in evolution from yeast to human, and their homolog genes in humans are named *ADCK3*, *ADCK1*, and *ADCK2,* respectively. For the first time, the similarity of Coq8 and UbiB with protein kinases was noted by Leonhard et al. A more in-depth analysis of the UbiB protein family categorizes it as atypical kinases (Leonard et al., 1998; Manning et al., 2002). Bioinformatic analysis indicated that the UbiB protein family retains some of the motifs conserved in canonical protein kinases such as PKL II, IV, V, (Leonard et al., 1998; Stefely et al., 2015). However, there are motifs in the UbiB protein family that distinguish them from other PKLs, such as an alanine rich loop that replace the canonical glycine-rich loop.

Eleven yeast genes, *COQ1-COQ11,* are essential for the biosynthesis of CoQ, which is a crucial lipid that plays a vital role in mitochondrial respiratory electron transport (Awad et al., 2018). Coq8, the best studied member of the UbiB protein family in *S. cerevisiae*, is critical for biosynthesis of CoQ and its depletion leads to respiration

deficiency in non-fermentable carbon source (Do et al., 2001). Although there is no evidence supporting the kinase activity of Coq8, it has been recently reported that Coq8 possesses an ATPase activity that is activated by binding to membranes containing cardiolipin (Reidenbach et al., 2018). Stafely et al. have provided valuable evidence by solving the structure of ADCK3, the homolog of Coq8 in humans, showing how ADCK3 binds to ATP. Furthermore, the crystal structure of ADCK3 showed that its N-terminal extension occludes the cleft that binds peptide substrate. It indicates that ADCK3 might not be able to use proteins as substrates for phosphorylation. ADCK3 also does not bind adenine nucleotides in a divalent cation-dependent manner, a common feature of protein kinases. This also supports the idea that ADCK3 is not a genuine protein kinase (Stefely et al., 2015; Tan et al., 2013).

MCP2, the other member of the UbiB protein family in *S. cerevisiae*, is the multi copy suppressor of loss of function ERMES complex indicating its role in mitochondrial phospholipid homeostasis (Tan et al., 2013). Although deletion of *MCP2* does not affect cell growth, immense overexpression of *MCP2* is toxic for the cells. Additionally, it has been shown that overexpression of *MCP2* partially restores the alterations in mitochondrial lipid composition of cells lacking Mdm10 (Tan et al., 2013). It strengthens the idea that Mcp2 might be involved in the lipid metabolism of mitochondria. Besides, it has been demonstrated that cells lacking *TGL2* and *MCP2* simultaneously have a tremendous growth defect and a lower amount of CL and PE (Odendall et al., 2019). Tgl2 is a mitochondrial protein with the predicated lipase domain (Grillitsch and Daum, 2011). Although the exact molecular function of Tgl2 is not clear in the mitochondria, enriched Tgl2 has lipolytic activity toward diacylglycerol (DAGs) and triacylglycerol (TAGs) (Ham et al., 2010). Odendall et al. have also reported that three amino acid residues of Mcp2, located in an annotate kinase domain of Mcp2, are crucial for restoring growth defect of loss of function ERMES (Odendall et al., 2019). It indicates that the annotated kinase domain of Mcp2 is essential for its function. Mco76 is the least studied protein in the ADCK like protein family, and it is uncharacterized.

1.7 The aim of the study

To fully understand different aspects of mitochondrial form and function, it is necessary to elucidate the function of uncharacterized mitochondrial proteins. The UbiB protein family has three members in *S. cerevisiae, Coq8, Mcp2, and Mco76,* all of which are evolutionary conserved from yeast to humans. Mutations in the UbiB protein family members have been linked to several human diseases. Therefore, it has potential therapeutic advantages to better understand the molecular function of the UbiB protein family. This study is focused on *MCO76,* which has been uncharacterized so far and this thesis aimed to gain novel insight into the molecular function of Mco76.

First, it is necessary to determine the localization and topology of Mco76 in the mitochondria. Second, it is crucial to discover the biochemical interacting partners of Mco76 as well as its genetic interactions. To this end, after determining the topology of Mco76 in mitochondria, its biochemical interactors were determined using biochemical approaches. This allowed obtaining a deeper insight into the function of Mco76 in mitochondria. Second, using cell biological approaches, genetic interactions of MCO76 were determined. Genetic interactions of *MCO76* also elucidated its function more in detail. Last but not least, the effects of deletion and overexpression of *MCO76* on mitochondrial structure and morphology were studied using cell biological approaches.

2. Materials and methods

2.1 Molecular biology methods

2.1.1 DNA isolation

2.1.1.1 Isolation of genomic DNA from yeast *S. cerevisiae*

Genomic DNA from yeast cells was isolated using Wizard Genomic DNA Purification kit (Promega) according to the manufacturer´s instructions. First, yeast cells were inoculated in 5 mL YPD medium and grown overnight at 30°C, shaking at 140 rpm. Cells were harvested from 5 mL of culture by centrifugation at 3,000 x g, 5 mins at RT. Cells were resuspended in 293 µL of 50 mM EDTA, pH 8.0. Then 7.5 µL of 10 mg/mL of zymolyase was added to the resuspended cells, and incubated for 60 min at 30°C. Cells were centrifuged at 16,000 xg for 2 mins at RT, and the pellet was resuspended in 300 µL of Nuclei Lysis Solution. This was followed by adding 100 µL of Protein Precipitation Solution and incubating on ice for 5 min. Proteins were pelleted by centrifugation at 16,000 xg for 3 min at RT and supernatant was transferred to a new microcentrifuge tube containing 300 µL isopropanol. Precipitated DNA was pelleted by centrifugation at 16,000 xg, 2 mins at RT. The pellet containing DNA was washed with ice cold 70% ethanol and centrifuged at 16,000 xg, 2 mins at RT. 50 µL of DNA Rehydration Solution containing 100 µg/mL RNase was added to DNA pellet and incubated at 37°C for 15 mins. DNA was rehydrated by incubation at 65°C for 1 hour and stored at -20°C until use.

2.1.1.2 Isolation of plasmids DNA from *E. coli*

To isolate high copy number plasmid DNA from *E. coli*, 5-10 mL of LB media containing 1µg/mL of ampicillin were inoculated with a single colony and cultivated at 37°C overnight. Cells from 1.5 mL of the culture were harvested by centrifugation at 10,000 xg for 1 min. The supernatant was discarded, and the pellet was resuspended in 100 µL of buffer P1. Cell lysis was achieved by adding 200 µL of P2 buffer. Cell suspension was mixed gently by inverting the tubes six times to prevent shearing the genomic DNA into small fragments since these fragments would subsequently lead to contamination of the plasmid DNA. Later 150 µL of ice-cold buffer P3 was added to the lysates to neutralize the pH and precipitate proteins and genomic DNA. The precipitate

was pelleted by centrifugation for 10 min at 20,000 ×g and 4°C. The supernatant containing plasmid DNA was transferred to a new reaction tube, and the same centrifugation step was repeated. Precipitation of plasmid DNA was achieved by adding 600 µL of ice-cold isopropanol. The DNA was pelleted by centrifugation for 10 min at 20,000 ×g and 4°C. The DNA pellet was washed with 600 µL of 70% ethanol at -20°C. The DNA pellet was dried entirely and then resuspended in 30 µL of sterile Millipore water. After determining the concentration, its concentration was adjusted to 1mg/ mL and stored at -20 4°C.

Buffer-P1 (stored at 4°C):

50 mM Tris-Base, 10 mM EDTA, 0.1 mg/ mL RNAse A

Buffer-P2 (stored 25°C):

0.2 M NaOH, 1% (w/v) SDS

Buffer-P3 (stored bei 4°C):

60 mL 3 M Kaliumacetat, 11.5 mL acetic acid, 28,5 mL H2O

Low copy number plasmid DNA was isolated from *E. coli* by NeucleoSpin Plasmid purification kit (Macherey-Nagel) according to the manufacturer's instruction. Briefly, a single bacterial colony was inoculated in 5 mL of LB medium containing 100 µg/mL of ampicillin and grown overnight at 37°C. Cells were harvested by centrifugation at 11,000 xg, 10 min, RT. The cells were resuspended in ice-cold 500 µL Buffer A1. The resuspended cells were lysed by addition of 500 µL Buffer A2, and the cell suspension was inverted six times gently. After 5 min of incubation at RT, 600 µL of Buffer A3 was added to neutralize the solution and precipitate proteins. Precipitated proteins were pelleted by centrifugation at 11,000 xg for 10 min at RT. 750 µL of the cleared solution was transferred to a NucleoSpin Plasmid column. The cleared solution was passed through the silica membrane by centrifugation 10,000 xg, 1 min at RT. Silica membrane wash with 600 µL of Buffer A4. Plasmid DNA was eluted from silica membrane by addition 30 µL of Millipore water and centrifugation with 11,000 xg for 1 min. DNA concentration was measured and the solution was stored at -20°C.

2.1.2 Amplification of DNA fragments

The Polymerase Chain Reaction (PCR) is used to amplify of specific DNA sequences over several reaction cycles. A cycle consists of the three steps of denaturing the double-stranded (ds) DNA, annealing of complementary oligonucleotides (primers), and synthesizing the DNA by thermostable DNA polymerase. Phusion-HF, a

commercially available high fidelity DNA polymerase from NEB, made by fusing Pyrococcus-like enzyme with a processivity enhancing domain, was used for PCR. Each 50 µL of PCR mixture contained 2 U polymerase, 10 µL of 5X Phusion-HF, 50 pmol of forward primers and 50 pmol reverse primers, 100 µM of the four deoxyribonucleoside triphosphates (dNTPs), 50 ng of genomic or 5 ng of plasmid DNA. The following PCR program was used for amplifying DNA fragments, if not mentioned otherwise:

Nuclease inactivation + Denaturation of DNA	98°C, 5 min
DNA amplification cycle:	30-35 cycles
1. DNA denaturation	95°C, 30 s
2. Annealing of primers	55°C, 30 s
3. Extension of primers	72°C, 1 min/kbp
Final extension and completion of reaction	72°C, 10 min

Colony PCRs were performed on bacterial single colons by resuspending single colones in 10 µL final PCR reaction Mix. Amplification of DNA fragments for site directed mutagenesis has been achieved by using phosphorylated oligonucleotides.

2.1.3 Detection and analysis of DNA

2.1.3.1 Quantification of DNA

To estimate DNA concentration, the absorbance of 2 µL of DNA sample at 260 nm was measured by NanoDrop.

2.1.3.2 Agarose gel electrophoresis

Analysis of DNA fragments and PCR products were achieved by gel electrophoresis. 1% (w/v) agarose was boiled in TAE buffer in a microwave oven for approximately 1-2 min until agarose entirely dissolved in the buffer. After cooling down the agarose solution, ethidium bromide was added to the final concentration of 0.5 µg/mL. The agarose mixture was solidified under the hood while a comb with a proper number of wells was inserted in the agarose gel. DNA samples were pre-mixed with commercially available Gel Loading Dye, Purple (6X) from NEB in 1:5 ratios and were loaded in the wells of solidified agarose gels. Gels were run at constant voltage, 100-120 V, depending on their size. Separated DNA fragments were visualized under UV light (366 nm).

TAE buffer:

40 mM Tris-acetate, pH 7.5, 20 mM Na-acetate, 1 mM EDTA

2.1.3.3 DNA extraction from agarose gels

DNA was extracted from agarose gel by Wizard SV Gel and PCR clean-up system from Promega. DNA band of interest was cut out by scalpel and transferred to a 1.5 mL tube. Subsequently, 600 µL of Membrane binding solution was added to the tube and incubated at 60°C for 10 min while shaking at 1,000 rpm. The dissolved gel was transferred to SV minicolumn assembly and incubated for 1 min. The dissolved gel was passed through the silica membrane by centrifugation at 16,000 xg for 1 min. Flow through was discarded from the collecting tube and silica-membrane washed twice by 700 µL of Washing Buffer containing 80% ethanol. Silica membrane was air dried, and subsequently, DNA was eluted from the silica membrane by adding 30 µL of water and centrifugation at 16,000g for 1 min.

2.1.4 Cleaning of PCR products

DNA fragments were either cut out from agarose gels and extracted therefrom or, directly after PCR reaction, were purified using mini-centrifugation columns. For this purpose, a kit from Promega was used according to the manufacturer's instructions (Wizard SV Gel and PCR Clean-Up System).

2.1.5 Manipulation of DNA with enzymes

2.1.5.1 Restriction Digestion

DNA sequence-specific digestion was carried out using appropriate endonucleases from New England Biolabs (NEB). For preparation purposes, 10 micrograms of DNA were digested with 20 U of appropriate endonucleases in the recommended buffer from the manufacturer. 50 µL of the total reaction solution was incubated at 37° C for 2 hours, and the reaction was stopped by incubation of solution at 67° C. For analytical purposes, one microgram of DNA was digested with two units of appropriate endonucleases in the recommended buffer. Later, digestion products were analyzed by agarose gel electrophoresis, and in case of preparation purposes, digestion products of interest were purified from agarose gel.

2.1.5.2 Phosphorylation of oligonucleotides

T4 Polynucleotide Kinase (PNK) from NEB was used for phosphorylation of the 5′ end of oligonucleotides. To do so, 750 pmol of oligonucleotides were incubated with 0.5 units of PNK in the presence of 1 mM ATP and appropriate PNK buffer recommended by the manufacturer. The reaction solution was incubated for 1 hour at 37° C. Deactivation of PNK enzyme was achieved by incubation of reaction solution at 65° C for 20 mins. Phosphorylated oligonucleotides were used directly for PCR reaction.

2.1.5.3 Ligation

In case of site directed mutagenesis, 100 ng of purified PCR product (linear) was ligated by 10 U of T4 DNA ligase (NEB) in T4 ligase buffer at 25°C for 4 h. 5 µL of ligation mixture was used to transform 75 µL of competent *E. coli* cells.

T4 ligase buffer

(50 mM Tris-Cl, 10 mM MgCl2, 1 mM ATP, 10 mM DTT, pH 7.5)

2.1.5.4 Gibson cloning

Gibson cloning technique allows for successful assembly of multiple DNA fragments, regardless of fragments length or end compatibility. Gibson assembly joins DNA fragments in a single tube by an isothermal reaction. There are three enzymatic activities that occur in a single tube during Gibson cloning. First, T5 exonuclease (NEB) creates single-stranded 3′ overhangs that facilitate the annealing of DNA fragments with sharing complementary strands at one end. Then Phusion DNA polymerase (NEB) fills in gaps within each annealed fragment. In the end, Taq DNA ligase (NEB) seals nicks in the assembled DNA. Vectors were cut by proper endonucleases and DNA fragments were produced by PCR amplification using primers which adds proper homology sequence to the ends of DNA fragments. DNA fragments and cut vectors were first purified by Wizard SV Gel and PCR clean-up system and DNA concentrations were determined. Different DNA fragments and cut vectors were combined in equimolar ratio to a final volume of 5 µL. This was added to 15 µL of Gibson Master Mix and incubated at 50°C for one hour and 8 µL of final reaction was used for transformation into *E. coli*.

Gibson Assembly Master Mix

Reagents	**concentrations**
PEG 8,000	10%
Tris-HCl, pH 7.5	200 mM
$MgCl_2$	20 mM
DTT	20 mM
dNTP	0.4 mM
NAD	2 mM
Phusion DNA polymerase	0.033 unit/µL
Taq DNA ligase	5.3 unit/µL
T5 exonuclease	0.005 unit/µL

2.1.6 Plasmid and cloning strategies

2.1.6.1 Overview of constructs used

Construct	**Vector**	**reference**
Prom-Mco76-Ter	pRS316	This thesis
Prom-Mco76-3xHA	pRS316	This thesis
Prom-Mco76-Ter(K275A)	pRS316	This thesis
Prom-Mco76-Ter(D288A)	pRS316	This thesis
Prom-Mco76-Ter(E330A)	pRS316	This thesis
Mco76	pYES2	This thesis
Mco76 (D288A)	pYES2	This thesis
Mco76 (E330A)	pYES2	This thesis
Mco76 (L275E)	pYES2	This thesis
pCO437		(Jakubke et al., 2021)

2.1.6.2 Cloning strategies

2.1.6.3 *MCO76* constructs under endogenous promoter

MCO76 with its endogenous promoter (800 base pair up stream of the start codon) and endogenous terminator (300 base pairs downstream of the stop codon) was cloned into pRS316 vector using *XhoI* and *HindIII* restriction sites by Gibson cloning strategy. The DNA fragment was amplified from genomic DNA of wild type yeast cells by following primers:

R *XhoI YPL109c*

5'-CTTACCGGGCCCCCCCTCGACGTACCGTTGCCTTATTGTTC-3'

F *HindIII YPL109C* (gib)

5'-GGTACCGGGCCCCCCCTCGAGGCTACCGTTGCCTTATTGTTC-3'

in order to delete the intron sequence from pRS316Mco76 construct, two DNA fragments were amplified excluding intron and they were cloned in pRS316 vector using XhoI and *HindIII* restriction sites by Gibson cloning strategy. A DNA fragment was amplified from *MCO76* promoter to the 5' of intron and another DNA fragment was amplified from 3' of intron to the end of *MCO76* terminator using the following four primers.

R *XhoI YPL109C*

5'-CTTACCGGGCCCCCCCTCGACGTACCGTTGCCTTATTGTTC-3'

F *HindIII YPL109C* (gib)

5'-GGTACCGGGCCCCCCCTCGAGGCTACCGTTGCCTTATTGTTC-3'

R intron deletion

5'-CTTACCGGGCCCCCCCTCGACGTACCGTTGCCTTATTGTTC-3'

F intron deletion

5'-CCAAACTTGGACTTATTTGAAAGTTCGCTGCCTATATTACGTG-3'

2.1.6.3.1 Mco76-3xHA under the endogenous promoter

Mco76-3xHA was cloned under its endogenous promoter and ADH1 terminator in pRS316 vector using *XhoI* and *HindIII* restriction sites by Gibson cloning. DNA

fragment was amplified from yeast cells genome in which 3xHA tag was inserted chromosomally in the C-terminus of *MCO76* open reading frame. These two primers were used to amplify the DNA fragments.

F *HindIII YPL109C* (gib)

5'-GCAGGAATTCGATATCAAGCTTGGTACTGGAAAGATCGCGTTC-3'

Gib(*XhoI*)ADH1terR1

5'-ACCGGGCCCCCCCTCGAGGTAGAGGTGTGGTCAATAAG-3'

To delete the intron sequence from pRS316Mco76-3xHA construct, the same strategy has been deployed as it is described for the deletion of the intron from pRS316Mco76 construct. Two DNA fragments were amplified excluding the intron and they were cloned in pRS316 vector using *XhoI* and *HindIII* restriction sites by Gibson cloning strategy. A DNA fragment was amplified from the beginning of *MCO76* promoter to the 5' of the intron and another DNA fragment was amplified from 3' of the intron to the end of the ADH1 terminator using the following four primers.

F *HindIII YPL109C* (gib)

5'-GCAGGAATTCGATATCAAGCTTGGTACTGGAAAGATCGCGTTC-3'

Gib(*XhoI*)ADH1terR1

5'-ACCGGGCCCCCCCTCGAGGTAGAGGTGTGGTCAATAAG-3'

R intron deletion

5'-CACGTAATATAGGCAGCGAACTTTCAAATAAGTCCAAGTTTGG-3'

F intron deletion

5'-CCAAACTTGGACTTATTTGAAAGTTCGCTGCCTATATTACGTG-3'

2.1.6.3.2 Mco76(K275A), Mco76(D288A) and Mco76(E330A) under endogenous promoter

Cloning of Mco76(K275A), Mco76(D288A), and Mco76(E330A) in pRS316 vector was achieved by site directed mutagenesis of the pRS316Mco76 construct. Mutations were added to the construct by amplification of pRS316Mco76 using two phosphorylated primer pairs containing mismatched base pairs. Blinds of each PCR product was annealed as it is described above and used for the transformation of *E. coli.*

*YPL109C*_K275A_for

5’-GCGATCTTGCATCCAAATGTAAG-3’

*YPL109C*_K275A_rev

5’-GATGGCACACCAACGATTTC-3’

*YPL109C*_D288A_for

5’-GCTTTGAAAATAATGAAATTCTG-3’

*YPL109C*_D288A_rev

5’-TCTCCGGATCTGAGATCTTAC-3’

*YPL109C*_E330A_for

5’-GCGGCGTTAAACCTGGAAAG-3’

*YPL109C*_E330A_rev

5’-AATTCTTAGATCCAACTGAATA-3’

2.1.6.3.3 Mco76 under the GAL1 promoter

Overexpression of *MCO76* was achieved by cloning of the *MCO76* open reading frame in the pYES2 vector under Gal1 promoter. In order to exclude intron sequence in the final construct *MCO76* sequence was amplified from genomic DNA of yeast wild type strain in two different fragments. BamHI restriction site was used to delete the intron and by using SacI and NotI restriction sites, the open reading frame excluding the intron was cloned into the pYES2 vector.

YPL109C(*SacI*)_s

5’-CCCGAGCTCATGTCATTTTTAAAGTTCGC-3’

YPL109C-int(*EcoRI*)_as

5’-CCCGAATTCACGTAATATAGGCAGCGAACTTTCAAATAAGTCCAAG-3’

YPL109C-int(*EcoRI*)_s

5’-CGTGAATTCGGGTTTAAGC-3’

YPL109C(*NotI*)_as

5’-CCCGCGGCCGCTTAATAATTAGGACACAATTG-3’

2.1.7 Transformation of *E. coli* with plasmid DNA

80 µL of competent *E. coli* XL1-Blue were thawed on ice. 5 µL of ligation mixture, 8 µL of Gibson final reaction, or 5 µg of purified plasmid were used per transformation. After incubation of cells for 10 mins on ice, the cells were subjected to heat shock at 42°C for 1 min. After 5 mins incubation of cells on ice, 1 mL of LB was added to the cell suspension and incubated at 37°C for 1 hour while shaking. Finally, cells were harvested by a centrifugation step at 11,0000 xg for 1 min and plated on LB agar plates with appropriate selection markers. Plates were incubated at 37° C for 16 hours.

2.1.8 Yeast genetics methods

2.1.8.1 *S. cerevisiae* strains used

Strain name	**Genotype**	**Reference**
YPH499 (WT)	MATa *ade2-101 his3-Δ200 leu2- trp1-Δ63*	(Sikorski
Δ*mco76*	YPH499, *mco76::HIS3*	This study
Δ*mcp2*	YPH499, *mcp2::HIS3*	This study
Δ*ups1*	YPH499, *ups1::KAN*	This study
Δ*ups1*	YPH499, *ups1::LEU2*	This study
Δ*crd1*	YPH499, *crd::Leu2*	This study
Δ*psd1*	YPH499, *psd1::Leu2*	This study
Δ*gep4*	YPH499, *gep4::Leu2*	This study
Δ*ups2*	YPH499, *ups2::Leu2*	This study
Δ*mdm35*	YPH499, *mdm35::Lue2*	This study
Δ*taz1*	YPH499, *taz1::Leu2*	This study
Δ*cld1*	YPH499, *cld1::Leu2*	This study
Δ*mco76*Δ*mcp2*	YPH499, *mcp2::HIS3 mco76::Kanmx6*	This study
Δ*ups1*Δ*mco76*	YPH499, *mco76::HIS3 ups1::Leu2*	This study
Δ*ups1*Δ*mco76*	YPH499, *mco76::HIS3 ups1::KANMX6*	This study
Δ*mco76*Δ*mcp2*	YPH499, *mcp2::HIS3, mco76::KANMX6*	This study
Δ*crd1*Δ*mco76*	YPH499, *mco76::HIS3, crd::LEU2*	This study
Δ*psd1*Δ*mco76*	YPH499, *mco76::HIS3, psd1::LEU2*	This study
Δ*gep4*Δ*mco76*	YPH499, *mco76::HIS3, gep4::LEU2*	This study

Δups2Δ*mco76*	YPH499, *mco76::HIS3, ups2::LEU2*	This study
Δ*mdm35*Δ*mco76*	YPH499, *mco76::HIS3, mdm35::LEU2*	This study
Δ*taz1*Δ*mco76*	YPH499, *mco76::HIS3, taz1::LEU2*	This study
Δ*cld1Δmco76*	YPH499, *mco76::HIS3, cld1::LEU2*	This study
Δ*ups1*Δ*mcp2*	YPH499, *ups1::KANMX6, mcp2::HPHNT1*	This study
Δ*ups1*Δ*mcp2*Δ*mco76*	YPH499, *mcp2::HIS3, mco76::kanMX6,*	This study
Mco76-3xHA	YPH499, *mco76::MCO76-3xHA-HIS3*	This study
Mco76-3xMyc	YPH499, *mco76::MCO76-3xMyc-TRP1*	This study
Por1-3xHA	YPH499, *por1::POR1-3xHA-HIS3*	This study
Om14-3xHA	YPH499, *om14::OM14-3xHA-HIS3*	This study
Δ*mic60* Om14-3xHA	YPH499, *mic60::HIS3, om14::OM14-3xHA-TRP1*	This study
YPH499mKate	YPH499, *HO-PGKpr-su9-KATE2::KANMX*	This study
Δ*mco76*mKate	YPH499, *mco76::HIS3,HO-PGKpr-su9-KATE2::KANMX*	This study
Δ*ups1*mKate	YPH499, *ups1::Leu2,HO-PGKpr-su9-KATE2::KANMX*	This study
Δ*ups1*Δ*mco76*mKate	YPH499, *ups1::Leu2,mco76::HIS3, HO-PGKpr-su9-KATE2::KANMX*	This study
Mic10-3xHA	YPH499, Mic10-3xHA*::HIS3*	(Harner et
Mic60-3xHA	YPH499, *Mic60-3xHA::KanMX*	(Harner et

2.1.8.2 Transformation of yeast cells

Required yeast cell strains were inoculated in 5 mL of YPD media overnight at 30°C, 140 RPM. The next day, 20 mL of YPD media were inoculated with overnight culture to OD_{600} ≃0.2 and incubated at 30°C for 4-5 hours. Cells from 1.5 mL of this culture were harvested by centrifugation at 11,000 g for 1 min at RT. Cells were resuspended in 100 µL of 0.1 M lithium acetate and harvested by centrifugation at 11,000g for 1 min at RT. Then 200 µL of 40% (w/v) PolyEthylene Glycol 6,000 (PEG), 32 µL of 1 M lithium acetate were added and the mixture was vortex for 30-60 seconds. After adding 50 µg of denatured salmon sperm DNA, cells were vortexed for 30 seconds. For transformation of yeast cells with plasmid DNA, 1-2 µg of plasmid DNA and for homologous recombination, 5 µL of PCR product were added to the cell suspension and

vortexed for 30 seconds. After incubation for 40 min at 30 ° C with mild shaking, a heat shock for 20 mins at 42 ° C followed. The transformed cells were then harvested by centrifugation at 2,500 xg for 5 mins at RT. The cell pellet was resuspended in 1 mL of YPD medium and incubated for 1 hour at 30°C with shaking. Cells were harvested by centrifugation at 2,500 xg for 5 mins at RT and resuspended again in 1 mL of sterile water. After centrifugation of cells at 2,500 xg for 5 mins at RT, the pellet was finally resuspended in 100 µL sterile water, spread out on a plate with the appropriate selection marker, and incubated at 30°C.

2.1.9 Genetic manipulation of *S. cerevisiae*

2.1.9.1 Deletion of genes from genome

The deletion of genes was carried out via homologous recombination of the His3 or Leu2 gene from *Saccharomyces Pombe* or insertion of geneticin resistance gene (*KanMx*) in the corresponding loci (Janke et al., 2004; Longtine et al., 1998). The deletion cassette was amplified using the PCR method. The plasmid pFA6a-His3MX6, pIZZA 73-LEU2, and pFA6a-kanMX6, served as templates. The primers used are composed of the 45 nucleic acids upstream of the start codon or the 45 nucleic acids after the stop codon of the respective open reading frames and a plasmid-specific sequence. After purification, the amplified DNA fragment was transformed into the YPH499 wild type strain. The selection was carried out using synthetic medium without Histidine or Leucine or YPD plates supplemented with 200 µM of Geneticin (G418).

2.1.9.2 Overview of the primers used for the deletion of genes

YPL109c KO s

5`-AACCCTCACAGAATAGAGATAAAGAACATCAGAACCATCTGGGCACGGATCCCCGGGTTAATTAA-3’

YPL109c KO as

5`-CACGTGGAAGTCGCAATTATAAAAGATGCATAAAAAGAAAGAATAATCGATGAATTCGAGCTCG-3’

Primer *PSD1*-KO s

5’-TTCTTGGTCGTTATTTTTTGAAGAAGAAGGAAAAGCAAAGCCAGCATGTCAATTCGGATCCCCGGGTTAATT-3’

Primer *PSD1*-KO/His/HA as

5`-TACTATATACAGCAAAATAAATGCTAACTTTACATATGATTGCTTATCGATGAATTCGAGC TCG-3’

Primer *CRD1*-KO_s

5`-ACAAGCAGGCCTGGTAGCATAGTTTGGTCCCTAATAATTTAGTCACGGATCCCCGGGTTA ATTAA-3’

Primer *CRD1*-KO/His/HA_as

5`-CAAAATGAAAAGTCAGGACCCTTTTCAAAAAGGATCGCAATTATAATCGATGAATTCGAG CTCG-3’

*TAM41*_KO_s

5`-TTGAATTAATAGGAGCTGCTTTTTACTTTGATATATCCTGAAGTTCGGATCCCCGGGTTAA TTAA-3’

*TAM41*_KO_as

5`-AAAACATTTTTGATAAAAGATAATGTGTAGATAACATTGGATACAATCGATGAATTCGAGC TCG-3’

*PGS1*_KO_s

5`-GCTTGTCCATAATTGCTAATAGCATACTCAGGATAACATATATTACGGATCCCCGGGTTA ATTAA-3’

*PGS1*_KO_as

5`-TTATTTTTCCATATTTACAGGCGACATACTATGATAGAATAGAATATCGATGAATTCGAGC TCG-3’

*GEP4*_KO_s

5`-AACTGAAAGGCGGCAGTTACATTACATCGTCTCCTCTACCTAGTCCGGATCCCCGGGTTA ATTAA-3’

*GEP4*_KO_as

5`-TATATAAAAAATTAAAATGTTTTACTTTTTATTAAAGTTGCCTAAATCGATGAATTCGAGCT CG-3’

*CLD1*_KO_s

5`-AAGGTACACTAATACTTATACTGATTAATAAGGGTTAGCCTTTTACGGATCCCCGGGTTA ATTAA-3’

CLD1 KO as

5`-ATGTAAAAATTTCGTTATATAATGTAGATGCACAAGATTTCTTCAATCGATGAATTCGAGC TCG-3'

MDM35 KO s

5`-TTTGTGTTTTAACTTGAATTACAATAACAATAATACCAGTTTTATCGGATCCCCGGGTTAA TTAA-3'

MDM35 KO as

5`-TATTTACATGTTGAATAATGCACATTCTGTGCTAAAATATATACTAATCGATGAATTCGAG CTCG-3'

MCP2 KO s

5`-GAGCAAGATTATAGTTGAATGTTTCTTATTCGGTGTTGATAGTAGCGGATCCCCGGGTTA ATTAA-3'

MCP2 KO as

5`-TATAATTTTACGTATATATTTACAAGTAGAAAGAACGCTAACGATATCGATGAATTCGAGC TCG-3'

2.1.9.3 Insertion of C-terminal tag into the chromosome

The insertions of chromosomal C-terminal protein tags were also carried out via homologous recombination. The respective tag was amplified by PCR together with a selection cassette. The plasmids pYM1 for 3xHA tags and pYM23 for 3xMyc tags were used as templates(Janke et al., 2004). The sense primers used are composed of the 45 nucleic acids upstream of the stop codon of the respective open reading frame and a plasmid-specific sequence. The corresponding deletion primers could be used as an antisense primer. The amplified DNA fragment was transformed into the YPH499 wild type strain. Transformed cells were plated on SCD-Trp plates or YPD plates supplemented with 200 M of Geneticin (G418), and single colonies of transformed strains were tested for expression of tagged proteins.

Overview of the primers used for the insertion of chromosomal C-terminal protein tags

YPL109cKO/his s

5'-CAAATATACGATCTTGTCAGGACTGATCAATTGTGTCCTAATTATCGTACGCTGCAGGTCG AC-3'

YPL109c KO as

5’-CACGTGGAAGTCGCAATTATAAAAGATGCATAAAAAGAAAGAATACGTACGCTGCAGGTC GAC-3’

OM14 tagging F

5’-GACGGTATAATTTCAAAGAAATACTACTCCAGATACGACAAGAAAATCGATGAATTCGAG CTCG-3’

OM14 tagging R

5’-TATAGAAACTTATCACTTGACCGATGAAGAGGAAAGCACGTTTCCATCGATGAATTCGAG CTCG-3’

POR1 tagging F

5’-TCTGAACCTGTTCACAAGCTAGGTTGGTCTTTGTCCTTCGACGCTCGTACGCTGCAGGTC GAC-3’

POR1 tagging R

5’-ACATATATGGTATATAGTGAACATATATATATTAGATATATACGTATCGATGAATTCGAGCT CG-3’

2.1.9.4 Insertion of Kate2 fluorophore in HO locus.

In order to visualize mitochondria for fluorescent microscopy, sequence of KATE2 fluorophore was inserted in HO locus of genome by homologous recombination. First 10 µg of pCO450 plasmid was digested by NotI restriction enzyme (NEB). Later, 5 µL of whole digested mixture were used for transformation.

2.2 Cell biology methods

2.2.1 Bacterial culture and *E. coli* growth for plasmid isolation

E. coli was grown in LB medium 5 g/L yeast extract, 10 g/L bacto-tryptone, 10 g/L NaCl supplemented with 100 µg/mL of ampicillin. LB medium was sterilized by autoclaving and ampicillin was added freshly before use. 5 mL of LB media was inoculated with single colony of *E. coli* and incubated at 30°C for 16 hours.

2.2.2 Cultivation of *S. cerevisiae* in liquid cultures

YPD media was inoculated with a single colony of respected yeast cell strain, and cells were grown overnight at 30°C with 160 RPM shaking. For Drop dilution assay on YPD plates, cultures were diluted with fresh YPD media when it is needed so that cells remained at exponential phase. In the case of drop dilution assay on plates with synthetic media and preparation of whole cell lysate, cultures were diluted in fresh SCD, and cells were kept at exponential phase for at least 24 hours in SCD media.

To isolate the crude mitochondria, 10 mL of YPD or SCD media was inoculated with a single colony of a respective strain and incubated at 30°C overnight with 160 RPM. The next day, cultures were diluted in 100 mL of YPG or SCG media. Cultures were diluted constantly in fresh YPG or SCG to keep cells at the exponential phase.

2.2.3 Preparation of glycerol stocks from *S. cerevisiae*

For the preparation of stocks of *S. cerevisiae*, cells from solid medium plates were mixed with 15% (v/v) glycerol in water and stored at -80°C.

2.2.4 Analysis of the growth phenotype of *S. cerevisiae*

To analyze the effects of genetic manipulations, the growth rates of the different mutants were determined. The growth phenotype was examined on agar plates. For this purpose, the strains of interest were cultivated in the liquid medium and kept in the exponential phase by repeated dilution. The number of cells corresponding to 0.5 OD_{600} were harvested, and the cell suspensions were diluted to the same cell density with sterile water. Starting from these suspensions, dilution series were prepared (1:10, 1: 100, 1: 1000, 1: 10,000). 7 µL of each of the dilutions were dropped on YPD plates or SCD plates. The growth of strains was evaluated after 2-3 days of incubation at 24°C, 30°C or 37°C.

2.2.5 Chemical competent *Escherichia coli* cells

500 mL of LB-medium was inoculated with 5 ml overnight-culture of *E. coli* and incubated at 37°C and 160 RPM to reach OD_{600} of 0.4. The Culture was incubated on ice for 15 mins and the bacteria were spun down at 2,000 ×g for 15 mins at 4°C. The pellet was resuspended in 40 mL of CaCl2-solution and after 30 mins on ice, the bacteria were harvested by centrifugation at 2,000×g for 15 mins at 4°C. After resuspending the pellet in 20 mL CaCl2-solution, 4 mL of 100% glycerol were added,

and the bacteria were incubated on ice for 2 hours. 200 µL aliquots of the suspension were snap-freeze in liquid nitrogen and subsequently stored at -80°C.

2.2.6 Preparation of whole cell lysate

An equivalent of 2.5 OD_{600} of cells was collected by centrifuging yeast cultures at 2,500 xg for 5 mins at RT. Cells were resuspended in 0.5 mL of dH_2O and transferred to a 1.5 mL tube. After harvesting cells by centrifuging at 2500 xg for 5 min at RT, they were resuspended in 100 µL of dH2O. 100 µL of 0.2 M NaOH was added to cell suspension and incubated at RT for 5 mins. Cells were harvested by centrifugation at 10,000 xg for 1 min at RT and were resuspended in 50 µL of 2X Laemmli buffer supplemented with 5% β-Mercaptoethanol. Cell suspensions were heated at 95°C for 5 min at 10,000 RPM.

2.2.7 Fast crude isolation of mitochondria

Adding a tag to a protein of interest might lead to instability of protein and consequently its proteolytic degradation or it might lead to mislocalisation of the tagged protein. Analyzing fast crude mitochondria of yeast cells allows testing expression and mitochondrial localization of tagged proteins at the same time. Therefore, fast crude mitochondria was analyzed to test expression and localization of tagged proteins in yeast cells. The yeast strain of interest and wild type strain were inoculated in 5 mL of YPD and incubated at 30°C overnight with 160 RPM. The day after, cultures were diluted with fresh YPGal media for 24 hours to keep cells in the logarithmic phase of their growth. An equivalent of 20 OD_{600} of Cells was harvested and washed with 1 mL of ice cold water. The cells were resuspended in 800 µL of SMK buffer supplemented with 1 mM of PMSF. 200 µL of glass beads were measured with PCR tubes and added to the cell suspension. Cells were lysed by vigorous vortexing of samples for 30 seconds interrupted by incubation on ice for 30 seconds which was repeated four times. Non-broken cells and cell debris were pelleted with centrifugation of samples at 2,000 xg for 5 mins at 4°C. The supernatant was transferred to a new 1.5 mL tube and mitochondria were pelleted by a centrifugation step at 20,000g for 10 min at 4°C. 200 µL of supernatant (cytosolic fraction) was transferred to a new tube and subjected to TCA precipitation. TCA precipitation of proteins was carried out by adding 50 µL of 72% trichloric acid (TCA) to 200 µL of supernatant and incubating at -80°C for 30 mins. The precipitated proteins were pelleted by centrifuging at 21,000 ×g for 15 mins at 4°C. Pellet was washed with 1 mL of ice cold acetone and centrifuged at 21,000 ×g for 15 min at 4°C. Pellet of crude mitochondria and cytosolic fraction were resuspended in 50 µL of 2x Laemmli buffer supplemented with β-mercaptoethanol

and incubated at 95°C for 10 mins. Cytosolic fraction and crude mitochondria fraction were analyzed by SDS-PAGE and western blotting.

2.2.8 Isolation of crude mitochondria

For isolation of crude mitochondria, yeast cells were cultured in YPG or SCG to final OD_{600} of 1.0-1.4 if not mentioned otherwise and harvested by centrifugation for 5 min at 2,000 ×g at RT. Cells were resuspended in 20 mL of dH2O and harvested by centrifugation at 2,500 xg for 5 mins at RT. The supernatant was discarded, and after measuring the wet weight of cell pellets, they were resuspended in 20 mL of DTT buffer and incubated at 30°C for 10 mins under mild agitation. Cells were reisolated by centrifugation at 2,000 xg for 5 mins at RT and were resuspended in 10 mL of Sphaeroplast buffer. Cells were reisolated by centrifugation at 2,500 xg for 5 min and resuspended in 6.6 mL/g of Sphaeroplast buffer. The yeast cell wall was digested by Zymolase treatment. To this end, 6 mg of Zymolase were added per gram of wet cells weight and incubated for 30-45 mins at 30°C under mild agitation. Formation of sphaeroplast can be controlled by measuring the reduction of OD_{600} of diluted sphaeroplast solution in sorbitol and comparing it to measurement of OD_{600} of sphaeroblast solution, which is diluted in dH2O. Bursting of sphaeroplast in dH2O due to osmotic pressure leads to reduction of OD_{600} measurement by 80-90%. Sphaeroplasts were harvested by centrifugation at 2,000g for 5 min at 4°C and washed twice with 15mL of ice cold Lysis buffer. Sphaeroplast were lysed in 15 mL of ice cold Lysis buffer by 30 times mild pipetting of samples with Pipetman P5000 (Gilson, Middleton, USA) and 1 cm cut off P5000 tips. Sphaeroplasts were pelleted by centrifugation at 2,000 ×g at 4°C for 5 min and the supernatant was transferred to a new cold 50 mL falcon tube. Harvested unbroken sphaeroplast were lysed one more time exactly like previous step. 30 mL of pooled supernatant were subjected to centrifugation at 2,000 ×g at 4°C for 5 mins to pellet the cell debris. Mitochondria were harvested by centrifugation of supernatant at 14,000 ×g at 4°C for 10 mins. Mitochondria were gently resuspended in 10 mL of ice cold SM buffer and subjected to centrifugation at 14,000 ×g at 4°C for 10 mins. The pelleted mitochondria were then resuspended in 1 mL SM buffer and the concentration was determined by Bradford Assay. They were stored in SM buffer in 500 µg aliquots at -20° until further use.

DTT Buffer:

10 mM Tris-HCl (pH not adjusted) and 10 mM DTT

Sphaeroplast buffer:

20 mM Tris-HCl pH 7.4, 1 mM EDTA 1.2 M sorbitol

Lysis Buffer:

20 mM MOPS- KOH pH 7.2, 1 mM EDTA, 0.6 M sorbitol, 0.2 % (w/v) BSA, 1 mM PMSF

SM Buffer:

20 mM MOPS- KOH pH 7.2, 0.6 M sorbitol

2.2.9 Fractionation of mitochondria

A modified protocol by Pon L. et al (Pon et al., 1989) was used to generate and separate vesicles consisting of pure the OM, the IM, and vesicles consisting of both membranes. 10 mg of Freshly Isolated mitochondria was resuspended in 1.6 mL of SM buffer. Mitochondria were swollen by dropwise adding 16 mL of Swelling buffer under mild stirring. Samples were incubated for 30 mins at 4°C under mild stirring. 5 mL of 2.5 M of sucrose were added to the samples to increase the sucrose concentration of samples to 0.55 M. Samples were incubated for 15 min at 4°C under mild stirring. Vesicles were generated by intermittent sonication at 10% amplitude for 30 seconds and repeated four times. Each sonication cycle was intermitted by 30 seconds of breaks while samples were kept cool on ice. The remaining intact mitochondria were separated from generated vesicles by centrifugation of samples at 20,000 ×g at 4°C for 20 mins. The supernatant containing vesicles was transferred to a new tube and 0.3 mL of 2.5 M sucrose was loaded at the bottom of the tube. Vesicles were concentrated on a 2.5 M sucrose cushion at the bottom of the column by centrifugation at 118,000 ×g at 4°C for 100 mins. Concentrated vesicles were harvested by discarding the top part (2/3 of column length) of column, and disc shape concentrated vesicles were transferred to an ice cold potter Dounce-homogeniser. The suspension was homogenized by ten strokes in Teflon potter. Sucrose concentrations of samples were measured by refractometer and were adjusted to 0.6 M. Samples were loaded on a sucrose step gradient column (0.8 M, 0.96 M, 1.02 M, 1.13 M, 1.25 M sucrose in 20 mM MOPS-KOH pH7.4 and 0.5 mM EDTA). Different types of vesicles were separated by centrifugation at 200,000 ×g at 4°C for 12 hours. The gradient was divided into 17 fractions in which proteins were subjected twice to TCA precipitation. The fractions were analyzed by SDS-PAGE, Western Blot, and immunodecoration.

SM-Buffer:

0,6 M Sorbitol, 20 mM MOPS pH 7,4

2.2.10 Determination of the topology of mitochondrial proteins by protease treatment (proteolytic susceptibility assay)

To determine topology of mitochondrial proteins, crude isolated mitochondria were subjected to theProteinase K (PK) in; intact, burst and lysed form. Hence, 50 µg of mitochondria were diluted 1:10 in ice-cold SM buffer, swelling buffer or lysis buffer and incubated on ice for 20 mins. Resuspension of mitochondria in SM buffer preserves the OM integrity of mitochondria due to lack of osmotic pressure. The osmotic shock caused by the incubation of mitochondria with Swelling-buffer leads to a swelling of the matrix space and therefore causes tearing of the outer membrane. Mitochondria with a destroyed outer membrane are called mitoplasts. In mitoplasts, the intermembrane space (IMS) is open and inner membrane proteins are accessible to proteinase K (PK). Incubation in lysis buffer leads to the destruction of the mitochondrial membrane envelope, which makes all mitochondrial proteins, including matrix proteins, accessible for PK. 100 µg of PK was added to intact mitochondria, mitoplasts, and lysed mitochondria. The proteolysis was completed after 30 mins incubation at 4°C, and it was stopped by adding 1 mM PMSF and incubation of 10 more mins at 4°C. After centrifugation for 20 min at 20,000 ×g at 4°C, the pellet was resuspended in 500 µL of ice cold SM buffer. In order to inactivate residual PK, the proteins were subjected to TCA precipitation. The precipitates were resuspended in 2x Laemmli buffer and analyzed by SDS-PAGE, Western blot, and immunodecoration.

SM-Buffer:

0,6 M Sorbitol, 20 mM MOPS pH 7,4

Swelling-Buffer:

20 mM MOPS pH 7,4

Lysis-Buffer:

0,1% (v/v) TritonX-100, 20 mM MOPS pH 7,4

2.2.11 Determination of the membrane association of mitochondrial proteins by alkaline extraction

The association of proteins with the mitochondrial membranes was examined by the alkaline extraction assay. For this purpose, 100 µg of isolated mitochondria were diluted with SM buffer to a concentration of 1 mg/ml. The same volume of a 200 mM sodium carbonate solution was added and the mixture was incubated on ice for 30 min.

To separate the membrane proteins from the soluble proteins, the samples were centrifuged for 30 min at 91,000 × g and 4°C. (TLA55 rotor; Beckman Optima MAX-XP ultracentrifuge). The supernatant was transferred to a new 1.5 mL tube and the proteins were subjected to TCA precipitation. The pellet of membrane proteins and the precipitated soluble proteins were resuspended in 2x Laemmli buffer supplemented with 5% β-Mercaptoethanol and incubated for 10 mins at 95 °C. Samples were analyzed by means of SDS-PAGE, Western blot and immunodecoration.

SM Buffer:

20 mM MOPS-KOH pH7.4, 0.6 Molar Sorbitol.

2.2.12 Electron microscopy

To analyze the mitochondrial ultrastructure of the deletion mutants generated in this work, cells of these strains were examined by electron microscopy. For electron microscopy, cells were grown to logarithmic phase in SC-Gal media with proper selection marker and prepared essentially as described previously (Bauer et al., 2001; Unger et al., 2017). Very briefly, cells were fixed by 2% glutaraldehyde. Afterward, the cell wall was digested by zymolyase. Lipid membrane were fixed and stained by potassium Ferrocyanide-reduced osmium tetroxide. Then, yeast cells were embedded in agarose and uranyl acetate was used to further enhance the contrast. The sample was then dehydrated with a graded ethanol series and infiltrated with Epon using propylene oxide as an intermediate solvent. Ultrathin 50nm sections were poststained for 20min with 2% uranyl acetate and for 3min in lead citrate. Samples were examined in a Zeiss CEM 902 (Carl Zeiss, Oberkochen, Germany) transmission electron microscope operated at 80 kV. Micrographs were taken using a 1350 × 1050-pixel Erlangshen ES500W CCD camera (Gatan, Peasanton, CA) and Digital Micrograph software (version 1.70.16). Electron microscopy analysis was performed by Dr. Till Klecker.

2.2.13 Fluorescent microscopy (Figure 15)

For visualizing mitochondria, mitochondrial presequence of subunit 9 of Fo-ATPase from *Neurospora crassa* was fused to Kate2 fluorophore (mKate2). Nucleotide sequence of Fusion mKate2 was inserted into HO locus of yeas genome. Yeast cells were inoculated in YPD media and grown overnight at 30°C. Cell cultures were diluted in SCD media the day after and were kept at the logarithmic phase for 24 hours. The amount of cells corresponding to OD_{600} of 1 were harvested by centrifugation. Cells were vortex for 1 min and then washed with 1mL of sterile 1x PBS. Cells were

harvested again by centrifugation at 2500 xg for 3 mins. Cell pellets were resuspended in 200 µL and immobilized on µ-slide (ibidi). Beforehand, the bottom of chambers of µ-slide (ibidi) were coated with 1 mg/ml of Concanavalin A. After immobilizing cells in chambers, cells were covered with 400 µL of SCD media. Microscopy was performed at 30°C on a Nikon Ti2-Eclipse microscope equipped with a CFI Apochromat TIRF 100x/1.49 NA Oil Objective and a TwinCam LS dual camera splitter attached to two Photometric Prime 95B 25 mm cameras.

2.3 Protein biochemistry methods

2.3.1 Protein detection and analysis

Bradford assay (Bradford, 1976) was performed to determine protein concentration in the solution by using the Bio-Rad protein assay following the manufacturer's instructions. The standard plot for Bradford assay with bovine IgG (Bio-Rad) was created to determine the concentrations. Protein samples used for concentration estimation were either used directly or were diluted 5-10 folds. 10 µL of sample (diluted or undiluted) was added to 1 mL of 1:5 diluted Bradford reagent (Bio-Rad). Samples were incubated at RT for 10 mins. Afterward, absorbance was measured at 595 nm wavelength and concentration was determined by comparison with the standard curve.

2.3.2 Tricholoricacid (TCA) precipitation of proteins

TCA precipitation of proteins was performed to increase the concentration of proteins. Proteins were precipitated by adding 72% (w/v) trichloroacetic acid (TCA) to a final concentration of 12% (w/v). After subsequent 4-min incubation at −80 ° C., the precipitated proteins were pelleted by centrifugation for 15 mins at 21,000 × g and 4°C. A washing step with 1 mL of ice-cold acetone followed to remove the lipids and TCA. The precipitate was dried completely, resuspended in Laemmli buffer, and incubated at 95 ° C. for 5-10 min.

2.3.3 SDS-polyacrylamide-electrophoresis

Analysis of protein samples based on their molecular weight was done by discontinuous SDS-PAGE (Laemmli, 1970). Glass plates measuring 160 x 180 mm and spacer with approximately 1 mm thickness were used to cast the gels. The space between glasses on one side was sealed with sealing gel. Various acrylamide concentrations had been used in the separating gel, depending on the required resolution, between 10% and

18% and the concentration of bisacrylamide between 0.08% and 0.13%. Proteins were dissolved in 2x Laemmli supplemented with 5% β-mercaptoethanol, heated up for 5 mins at 95°C, and applied on a SDS-gel. The electrophoresis was carried out at 35 mA for 1-2 hour. The proteins were then transferred to a nitrocellulose membrane.

Sealing gel:

1% agarose in 25 mM Tris-HCl pH8.8

Resolving gel:

10-18% acrylamide, 0.08-0.13% bis-acrylamide, 375 mM Tris-HCl pH 8.8, 0.1% SDS, 0.1% APS, 0.03% TEMED

Stacking gel:

5% acrylamide, 0.03% bis-acrylamide, 60 mM Tris-HCl pH 6.8, 0.1% SDS, 0.05% APS, 0.1% TEMED

SDS running buffer:

50 mM Tris-HCl pH 8.3, 0.38 M glycine, 0.1% SDS

SDS sample buffer (Laemmli buffer):

60 mM Tris-HCl, 2% SDS, 5% β-mercaptoethanol, 10% glycerol, 0.02% bromophenol blue, pH 6.8

2.3.4 Blue-native polyavrylamide-gelelectrophoresis (BN-PAGE)

BN-PAGE was performed to determine the size of protein complexes under native conditions. To this end, 150 µg of isolated mitochondria was first pelleted by centrifugation for 12 min at 17,000 xg and 4°C. The pellet was resuspended in 50 µL of Schägger's BN buffer supplemented with 3% digitonin and solubilized for 15 min at 4°C (Wittig et al., 2006). In order to remove large membrane fragments, a centrifugation step was carried out for 15 min at 14,000 ×g at 4°C. The sample preparation and the run of the blue native polyacrylamide gel electrophoresis were carried out according to the manufacturer's instructions (NativePAGE Novex Bis-Tris Gel System, Invitrogen). After the electrophoresis, the proteins were transferred to a PVDF membrane (Roth) by wet-Western Blot method (40V, 2 hours at 4°C.). The protein complexes were analyzed using immunodecoration.

BN buffer (Schägger's BN buffer):

50 mM NaCl, 50 mM imidazole-HCl, 2 mM 6-aminohexanoic acid, 1 mM EDTA, pH 7.0 (at 4°C)

2.3.5 Transfer of proteins to nitrocellulose membrane

Proteins separated by SDS-PAGE were transferred to nitrocellulose membranes by wet western blot transfer method. Here a sponge soaked in transfer buffer was placed on the anode side followed by a Whatman paper, a nitrocellulose membrane, SDS-PAGE gel, another Whataman paper and another sponge at the top. Air bubbles between the individual layers were removed with the aid of a roller. The protein transfer to the membrane was carried out at 4°C for 1.5 hours at 380 mA. After the transfer, the proteins were stained by Ponceau solution. Before starting the immunodecoration, the membrane was completely destained with TBST.

Ponceau solution:

0.2% (w/v) Ponceau S, 3% (w/v) TCA, pH not adjusted

2.3.6 Transfer of protein to PVDF membrane

Protein complexes separated by BN-PAGE were transferred to PVDF membranes by wet western blot transfer method. Before use, the PVDF membrane was activated for 1 min in 100% methanol and equilibrated for 5 min in 1x BN transfer buffer. In order to make the epitopes more accessible for antibodies, the gel was incubated for 5 min in SDS running buffer and then briefly washed in 1x BN transfer buffer. Whatman filter papers were also soaked with 1x BN transfer buffer for 30 mins. One Whatman filter paper was placed on three wet sponges on the anode electrode followed by the PVDF-membrane, the BN-gel, two another Whatman filter papers and the cathode electrode plate. Transfer was performed at 40 mA for 2 hours. All buffers and protein transfer was performed at 4°C. After protein transfer to the membrane, the proteins were fixed on the membrane for 15 mins with 8% acetic acid. The Coomassie-stained membrane was completely destained with 100% methanol. BN transfer buffer before starting the immunodecoration.

1x NuPAGE Transfer Buffer, Invitrogen

2.3.7 Chemical crosslinking

To study protein-protein interactions of Mco76 protein in intact mitochondria, disuccinimidyl glutarate (DSG) and m-maleimidobenzoyl-N-hydroxysuccinimide ester

(MBS) crosslinkers were used. To this end, isolated crude mitochondria were diluted in SI buffer in 100 µL to the concentration of 1 mg/mL. DSG and MBS from stock solution (40 mM in DMSO) were added to the samples to the final concentration of 400 µM and incubated at 4°C for 30 mins. The reaction was stopped by addition of glycine (1M, pH 8.8) to final concentration of 100 mM and incubation at 4°C for 10 mins. Mitochondria were reisolated by centrifugation at 17,000 xg for 10 mins. at 4°C. Supernatant was discarded and the pellet was resuspenden in 2x Laemmli buffer supplemented with 5% β-Mercaptoethanol and incubated at 95°C for 10 mins.

SI buffer:

50 mM HEPES-KOH, 0.6 M Sorbitol, 75 mM KCl, 10 mM Mg(Ac)2, 2 mM KH2PO4, 2.5 mM EDTA, 2.5 mM MnCl2, pH 7.2

2.3.8 Affinity purification of Por1-Om14 complex.

To test interaction of Mco76 with Por1 and Om14, Por1-Om14-Om45 complex has been isolated via immunopurification of Po1-3xHA or Om14-3xHA by anti-HA agarose beads. 4 mg of crude isolated mitochondria were resuspended in 2 mL of IP buffer supplemented with 1% digitonin and 1 mM PMSF. Solubilization of crude mitochondria took place for 15 mins at 4°C while samples were rotating. Cleared lysates were achieved by centrifugation of lysates for 10 mins at 12,000 xg at 4°C. 1-2.5 % of cleared lysates were transferred to new 1.5 mL tubes and subjected to TCA precipitation. The rest of cleared lysates were incubated with 100 µL (50% slurry) of equilibrated anti-HA agarose beads (sigma) for 2 hours at 4°C while samples were rotating. Anti-HA agarose beads were pelleted by centrifugation at 2,000 xg for 30 seconds at 4°C. 75 µL of supernatants were transferred to new 1.5 mL tubes and subjected to TCA precipitation. Rest of the supernatant was discarded and agarose beads were washed four times with 1mL of IP buffer supplemented with 0.1 % digitonin. After the last washing step, bound proteins to the anti-HA agarose beads were eluted with 30 µL of 3x Laemmli buffer and incubated at 95°C for 10 min with mild agitation. Precipitated proteins of clear lysate before and after incubation with agarose beads were resuspended in 2x Laemmli buffer and incubated at 95°C for 10 min with mild agitation. Elutes were separated from anti-HA agarose beads and transferred to new 1.5 mL tubes. β-Mercaptoethanol was added to all samples to the final concentration of 5% (V/V) and incubated at 95°C for 10 mins.

Immunoprecipitation buffer:

50 mM Tris-HCl pH 7.4, 50 mM NaCl

2.3.9 Affinity purification of Mco76-3xHA complex

1 mg of isolated crude mitochondria were resuspended in 1mL of IP buffer supplemented with 1% digitonin and 1mM PMSF. Solubilization of crude mitochondria took place for 15 mins at 4°C while samples were rotating. Cleared lysates were achieved by centrifugation of lysate for 10 mins at 12,000 xg at 4°C. 50 µL of cleared lysates were transferred to new 1.5 mL tubes and subjected to TCA precipitation (Total fraction). The rest of cleared lysate was incubated with 40 µL (50% slurry) of equilibrated anti-HA agarose beads (sigma) for 2 hours at 4°C while sample where rotating. Anti-HA agarose beads were pelleted by centrifugation at 2,000 xg for 30 seconds at 4°C. 50 µL of supernatants were transferred to new 1.5 mL tubes and subjected to TCA precipitation (Unbound fraction). The remaining supernatants were discarded and agarose beads were washed three times with 1mL of IP buffer supplemented with 0.1 % digitonin. After the last washing step, bound proteins to the anti-HA agarose beads were eluted with 30 µLof 3x Laemmli buffer supplemented with 5% β-Mercaptoethanol and incubated at 95°C for 10 min with mild agitation. Precipitated proteins of clear lysate before and after incubation with anti-HA agarose beads were resuspended in 2x Laemmli buffer 5% β-Mercaptoethanol and incubated at 95 for 10 min with mild agitation.

Immunoprecipitation buffer:

50 mM Tris-HCl pH 7.4, 50 mM NaCl

2.3.10 Affinity purification of Mic60-3xHA and Mic10-3xHA

To test the interaction of Mco76 with Mic60 and Mic10, immunopurification of Mic60-3xHA or Mic10-3xHA by anti-HA agarose beads were performed. 4 mg of crude isolated mitochondria were resuspended in 2 mL of IP buffer supplemented with 1% digitonin and 1 mM PMSF. Solubilization of crude mitochondria took place for 15 mins at 4°C while samples were rotating. Cleared lysates were achieved by centrifugation of lysates for 10 mins at 12,000 xg at 4°C. 2.5 % of cleared lysates were transferred to new 1.5 mL tubes and subjected to TCA precipitation. The rest of cleared lysates were incubated with 75 µL (50% slurry) of equilibrated anti-HA agarose beads (sigma) for 2 hours at 4°C while samples were rotating. Anti-HA agarose beads were pelleted by centrifugation at 2,000 xg for 30 seconds at 4°C. 75 µL of supernatants were transferred to new 1.5 mL tubes and subjected to TCA precipitation. The rest of supernatant was discarded and agarose beads were washed four times with 1mL of IP buffer supplemented with 0.1 % digitonin. After the last washing step, bound proteins

to the anti-HA agarose beads were eluted with 35 µL of 3x Laemmli buffer and incubated at 95°C for 10 min with mild agitation. Precipitated proteins of clear lysate before and after incubation with agarose beads were resuspended in 2x Laemmli buffer and incubated at 95°C for 10 min with mild agitation. Elutes were separated from anti-HA agarose beads and transferred to new 1.5 mL tubes. β-Mercaptoethanol was added to all samples to final concentration of 5% (V/V) and incubated at 95°C for 10 mins.

Immunoprecipitation Buffer:

50 KPBS pH 8.0, 50 mM NaCl

2.4 Immunological methods

2.4.1 Affinity purification of antibodies

Specific antibody was extracted from antisera by affinity purification to improve specificity and reduce unspecific binding of antibodies. For the affinity purification of antibodies, the respective antigen which has an extra cysteine at one terminus, was coupled to Sulfo-link Coupling Gel (Thermo Fisher Scientific). For this purpose, the first 1 mL of Sulfo-link Coupling Gel (Thermo Fisher Scientific) was packed in a column and equilibrated with 6 mL of coupling buffer. At the same time respective antigen was diluted in coupling buffer to the concentration of 1mg/mL. Diluted antibody was incubated with equilibrated matrix in the column for 45 mins at RT with gentle agitation. Afterward the column was held in a stand clamp to let the matrix sediment by gravitation force for 30 mins. The column was washed with 3 mL of coupling buffer to remove the unbound antigens. The column was incubated with blocking buffer for 45 mins at RT to block the free binding sites on the column. The flow through was discarded and the column was washed with 16 mL of 1 M NaCl solution. The column was washed with NaN3-buffer and then stored for future use at 4°C.

The antigen-coupled matrix was equilibrated by rinsing with 10 mL of wash buffer1 for antibody purification. Subsequently, to remove weakly bind antigen, the column was washed with 10 mL of buffer 1, elution buffer 2, wash buffer 2, elution buffer 3 and again with wash buffer 1. Then, 6 mL of the antiserum was mixed with 24 mL of washing buffer 1 containing 1 mM PMSF, and 1× Roche Complete Protease Inhibitor for antibody purification. The antiserum solution was added to the column using a peristaltic pump and the flow through was incubated with column for the second time. This was followed by two washing steps with 10 mL of washing buffer 1 and 10 mL of washing buffer 3. Finally, the antibody was eluted by adding 10 mL of elution buffer 1,

elution buffer 2 and at last elution buffer 3 sequentially. The eluate was collected in 1ml fractions in separate 1.5 mL tubes. The pH of each fraction was neutralized by adding 100 µL of neutralization buffer 1 for elution buffer 1 and 2 or neutralization buffer 2 for elution 3. The protein concentration of the individual fractions was determined according to Bradford assay. The fractions with a high protein content were examined for their antibody content by means of Western blot and immunodecoration. The fractions with a high concentration of the desired antibody were stored at -20 ° C. The column was then washed with 10 mL of washing buffer 1 and stored at 4°C. with 0.05% (w/v) sodium azide in 2 mL of the same buffer.

Coupling Buffer:

50mM Tris, 5mM EDTA; pH 8.5

Block Buffer:

50 mM cysteine, 50 mM Tris, 5 mM EDTA; pH 8.5

Wash Buffer 1:

10 mM Tris / HCl; pH 7.5

Wash Buffer 2:

10 mM Tris / base; pH 8.8

Wash Buffer 3:

500 mM NaCl, 10 mM Tris / HCl; pH 7.5

Elution Buffer 1:

100 mM sodium citrate; pH 4.0

Elution Buffer 2:

100 mM glycine / HCl; pH 2.5

Elution Buffer 3:

100mM Na3PO4; pH 11.5

Neutralization Buffer 1:

1 M Tris / base; pH 8.8

Neutralization Buffer 2:

1 M glycine / HCl; pH 2.5

2.4.2 Immunodecoration of proteins with specific antibodies

For antibodies obtained from rabbit plasma, the following protocol was typically used. After the protein transfer to the nitrocellulose or PVDF membranes, the unspecific binding sites that were still free were saturated by incubation in blocking solution for 1-2 h at RT. The proteins were then decorated with specific antisera or affinity-purified antibodies for approximately 3 h at RT or overnight at 4°C. Depending on the affinity of antibodies for the antigens, these were diluted between 1:250 and 1: 5,000 in blocking solution. Three washing steps (10 min in TBST) was followed by incubation for 1-2 hour at RT with a second antibody (Goat Anti Rabbit-IgG Horseradish Peroxidase (Bio-Rad), Goat Anti Rabbit-IgG Alexa Fluor Plus 680 (invitrogen), Goat Anti Rabbit-IgG Alexa Fluor Plus 800 (Invitrogen), Goat Anti Mouse-IgG Alexa Fluor Plus 800 (Invitrogen)) which anti-immunoglobulin G from Rabbit was targeted. This was diluted 1:10,000 in block solution. The membranes were then washed three times as described above. The bound secondary antibodies were finally detected via a Licor Odyssey imager or the peroxidase using chemiluminescence. The reaction taking place for chemiluminescence was started by adding the solutions ECL1 and ECL2. The two solutions were mixed in a ratio of 1:1 just before use. The signals were detected by exposing the membranes to X-ray films (Fuji).

Blocking Buffer:

10 mM Tris-HCl; 150 mM sodium chloride; pH 7.5 with 5% (w/v) milk powder.

Washing Buffer:

10 mM Tris-HCl; 150 mM sodium chloride; pH 7.5

2.4.3 Immunodetection of proteins with purchased antibodies

Purchased antibodies were used to decorate triple HA tags and triple Myc tags (anti-HA, Santacruz; anti-Myc, Santacruz). These antibodies were used according to the manufacturer's instructions.

2.5 Lipid analysis

Lipidomics analyses were performed as described in (Papagiannidis et al., 2021). Aliquots corresponding to 1500-2000 pmol total lipid were subjected to acidic Bligh and Dyer extractions, except for CL and MLCL which were extracted using MTBE

(Matyash et al., 2008). Acidic Bligh and Dyer extractions were performed in the presence of internal lipid standards from a master mix containing 40 pmol d7-PC mix (15:0/18:1-d7, Avanti Polar Lipids), 25 pmol PI (17:0/20:4, Avanti Polar Lipids), 25 pmol PE and 15 pmol PS (14:1/14:1, 20:1/20:1, 22:1/22:1, semi-synthesized as described in Özbalci et al, 2013), 20 pmol PA (PA 17:0/20:4, Avanti Polar Lipids) and 5 pmol PG (14:1/14:1, 20:1/20:1, 22:1/22:1, semi-synthesized as described in Özbalci et al (Özbalci et al., 2013). Lipids recovered in the organic extraction phase were evaporated by a gentle stream of nitrogen. Prior to measurements, lipid extracts were dissolved in 10 mM ammonium acetate in methanol, diluted 1:10 and transferred into Eppendorf twin.tec 96-well plates. Mass spectrometric measurements were performed in positive ion mode on an AB SCIEX QTRAP 6500+ mass spectrometer equipped with chip-based (HD-D ESI Chip, Advion Biosciences) nano-electrospray infusion and ionization (Triversa Nanomate, Advion Biosciences) as described (Özbalci et al, 2013). The following precursor ion scanning (PREC) and neutral loss scanning (NL) modes were used for the measurement of the various lipid classes: +PREC 184 (PC), +NL141 (PE), +NL185 (PS), +NL277 (PI), +NL189 (PG), +NL115 (PA). Mass spectrometry settings: Resolution: unit, low mass configuration; data accumulation: 400 MCA; curtain gas: 20; Interface heater temperature: 60; CAD: medium. Data evaluation was done using LipidView (Sciex) and ShinyLipids, a software developed in house. For MS analysis of CL and MLCL, lipids were extracted by MTBE extraction as described in (Matyash et al., 2008) and further processing of sampels was performed as described in (Chowdhury et al., 2018). Lipid extracts were dried under a gentle nitrogen stream. Dried lipids were re-dissolved in 40% UPLC solvent B (90% 2 propanol/10% acetonitrile /0.1% formic acid/ 10 mM NH4HCO2) and transferred to silanized glass inserts (Phenomenex) using Hamilton syringes. The glass inserts were placed in Eppendorf tubes and centrifuged in an Eppendorf centrifuge at 9000 rpm for 1.5 minutes. Lipid samples were then subjected to UPLC-ESI-MS/MS analysis performed on an Ultimate® 3000 LC system (Dionex, Thermo Fisher Scientific) coupled to a Q Exactive Hybrid Quadrupole-Orbitrap instrument (Thermo Scientific). For LC separations, a ACQITY UPLC CSH C18 1.7µm, 1.0 x 150 mm column (Waters) was used. The column oven temperature was set to 55°C, the temperature of the autosampler was set to 20°C. The flow rate used was 100 µL/min. The solvent composition used was as follows: 60% acetonitrile/40% H2O/0.1% formic acid/10 mM NH4HCO2 (solvent A), 90% 2 propanol/10% acetonitrile /0.1% formic acid/ 10 mM NH4HCO2 (solvent B). The starting solvent composition was 40% solvent B/60% solvent A. The conditions of the gradient were as follows: 3 min: 50% solvent B, 9 min: 54% solvent B, 9.1 min: 70% solvent B, 17-22 min: 90% solvent B and 22.5-30 min: 40% solvent B. The MS analyses were performed in the negative ion mode. The

following ESI source parameters were used: sheath gas flow rate: 4 (a.u.), auxilliary gas flow rate: 0, sweep gas flow rate: 0, spray voltage: 4 kV, capillary temperature: 320°C, S lens RF level: 50. Full-MS scans were recorded using the following parameters: FWHM peaks: 15 s, resolution: 140,000 (at m/z 200) AGC-target: 1e6, maximum IT: 200 ms, scan range: m/z 500-2000. Data evaluation was performed using MassMap.

2.6 Media

2.6.1 *E. coli* Media

LB Media:

10g/L Bacto-Tryptone, 5g/L yeast extract, 10g/L sodium chloride

LB/AMP medium:

Autoclaved LB medium with 100µg/ml ampicillin

LB plates:

LB medium; 1.5% (w/v) agar For LBAmp plates, 100 µg / mL Ampicillin added

TBS buffer:

10 mM Tris / HCl; 150 mM sodium chloride; pH 7.5

TE bufer:

10 mM Tris/HCl 1 mM EDTA; pH 8,0

2.6.2 *S. cerevisiae* media

Synthetic medium (SC medium): 1.7 g/L Yeast Nitrogen Base without amino acids and ammonium sulfate; 5 g/L ammonium sulfate; 2g/L Drop out mix with 2% (w/v) glucose (SD) or 3% (w/v) glycerol (SCG) or 2% galactose (w/v).

Auxotrophic marker:

Adenine 20 mg/L; Uracil 20 mg/L; Histidine 30 mg/L; Leucine 30 mg/L; Lysine 30 mg/L; Methionine 30 mg/L; Tryptophan 30 mg/L.

Drop Out Mix (C):

L-Alanine (2.5 mM), L-Arginine (2.5 mM), L-Asparagine (2.5 mM), L-Aspartic acid (2.5mM), L-Cysteine (2.5 mM), L-Glutamine (2.5 mM), L-Glutamic acid (2.5 mM), L-Glycine (2.5 mM), L-Methionine (2.5 mM), L-Isoleucine (2.5 mM), L-Phenylalanine (2.5 mM), L-Proline (2.5 mM), L-Serin (2.5 mM), L-Threonine (2.5 mM), L-Tyrosine (2.5 mM), L-Valin (2.5 mM), Myo-Inositol (2.5 mM), 4-Aminobenzoic acid (PABA) (2.5 mM)

YP medium: 1% (w/v) yeast extract; 2% (w/v) bacto-peptone; pH adjusted to 5.5 with HCl Glucose was autoclaved separately as 40% (w/v) concentrated stock solutions and added to the autoclaved YP medium (YPD) or glycerol was autoclaved separately as 30% (w/v) concentrated stock solutions and added to autoclaved YP medium (YPG).

YPD-G418:

YPD medium with 500µg/ml Geneticin (G418).

2.7 Chemical reagents and equipments

2.7.1 Chemicals

All chemicals not listed in the chart below are provided by Merck, Darmstadt, GER

Manufacturers	**Chemicals**
Agfa-Gevaert, Germany	Developer, fixer for X-ray films
AMSBIO, England	Zymolyase 20T
AppliChem, Germany	Ampicillin, DTT, APS, H_2O_2, skimmed milk powder
Beckton Dickenson, Germany	Bacto tryptone
Bio-Rad Laboratories, Germany	Protein standard and reagents for protein determination, horseradish peroxidase-coupled Anti-rabbit and anti-mouse antibodies,
Carl Roth, Germany	Hygromycin B- solution, Roti®-PVDF-Membrane, Sucrose,
Fuji, Germany	Medical X-ray film Super RX 13 x 18 cm
GE Healthcare, Germany	Amarsham nitrocellulosese membrane, NHS-activated Sepharose 4 Fast Flow

Greiner bio-one, Austria	15- and 50-mL reaction vessels, Reaction vessels,
Invitrogen, Germany	DH5α, Goat Anti Rabbit-IgG Alexa Fluor Plus 680, Goat Anti Rabbit-IgG Alexa Fluor Plus 800, Goat Anti Mouse-IgG Alexa Fluor Plus 800, NativePAGE 5% G-250 Sample Additive, NativePAGE Sample Buffer, NativePAGE 4-16% Bis-Tris Gel, NativePAGE 3-12% Bis-Tris Gel, NativePAGE Cathode Buffer Additive (20x), NuPAGE Transfer Buffer (20x),
Metabion, Germany	Oligonucleotides
Macherey-Nagel, Germany	Blotting paper, RNA, DNA, and protein purification products
New England BioLabs, USA	DNA ladder 1 kb, DNA ladder 100 bp, restriction endonucleases and 10 × buffer for restriction endonucleases, Taq DNA polymerase, deoxynucleoside triphosphates (dNTPs), T4 DNA ligase and associated 10 x buffer, Phusion High-Fidelity DNA Polymeras
Promega, germany	Pure Yield Plasmid Mini Prep System
R&D Systems, UK	pYX242 vector
Roche Applied Sciences, Germany	Proteinase K, Protease Inhibitor Complete, EDTA-free
Santa Cruze, USA	HA Probe (7-a) mouse monoclonal IgG, c-Myc Mouse monoclonal IgG,
Serva, Germany	Acrylamid, Agar-Agar, Agarose, BSA Grade VIII (fatty acid free), PMSF, Yeast extract, Ponceau S, TEMED, HEPES,
Sigma, Germany	Amino Acids, Anti-HA agarose conjugate, Ammonium nitrate, ß-mercaptoethanol, DMSO , Ethanol, Glycerol, PEG 8,000, Spermidine (N-[3-aminopropyl]-1,4-butanediamine), Triton X-100, Tween20, Yeast Nitrogen Base
Thermo Fisher Scientific, USA	Page ruler plus prestained protein ladder, Unstained protein MW marker, Sulfo-link Coupling Gel

2.7.2 equipment

Equipment	**Manufacturers**
Autoclave Systec DX-150, D1167	Systec GmbH, Wettenberg, GER
Table top centrifuge 5424 R	Eppendorf, Hamburg, GER
Table top centrifuge 5424	Eppendorf, Hamburg, GER
Centrifuge multifuge X3R	Thermo Fisher Scientific GmbH, Ulm, GER
Centrifuge Optima Max Ultracentrifuge	Beckman Instruments, München, GER
Centrifuge Optima XPN-100 ultra	Beckman Instruments, München, GER
Developer machine AGFA Gevamatic 60	Agfa-Gevaert, Munich, GER
Erlenmeyer flask	Carl Roth, Gremany
Freezer -20	Liebherr, Ochsenhausen, GER
Freezer -80 TSX series	Thermo Fisher Scientific GmbH, Ulm, GER
Gas burner Fireboy eco 50/60 Hz, 5 W	Integra Biosciences AG, Wallisellen, CH
Gelelectrophoresis chamber PEGLAB	PEQLAB Biotechnologie GmbH, Erlangen, GER
Glass-teflon homogenizer	Workshop, Institute for Physiological Chemistry, LMU Munich
Incubator innova 42	New Brunswick Scientific GmbH, Nürtingen, Germany
Incubator innova 44	New Brunswick Scientific GmbH, Nürtingen, Germany
Magnetic stirrer RCT basic	IKA-Werke GmbH, Stafen, Germany
Peristaltic pump P-1	Biochrom Ltd., Cambridge, GB
pH-Meter Five easy F20	Mettler Toledo, Giessen, Germany

Photometer OF600	Implen GmbH, Schatzbogen, München
Photometer biophotometer plus	Eppendorf, Hamburg, GER
Pipettes	Gilson, Inc., Middleton, WI, USA
Pipet tips	STARLAB GmbH, Hamburg, Germayn
Power supply EPS 600	Pharmecia biotech
Power supply PEGLAB	PEQLAB Biotechnologie GmbH, Erlangen, GER
Pure water plant Milli-Q M	Merck, Darmstadt, GER.
Cuvettes semi-micro	Greiner Bio-One, Kremsmünster, Austria
Reaction tubes	Greiner Bio-One, Kremsmünster, Austria
Rotor TX1000	Thermo Fisher Scientific GmbH, Ulm,
Rotor FA-45-24-11	Eppendorf, Hamburg, GER
Rotor SW41Ti	Beckman Instruments, München, GER
Rotor TLS 55i	Beckman Instruments, München, GER
blotting chamber	Workshop, Institute for Physiological Chemistry, LMU Munich
Digital Sonifier W-250 D	Branson Ultrasonics, Brookfield, USA
Sterile Bench B Max Pro 190	Berner International GmbH, Elmshorn, Germany
Table shaker Thermomix comfort	Eppendorf, Hamburg, GER
Thermo cycler S1000	Bio-Rad Laboratories, Feldkirchen, Germany
Vortex Mixer Genie 2	Scientific industries, New York, USA
Weighing machine UPL 7231	VWR International GmbH, Darmstadt, Germany

3. Results

3.1 Mco76 is present in the inner mitochondrial membrane.

YPL109C has been named *MCO76* due to its predicted molecular weight and its mitochondrial localization in *S. cerevisiae* (Morgenstern et al., 2017). *MCO76* and its human homolog ADCK2 are not well characterized so far. To fully understand the topology of Mco76, it was necessary to find out how many transmembrane domains Mco76 has. To predict hydrophobic regions of Mco76, a query has been made by the amino acid sequence of Mco76 in DAS TM-segment prediction server (https://tmdas.bioinfo.se/DAS/index.html). Analysis of Mco76 amino acid sequence by DAS TM-segment prediction server showed that it contains two potential hydrophobic regions, one close to its N-terminus (125aa-142aa) and the other one close to its C-terminus (573 aa -582aa) (Figure 3.1A, B, C). Additionally, *In silico* analysis by Mitofates, revealed that Mco76 has an potential N-terminal mitochondrial targeting sequence (amino acid 1-7) with a mitochondrial protein peptidase (MPP) cleavage site at amino acid 14(Figure 3.1 C) (Fukasawa et al., 2015).

At the beginning of this work, whole cells lysates were prepared from yeast wild type cells and deletion *Δmco76* strain cells which subjected to SDS-PAGE and immunodecoration. Immunodecoration against the endogenous Mco76 revealed that Mco76 has a molecular mass of approximately 60 kDa which is substantially smaller than the predicted molecular mass of Mco76 (Figure 3.2 A).

Submitochondrial localization of a protein can provide a potential hint into its function. To analyze submitochondrial localization of Mco76, mitochondria of yeast strain expressing Mco76-3×HA were subjected to proteolytic susceptibility assay (Figure 3.2 B). Immunodecoration of untreated mitochondria using a specific antibody against the HA-tag (α-HA) revealed a band with an apparent molecular mass of 63 KDa (Figure 3.2 B). First, intact mitochondria were treated with proteinase K which leads to degradation of the OM proteins like Tom70. However, subjecting intact mitochondria of cells expressing Mco76-3×HA to proteinase K indicates that Mco76 is not located in the OM. Second, Mitochondria were treated with hypotonic buffer to disrupt the OM and release of soluble proteins of IMS. Soluble proteins in IMS are not retained in mitochondria after disruption of the OM and reisoloation by centrifugation. Presence of Mco76-3xHA signal in the second lane (Figure 3.2 B) suggested that Mco76 is not a soluble protein of IMS. Third, Proteins of the IM such as Tim50 can be degraded by

proteinase K when the OM is disrupted. Finally, both membranes need to be lysed by treatment of mitochondria with detergents such as TritonX-100 (TX) to degrade proteins present in the matrix space. Immunodecoration against the HA-tag of Mco76-3xHA revealed that it behaves similarly as Tim50 indicating that it is present in the IM (Figure 3.2 B).

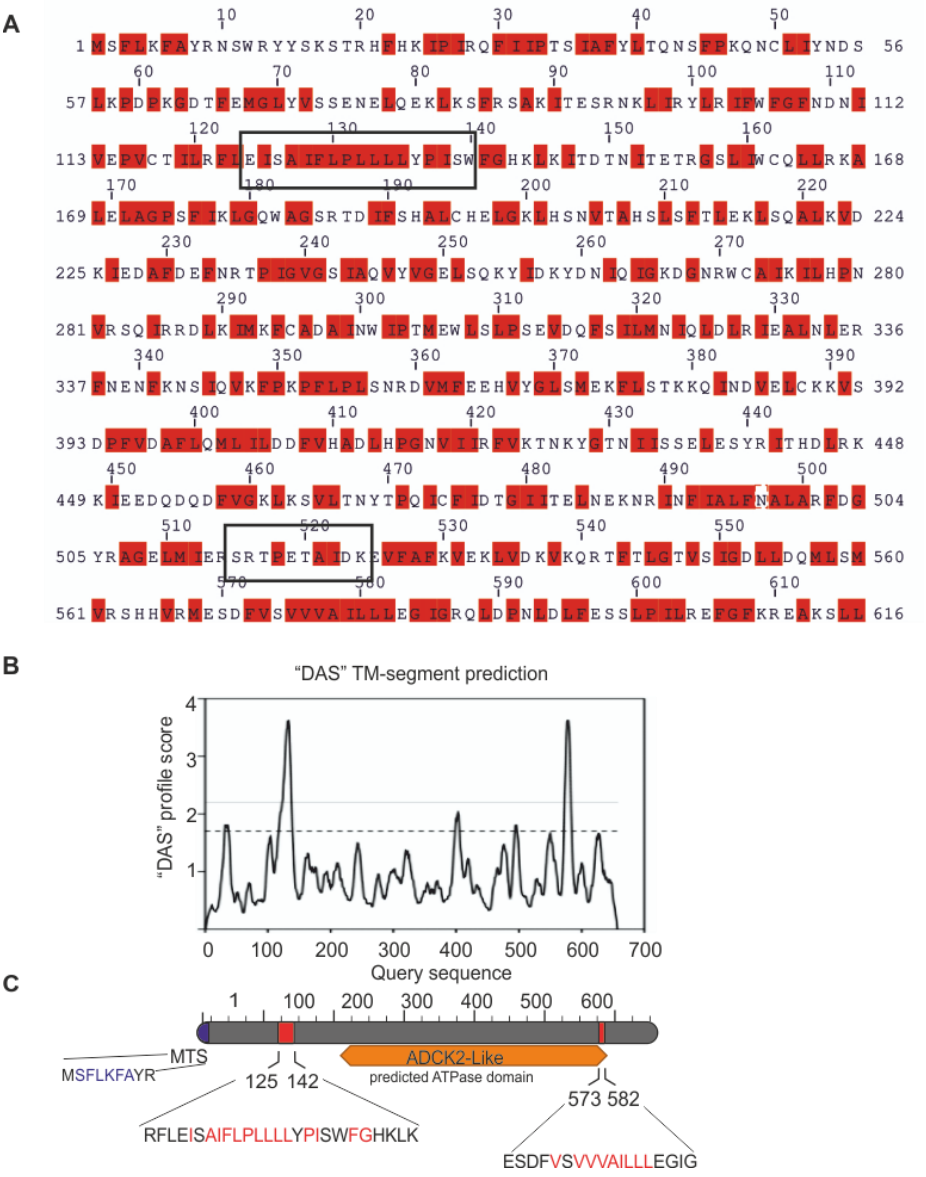

Figure 3.1 Hydrophobic regions of Mco76.

A)Amino acid sequence of Mco76. Hydrophobic amino acids were highlighted in red. Black boxes refer to predicted transmembrane domains by DAS prediction server.

B) Dense alignment surface (DAS) profile score of the amino acid sequence of Mco76. The Dashed line representing loose cut off and the solid line represents the stringent cut-off.

C)Schematic annotated domains of Mco76. The orange region of Mco76 shows the Aarf domain containing kinase 2 like protein domain (ADCK2-Like/ATPase) (amino acid 200 to 538). Red boxes indicate hydrophobic regions of Mco76.

Proteolytic susceptibility assay revealed the submitochondrial localization of the protein of Mco76. However, the result of proteolytic susceptibility assay cannot demonstrate whether Mco76 is peripherally attached to the IM or it spans the IM. The alkaline extraction assay was performed to examine whether Mco76 is a transmembrane protein (Fujiki et al., 1982). In this method, membrane vesicles are converted into membrane sheets uses alkaline pH. The soluble proteins inside vesicles and peripheral proteins associated with membranes are released into the supernatant fraction. Only integral transmembrane proteins remain associated with the membrane stay in the pellet. Mco76-3×HA was present predominantly in the pellet fraction (P) of the alkaline extraction assay, similarly to the transmembrane protein Tom70 and Tim50, while the soluble matrix protein, Hep1, accumulates in the supernatant fraction (S) (Figure 3.2 C). These results strongly suggest that Mco76 is embedded in the IM with its C-terminus is present in IMS (Figure 3.3 D).

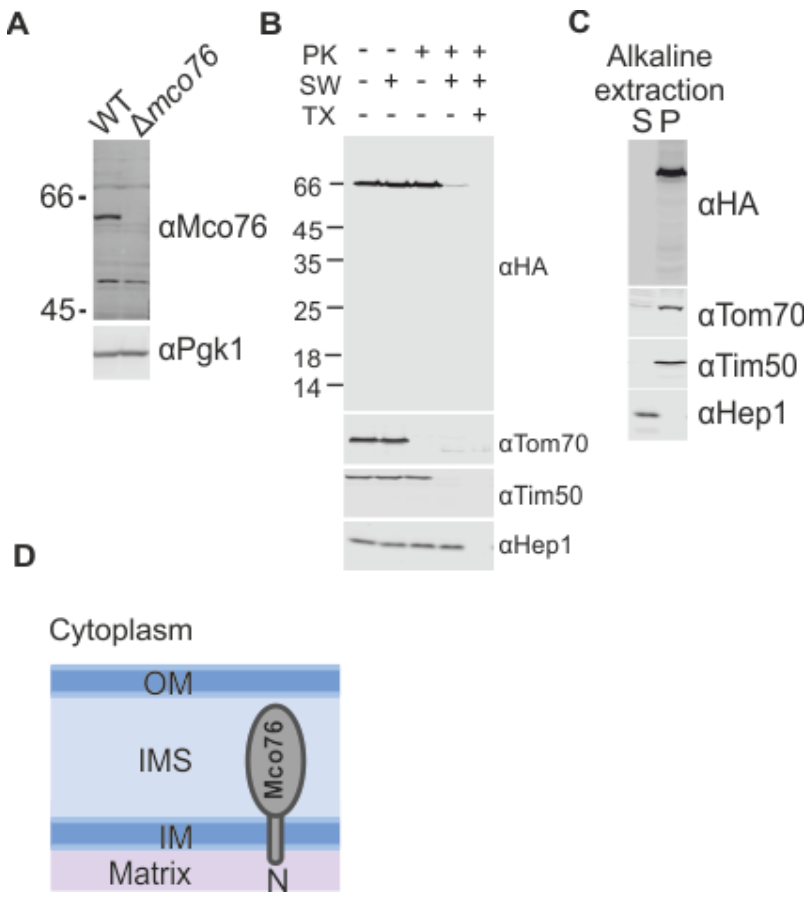

Figure 3.2 Mco76 is located in the inner membrane of mitochondria.

A) Mco76 has an apparent molecular weight of 60 kDa. Whole cell lysate prepared from wild type cells and deletion mutant Δ*mco76* cells.

B) Topological analysis of Mco76 by proteolytic susceptibility assay. Crude mitochondria of Mco76-3×HA expressing cells were isolated by differential centrifugation subjected to proteolytic susceptibility assay. First, mitochondria were left untreated. Then mitochondria were exposed to hypotonic media to disrupt the OM (SW). At last, mitochondria were lysed using a buffer containing 0.1% TritonX-100 (TX). Proteinase K (PK) was added as indicated. Samples were analyzed by SDS-PAGE and immunoblotting using the indicated antibodies.

C)Mitochondria were subjected to alkaline extraction to separate soluble and membrane proteins. After incubation in 100mM Na2CO3, membranes were spun down for 30 min at 145.000 xg. Proteins in the supernatant (S) were subjected to TCA precipitation and afterward resuspended in SDS sample buffer. The pellet (P) was directly resuspended in the SDS sample buffer. Samples were analyzed by SDS-PAGE and immunoblotting using the indicated antibodies.

D) Schematic presentation of the topology of Mco76 in mitochondria.

3.2 Mco76 is enriched in contact site fractions

To analyze submitochondrial localization of Mco76 more in detail, I performed the mitochondrial fractionation assay, a modified version of the assay that led to the identification of MICOS complex (Harner et al., 2011). In brief, mitochondria were isolated from a yeast strain expressing Mco76-3×HA. First, mitochondria were treated with hypertonic buffer followed by hypotonic buffer to separate the IBM from the OM (Figure 3.3). Afterward three different types of vesicles were generated by mild sonification (Figure 3.3).

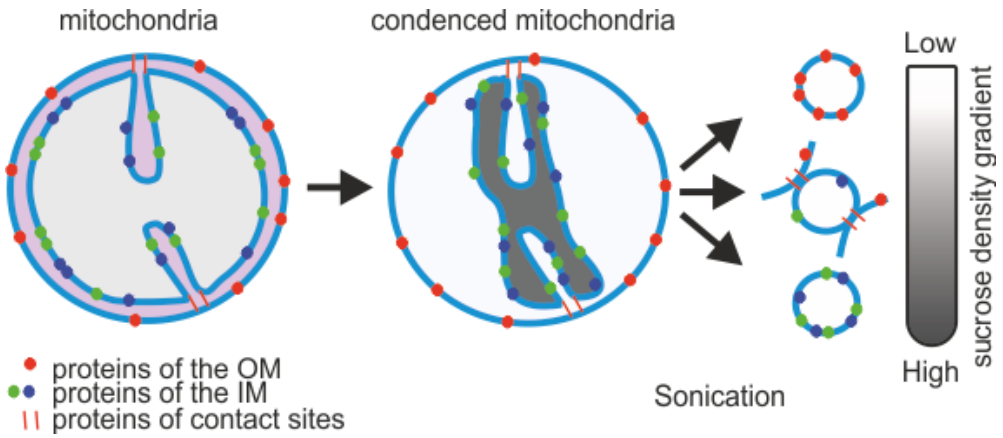

Figure 3.3 Schematic presentation of the mitochondrial fractionation assay.

The first type of vesicles consists of the OM, and the second type of vesicles consists of IM. But the third type of vesicles consists of both the OM and the IM of mitochondria

due to the presence of stable contact sites between the two membranes. As a result of the tremendous difference in protein to lipid ratio of the OM and the IM, the generated vesicles differ in their density. Hence, these different vesicles can be separated by density gradient ultracentrifugation (Figure 3.3).

The gradient was harvested in seventeen fractions, and proteins present in the various fractions were analyzed by SDS-PAGE and immunodecoration. To determine the separation of the OM proteins, the IM proteins, and the CS proteins, the distribution of the respective marker proteins Tom40 (OM), Tim17 (IM), and Mic27 (CS) were analyzed in different fractions (Figure 3.4 A). In addition, the relative abundance of Tom40, Tim17, Mic27, and Mco76-3×HA were calculated and plotted (Figure 3.4B). Immunodecoration against Tom40 revealed that top fractions (fraction numbers 3 to 6) are composed of proteins of the OM. Proteins of the IM represented by Tim17 are enriched at the bottom fraction (fraction numbers 17) and they are not present at top fractions (fraction numbers 3 to 6). This indicates the successful separation of OM and IM vesicles (Figure 3.4 B). Proteins in contact sites represented by Mic27 are enriched at intermediate density fractions and the most bottom fractions (fraction numbers 10 to 15). They are also clearly distinguishable from IM proteins (fraction 17) (Figure 3.4 B). Mco76-3xHA is mainly present in the middle density fractions and the most bottom fraction. Strikingly, this assay revealed that the distribution of Mco76-3xHA is similar to the relative abundance of Mic27 (Figure 3.4 B). It indicates that Mco76-3xHA is present at contact sites like Mic27, subunit of MICOS complex. Since Mco76 itself is anchored in the IM these results suggest that it might interact with proteins of the OM.

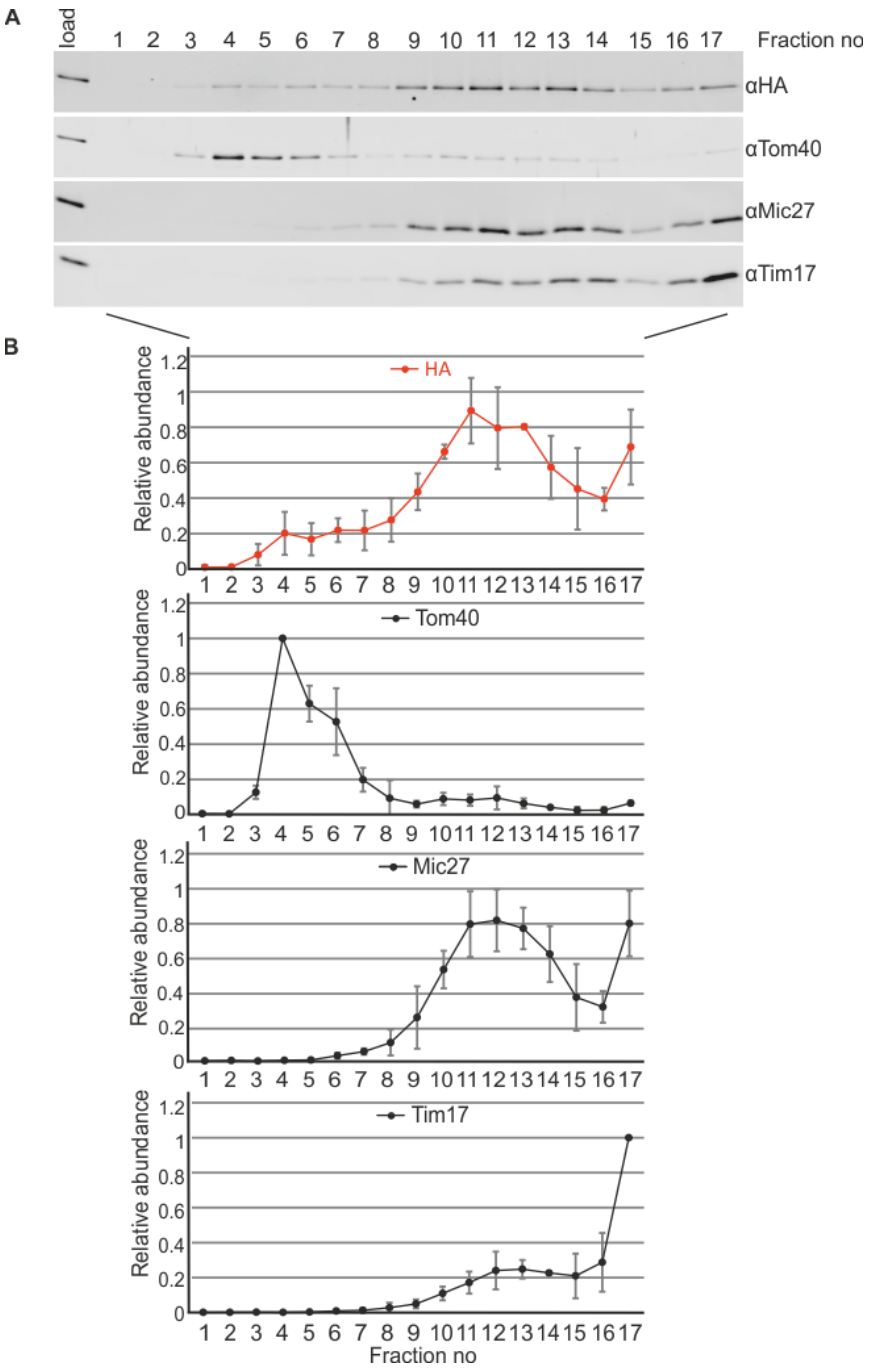

Figure 3.4 Mco76 is enriched in intermediate fractions.

A) Mitochondria of a Mco76-3xHA expressing strain were isolated, subjected to mitochondrial fractionation. The sucrose gradient was fractionated, the proteins in the fractions were subjected to TCA precipitation and analyzed by SDS-PAGE and immunoblotting using the indicated antibodies.

B) The graph shows mean values of the distribution of Mco76-3xHA and the marker proteins for the OM (Tom70), the IM (Tim17), CS (Mic27) of three independent experiments. To calculate the relative abundance of each protein among the fractions, first, the highest signal intensity of immunodecoration was determined for each protein. Then the signal intensity of each fraction for each protein was divided by the highest signal intensity of that specific protein. Error bars indicate standard deviation.

3.3 Mco76 forms a high molecular weight complex

Fractionation of mitochondria revealed that Mco76 was present at contact sites indicating it might form a high molecular weight protein complex like MICOS complex . Formation of the Mco76 containing protein complex was analyzed by native gel electrophoreses. Interestingly, BN-PAGE revealed that Mco76-3×HA is present in a protein complex of approximately 440 kDa. However, a small yet reproducible fraction is detectable at approximately 640 kDa (Figure 3.5 A). Since the composition of the Mco76 containing protein complex is unknown, first, a homotypic interaction of Mco76 was tested. To this end, a yeast strain expressing a 3xHA-tagged and a 3xMyc-tagged version of Mco76 simultaneously was generated. Isolated mitochondria of the generated yeast strain was subjected to immunoprecipitation assay using anti-HA agarose beads. Co-isolation of Mco76-3×Myc with Mco76-3×HA clearly shows that Mco76 interacts in a homotypic manner (Figure 3.5 B). The finding that Mco76 interacts with itself is interesting but the function of this homo-oligomer remains unclear so far. Additionally, whether this homotypic interaction is responsible for its presence at CS is still open.

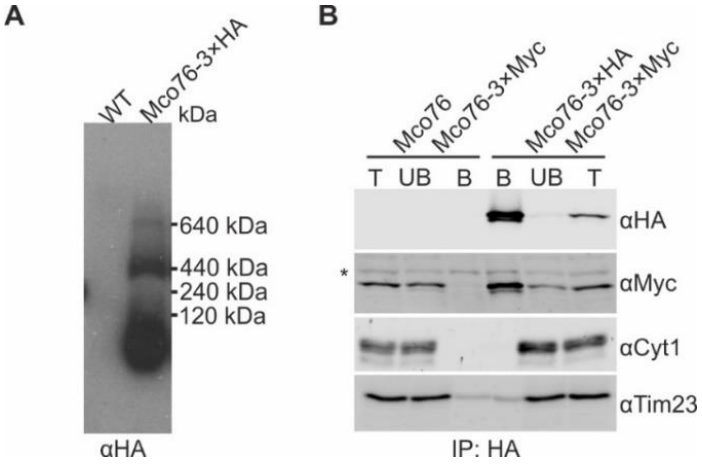

Figure 3.5 Mco76 forms a high molecular complex by homotypic interaction.

A) Mitochondria isolated from wild type yeast cells and a yeast strain expressing Mco76-3xHA were solubilized in a buffer containing 1% (w/v) digitonin. Cleared lysates were subjected to BN-PAGE analysis. Mco76-3xHA containing complexes were detected by immunoblotting with an anti-HA antibody.

B) Mitochondria of strains expressing Mco76-3xMyc in the presence of untagged or HA-tagged Mco76 were isolated. Digitonin (1%, w/v) lysed mitochondria were subjected to immunoprecipitation using anti HA affinity agarose. Bound proteins were eluted with SDS sample buffer. Total lysate (T; 5%), unbound protein (UB; 5%), and bound protein (B; 100%) were analyzed by SDS-PAGE and immunodecoration using the indicated antibodies. Asterisk indicates unspecific bands.

3.4 Mco76 does not interact with Mic10 and Mic60

Presence of Mco67 in intermediate fractions suggests that it might interact with other proteins that present in the intermediate fractions like subunits of MICOS complex such as Mic10 and Mic60. To test this idea, immunoprecipitation of Mco76-3×HA was performed. Therefore, crude isolated mitochondria of cells expressing Mco76-3×HA was lysed by Digitonin 1%(W/V), and the lysate was subjected to immunopurification using anti-HA agarose beads (Figure 3.5). Co-immunoprecipitations of Mic60 and Mic10 with Mco76-3×HA were analyzed by immunodecoration against Mic10 and Mic60 in the elution fraction (Figure 3.6 A). Analysis of interactions of Mco76 with Mic60 and Mic10 suggests that Mco76 does not interact with Mic10 and Mic60, indicating Mco76 is not a subunit of MICOS. However, it was still possible that interactions of Mco76 with Mic10 and Mic60 were disturbed due to the presence of HA tag on the c-terminus of Mco76.

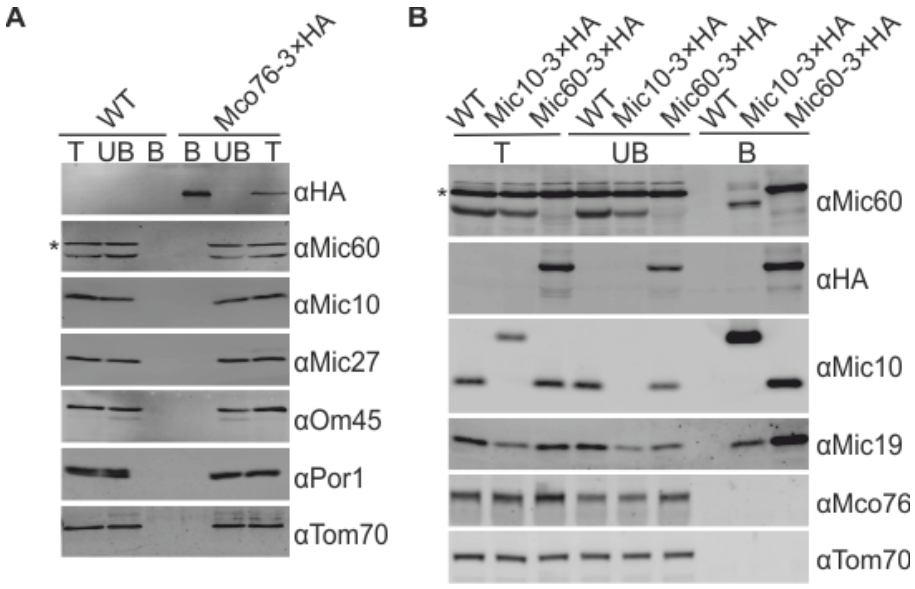

Figure 3.6 Mco76 does not interact with Mic10 and Mic60.

A)Mitochondria isolated from wild type yeast cells and a yeast strain expressing Mco76-3xHA were solubilized in a buffer containing 1% (w/v) digitonin. Lysed mitochondria were subjected to immunoprecipitation using anti HA affinity agarose. Bound proteins were eluted with SDS sample buffer. Total lysate (T; 2.5%), unbound protein (UB; 2.5%), and bound protein (B; 100%) were analyzed by SDS-PAGE and immunodecoration using the indicated antibodies.

B)Immunoprecipitation of Mic10-3×HA and Mic60-3×HA. Analysis as in Figure 3.6 **A**)

Therefore, immunoprecipitation of Mic60-3×HA and Mic10-3×HA were performed to investigate the co-precipitation of Mco76 with Mic60-3×HA and Mic60-3×HA. Crude isolated mitochondria of cells expressing Mic60-3×HA or Mic60-3×HA were lysed by Digitonin 1%(W/V), and lysate was subjected to immunopurification using anti HA-

agarose beads. Immune decoration against Mic19, Mic10, and Mic60 of elution fractions clearly showed that Mic60-3×HA and Mic60-3×HA were able to form interactions with other subunits of MICOS complex. However, immunodecoration against Mco76 of the elution fractions showed that Mco76 does not interact with Mic60-3×HA and Mic60-3×HA. This clearly suggests that Mco76 is not the subunit of the MICOS complex.

3.5 Mco76 interacts with additional proteins

Preceding results suggested that Mco76 forms a complex by homotypic interaction. However, the presence of Mco76 in intermediate fractions implies its interaction with OM proteins. Crosslinking experiments in intact mitochondria were performed to test whether Mco76 interacts with other proteins than itself. Isolated mitochondria of Mco76-3×HA expressing cells were subjected to cross-linker reagents, Di(N-succinimidyl) glutarate (DSG), and m-maleimidobenzoyl-N-hydroxysuccinimide ester (MBS). Chemical crosslinks containing Mco76 and unidentified proteins were analyzed by SDS-PAGE and immunodecoration against HA tag (Figure 3.7).

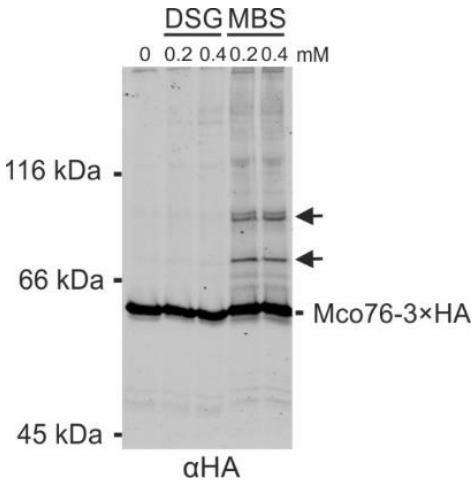

Figure 3.7 Mco76 interacts with several proteins.

Isolated mitochondria of a Mco76-3xHA expressing strain were exposed to DMSO only or the chemical crosslinkers DSG and MBS at the indicated concentrations. The reaction was stopped by the addition of an excess of glycine. Mitochondria were harvested and resuspended in the SDS sample buffer. Samples were analyzed by SDS-PAGE and immunoblotting with an anti-HA antibody. Arrows indicate to Mco76-3×HA containing crosslinks.

No Mco76 containing crosslinks were observable after incubation of mitochondria with DSG. However, in the presence of MBS, Mco76-3×HA appeared in two crosslinked species around 70 kD and 90 kD (Figure 3.7). These results indicated that Mco76 interacts with two proteins other than itself. Since Mco76 shows an apparent mass of

about 60kDa the interaction partners should be approximately 15 kDa and 35 kDa in size. Two abundant OM proteins with these approximate molecular masses are Porin and Om14. The question of whether Mco76 forms a complex with Porin and OM14 will be addressed in the following section.

3.6 Mco76 interacts with proteins of the OM, Om14 and Por1

The presence of Mco76 in intermediate fractions and interaction of Mco76 with small proteins, around 15 and 35 KDa, led us to investigate Mco76 interaction with small and abundant proteins of the OM. Om14 and Por1 are candidates that meet these criteria. To test this, co-immunoprecipitation of Om14-3×HA and Mco76 was performed. Therefore, crude isolated mitochondria of cells expressing Om14-3×HA were lysed by Digitonin 1%(W/V), and lysate were subjected to immunopurification using anti-HA agarose beads. Strikingly, Mco76 was successfully co-precipitated with OM14-3xHA (Figure 3.8 A). Evidently, the Mco76-Om14 complex forms a contact site between the IM and the OM.

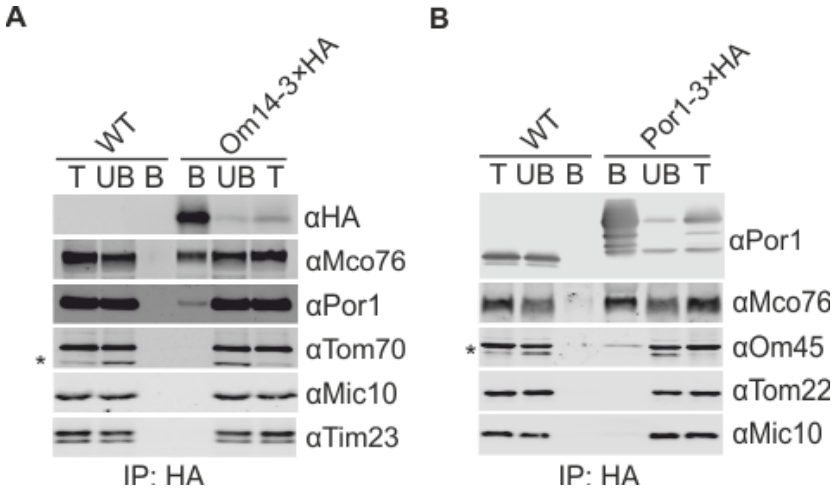

Figure 3.8 Mco76 forms a contact site by interacting with OM14 and Por1.

A) Mitochondria of wild type yeast and the yeast strain expressing OM14-3xHA were isolated and lysed in buffer containing 1% (w/v) digitonin. Lysed mitochondria were subjected to immunoprecipitation using anti HA affinity agarose. Bound protein was eluted with SDS sample buffer. Total lysate (T; 2.5%), unbound protein (UB; 2.5%), and bound protein (B; 100%) were analyzed by SDS-PAGE and immunodecoration using the indicated antibodies. Asterisk indicates unspecific bands.

B) Mitochondria of wild type yeast cells and a yeast strain expressing Por1-3xHA were isolated and lysed in buffer containing 1% (w/v) digitonin. Lysed mitochondria were subjected to immunoprecipitation using anti HA affinity agarose. Bound protein was eluted with SDS sample buffer. Total lysate (T; 1%), unbound protein (UB; 1%), and

bound protein (B; 100%) were analyzed by SDS-PAGE and immunodecoration using the indicated antibodies. Asterisk indicates unspecific bands.

Lauffer et al. have shown that Por1, Om14, and Om45 form a complex in the OM (Lauffer et al., 2012). So, I asked the question whether Mco76 interacts with Por1. To test this possibility a yeast strain expressing a 3×HA tagged version of Por1 was generated. Mitochondria were isolated from this strain, solubilized with Digitonin 1%(W/V), and subjected to immunopurification using anti-HA beads. Interestingly, Mco76 was also co-immunoprecipitated with Por1 (Figure 3.8 B). At last co-immunoprecipitation of Om45-3×HA with Mco76 was analyzed since it has been shown that Por1 and Om24 interact with Om45 (not shown in this thesis). However, tagging of Om45 with 3xHA led to degradation of Om45. Consequently, it was not possible to immunoprecipitate Om45. In conclusion, a novel contacts site between IM and OM of mitochondria composing of Mco76, Por1, Om45 and Om14 has been discovered in this study.

3.7 The Mco76 containing contact site is independent of MICOS complex

MICOS complex is essential for the formation of virtually all so far identified contact sites between the IM and the OM (Bohnert et al., 2012; Darshi et al., 2011; Harner et al., 2011; Modi et al., 2019; von der Malsburg et al., 2011; Xie et al., 2007; Zerbes et al., 2012). Upon deletion of *MIC60*, the core subunit of MICOS complex, MICOS complex dissociates, and CS which are formed by Mic60 are abolished. To investigate the possibility that CS containing Mco76 is formed independent of CS mediated by Mic60, I analyzed the interaction of Mco76 with Om14 in the absence of Mic60. To this end, a yeast strain was generated that lacked Mic60 while it expresses Om14-3×HA. Mitochondria from this strain were isolated, solubilized with digitonin and subjected to immunopurification. Remarkably, Mco76 and Por1 were co-immunoprecipitated with Om14-3×HA independent of the presence of Mic60 (Figure 3.9). This indicates that assembled MICOS is not necessary for forming of CS formed by Mco76, Por1, andOm14 complex. In conclusion, a novel contact site between the OM and the IM has been identified, which is composed of Mco76, Por1, Om45, and Om14. Strikingly, the formation of this CS is independent of the MICOS complex.

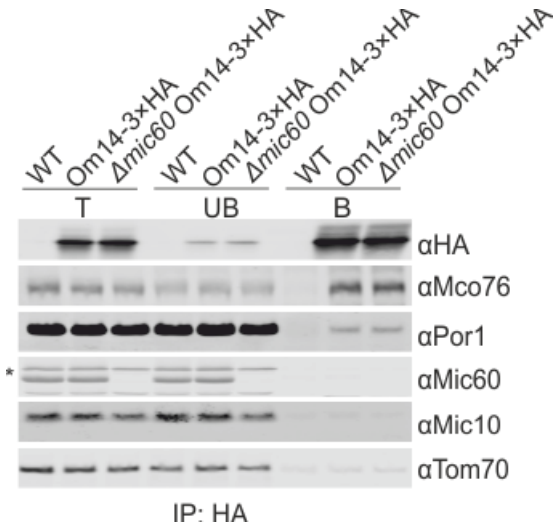

Figure 3.9 Interaction of Mco76 with Om14 is independent of Mic60 mediated contact sites.

Mitochondria of yeast strain WT, Om14-3×HA, and Δmic60 Om14-3×HA strains were lysed in buffer containing 1% (w/v) digitonin. Lysed mitochondria were subjected to immunoprecipitation using anti-HA affinity agarose. Bound proteins were eluted with SDS sample buffer. Total lysate (T; 1%), unbound protein (UB; 1%), and bound proteins (B; 100%) were analyzed by SDS-PAGE and immunodecoration using the indicated antibodies. Asterisk indicates unspecific bands.

3.8 Overexpression but not deletion of *MCO76* leads to defect in cell growth.

The analysis of the topology of Mco76 and the identification of its biochemical interactors revealed that Mco76 forms a CS between the IM and the OM. however, the function of Mco76 is unknown so far. In order to gain initial information of Mco76 function, the effect of the deletion and the overexpression of *MCO76* on cell growth was analyzed by drop dilution assays. Hence, *MCO76* was deleted by standard methods. The drop dilution assay was performed on rich plates containing fermentable or nonfermentable carbon sources to analyze the effect of depletion of Mco76. Interestingly, yeast cells lacking Mco76 did not show any growth defect, neither on fermentable nor on nonfermentable carbon sources, indicating that Mco76 is not directly involved in essential functions of mitochondria (Figure 3.10).

An overexpression strain of *MCO76* was generated by transforming the deletion strain Δmco76 with pYES2 plasmid bearing the *MCO76* coding sequence under the control of a Gal1 promoter. This allows the induction of gene expression through growth on galactose containing medium whereas it is repressed through growth on glucose

containing medium. Cell growth analysis of the *MCO76* overexpression strain was studied on synthetic medium containing glucose (SCD) or galactose (SCGal) in compared to wild type cells and cells of an *MCO76* deletion strain harboring the empty plasmid. Surprisingly, drop dilution assay revealed that growth of *MCO76* overexpression strain was impaired significantly in all tested temperatures (Figure 3.10). This indicates the high level of Mco76 in the mitochondria disturbs cell growth. However, how overexpression of *MCO76* affects the cell growth is not clear yet.

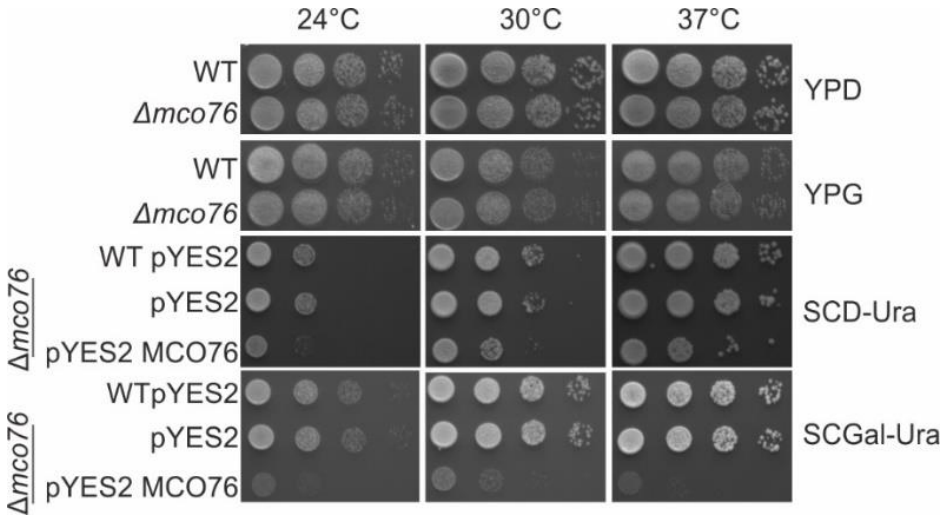

Figure 3.10 Overexpression but not deletion of *MCO76* leads to cell growth defect.

Growth analysis of wild type, *MCO76* deletion, and *MCO76* overexpression strains by drop dilution assay. Cells were grown On YPD media then the amount of cells corresponding to OD_{600} of 1 was harvested, washed, and resuspended in water. Cell suspensions were diluted 1:10 four times serially and spotted on indicated plates. To perform the drop dilution assay on plates with synthetic media, cells were shifted to SCD media for dropping on agar plates containing SCD and SCGal-Ura media for dropping on agar plates containing SCGal-Ura, 30 hours before harvesting.

3.9 Mitochondrial morphology and ultrastructure are altered in the *MCO76* overexpression strain.

Mic60, which forms CS between the OM and the IM, is critical for formation and maintenance of mitochondrial ultrastructure (Rabl et al., 2009). Interestingly, deletion and overexpression of *MIC60* alters the structure of the IM (Rabl et al., 2009). Interacting studies have shown that Mco76 forms a contact site between the IM and the OM. Therefore, I tested whether deletion or overexpression of *MCO76* alters mitochondria morphology or ultrastructure. Visualization of mitochondria in the *MCO76*

deletion and overexpression strains was achieved by using mtGFP. mtGFP is transported into the mitochondrial matrix by the addition of the Sue9 mitochondrial targeting sequence on its N-terminus. Fluorescence microscopy images of cells lacking Mco76 clearly showed that deletion of *MCO76* does not affect mitochondria morphology (Figure 3.11 A). However, *MCO76* overexpression leads to the formation of big mitochondrial aggregates (Figure 3.11 A). Quantitative analysis revealed that about 60% of cells with an elevated level of Mco76 contained mitochondrial with abnormal morphology (Figure 3.11 B). Since mitochondrial morphology and ultrastructure are intimately linked, electron microscopy (EM) was used to study this level of mitochondrial organization in cells lacking or overexpressing *MCO76*. Similar to previous observation by fluorescent microscopy, no changes in the ultrastructure of mitochondria have been observed in the deletion strain Δ*mco76*, cristae appeared normal in mitochondria of the cells lacking Mco76 (Figure 3.11 C). Intriguingly, the ultrastructure of mitochondria in cells overexpressing *MCO76* was altered dramatically. These cells harbored mitochondria that lacked cristae completely or had fewer number of cristae compare to the wild type cells or cells of the deletion strain Δ*mco76* (Figure 3.11 C). Furthermore, mitochondria appeared to be bigger in cells overexpressing *MCO76*, and aggregates of mitochondria are observable too. Altogether, fluorescence microscopy and electron microscopy results showed that both mitochondrial morphology and ultrastructure are drastically affected by overexpression of *MCO76* (Electron and fluorescence microscopy analysis were performed by Dr. Till Klecker and coworkers, University of Bayreuth).

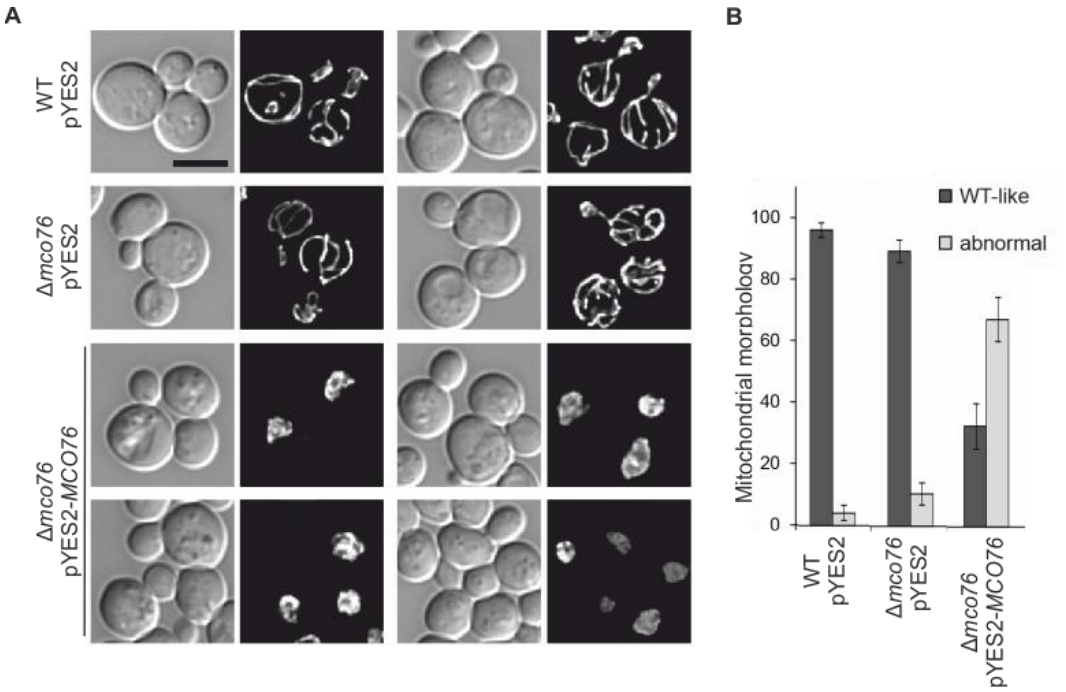

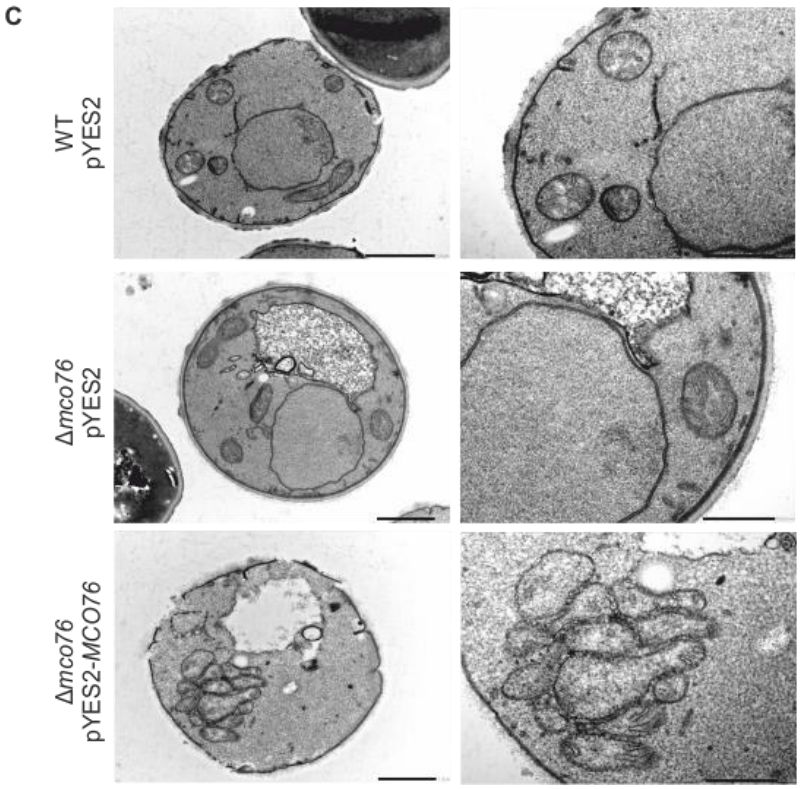

Figure 3.11 Mitochondrial ultrastructure is altered in the cells overexpressing *MCO76*.

A) Overexpression of *MCO76* disturbs the mitochondrial morphology. Mitochondria were visualized using mitochondrially targeted GFP. Cells were grown to log phase in SCGal-Ura and then examined by differential interference contrast and fluorescence microscopy. Size bar, 5 µm.

B) Quantification of the strains depicted in **A**. The average percentages of three independent experiments with at least 100 cells per experiment are shown. Error bars indicate standard deviation.

C) Effect of overexpression and deletion of *MCO76* on mitochondrial ultrastructure. Electron micrographs of mitochondria of wild type cells, cells overexpressing *MCO76*, or lacking Mco76. Cells were fixed with glutaraldehyde and sections contrasted with OsO4. Size bar, 100 nm. Electron and fluorescence microscopy analyses were performed in collaboration with Dr. Till Klecker.

3.10 Formation of mitochondrial protein complexes is affected by overexpression of *MCO76*

Mitochondrial proteincomplexes such as MICOS and F_1F_O-ATP synthase play essential roles in formation and maintenance of mitochondrial ultrastructure. So, changes in mitochondria ultrastructure in the cells overexpressing *MCO76* led us to test whether the formation of mitochondrial protein complexes like F_1F_O-ATP synthase complex and

MICOS are affected by overexpression of *MCO76*. To do so, Blue native page (BN-PAGE) using isolated mitochondria of wild type cells, cells lacking Mco76, and cells overexpressing *MCO76* was performed (Figure 3.12 A).

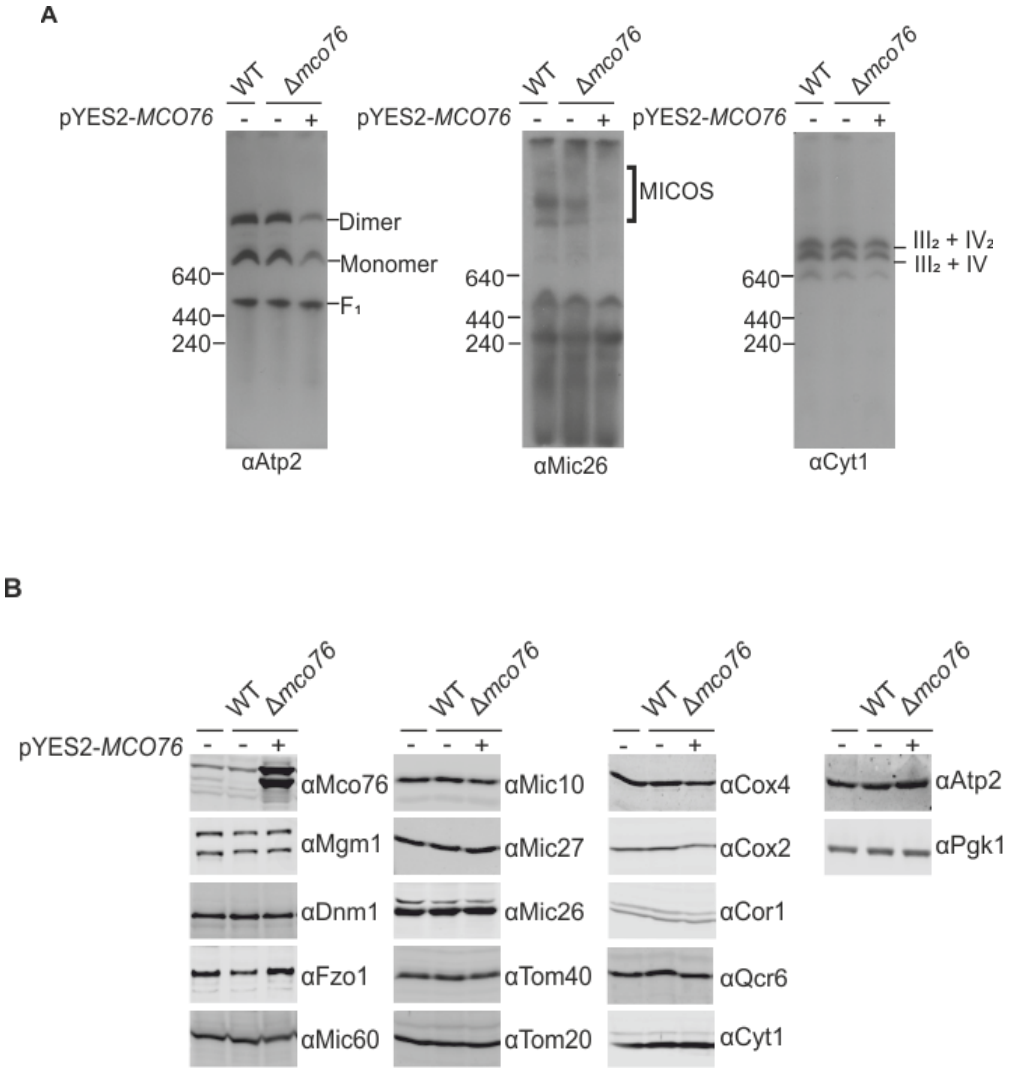

Figure 3.12 Formation of mitochondrial protein complexes is disturbed in the *MCO76* overexpression strain.

A)Assembly state of mitochondrial protein complexes. Yeast cells were grown in SCGal-Ura media. Isolated mitochondria (50µg or 150 µg) of the indicated strains were lysed in buffer containing digitonin (3% w/v), and cleared lysates were subjected to BN-PAGE. Assembly of F_1F_O ATP-synthase, respiratory chain supercomplexes, and the MICOS complex were analyzed by immunoblotting using antibodies against Atp2, Cyt1, and Mic26.

B) Effect of overexpression and deletion of *MCO76* on steady state levels of mitochondrial proteins. Wild type yeast cells and yeast cells in which *MCO76* was deleted or overexpressed were grown to log phase in the synthetic media containing galactose. Whole-cell extracts were prepared and samples were analyzed by SDS-PAGE, and immunodecoration using the indicated antibodies.

Immunoblotting revealed that F_1F_O-ATP synthase and MICOS complex are considerably reduced in *MCO76* overexpression strains, but respiratory super complexes were not affected by *MCO76* deletion or overexpression (Figure 3.12 A). These data are in line with the altered mitochondrial ultrastructure which was observed by EM. In addition, steady state levels of various mitochondrial proteins were analyzed in order to test whether reduction in the assembly of MICOS and F_1F_O-ATP synthase complexes were due to changes in steady state level mitochondrial proteins. Strikingly, it was found that steady state level of MICOS subunits such as Mic60, Mic27, Mic10 is not affected by deletion or overexpression of *MCO76* (Figure 3.12 B). Additionally, overexpression and deletion of *MCO76* do not affect the steady level of proteins that are involved in fusion and fission, such as Mgm1, Fzo1, and Dnm1 (Figure 3.12 B).

3.11 *MCO76* has negative genetic interaction with *UPS1* and *CRD1*.

Mco76 belongs to the UbiB protein family. Coq8 and Mcp2 are the other members of this protein family in *S. cerevisiae.* Coq8 is required for the maintenance of CoQ levels, and Mcp2 has been proposed to be involved in the mitochondrial phospholipid hemostasis. For instance, it has been shown that deletion of *MCP2* alleviates the growth phenotype of cells lacking Ups1(Odendall et al., 2019; Poon et al., 2000; Tan et al., 2013). Due to the similarity of Mcp2 and Mco76, genetic interactions of *MCO76* with genes of proteins that are involved in phospholipid metabolism of mitochondria were studied. The *MCO76* open reading frame has been deleted in different deletion mutant backgrounds such as *UPS1*, *CRD1*, *CLD1*, *TAZ1 GEP4*, *UPS2*, *MDM35*, *PSD1*, and *TAM41* in order to produce double mutant strains. Drop Dilution assay has been performed to analyze the growth of all mutant strains. Strikingly, growth analysis of double deletion strains revealed that deletion of *MCO76* from cells lacking Ups1 decreases the cell growth dramatically in synthetic media in all tested temperatures (Figure 3.13). Such growth defect phenotype has not been observed for the same double deletion strain in rich media. Additionally, it has been observed that the deletion of *MCO76* from mutant strain Δ*crd1* affects cell growth. However, this phenotype was only observed at higher temperatures (Figure 3.13). No further growth defects have been observed among the other double deletion mutant strains generated. Growth analysis of double deletion mutant *Δmco76Δups1* and *Δmco76Δcrd1* clearly shows that Mco76 is important for the function of mitochondria when Crd1 or Ups1 are depleted from the cells. This indicates that Mco76 might be involved in phospholipid homoeostasis of mitochondria like Mcp2.

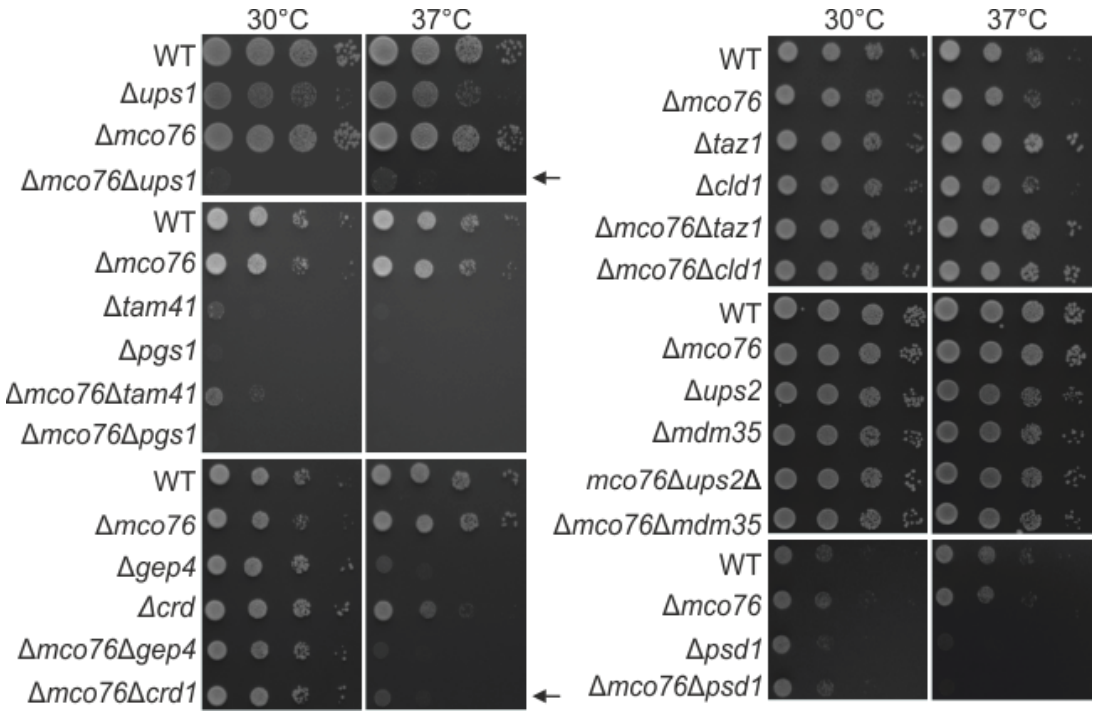

Figure 3.13 *MCO76* shows negative genetic interactions with *UPS1* and *CRD1*.

Growth analysis of yeast single and double deletion mutants. Yeast wild type cells, cells of the indicated single deletion mutants, and respective double deletion mutants were grown overnight on YPD at 30°C. Cells were shifted to the synthetic media containing glucose and cultured for a further 30h while keeping them at the logarithmic phase. Cells were harvested at the logarithmic phase and the growth was analyzed by drop dilution assay.

3.12 Conserved residue, Glutamic acid 330, in the predicted kinase domain of Mco76 is crucial for the function of Mco76.

Bioinformatics analysis of the UbiB protein family revealed an ATPase like domain (ADCK-like) (AA 230-AA590) (Leonard et al., 1998). Members of the UbiB protein family retain some conserved domains of the PKL super family, such as PKL II, IV, and V. However, the UbiB protein family contains some unique features that distinguish them from the other PKLs. However, structural analysis of Coq8 and ADCK3 by Stefely et al. showed that Coq8 and ADCK2 do not retain kinase activity (Stefely et al., 2015).

Previous studies showed that three conserved residues of Mcp2 K210, D222, and E256 are vital for its function(Odendall et al., 2019). Protein sequence alignment of Mcp2 and Mco76 reveals the three corresponding residues in Mco76 are K275, D288, and E330. These residues are present in the conserved motives of the ADCK-like (ATPase) domain. In addition, these three residues are highly conserved in this protein family

throughout evolution (Figure 3.14 A). Therefore residues, K275, D288, and E330 were mutated to alanine to test whether they are essential for the function of Mco76. To assess the importance of these residues for the function of Mco76, I analyzed the ability of mutated versions of Mco76 to the restore growth defect of double deletion strain *Δmco76Δups1.* To this end, cells lacking both Mco76 and Ups1 were transformed with plasmids expressing wild type Mco76, Mco76 K275A, Mco76 D288A, and Mco76 E330A under its endogenous promoter to have the protein expression close to wild type proteins levels.

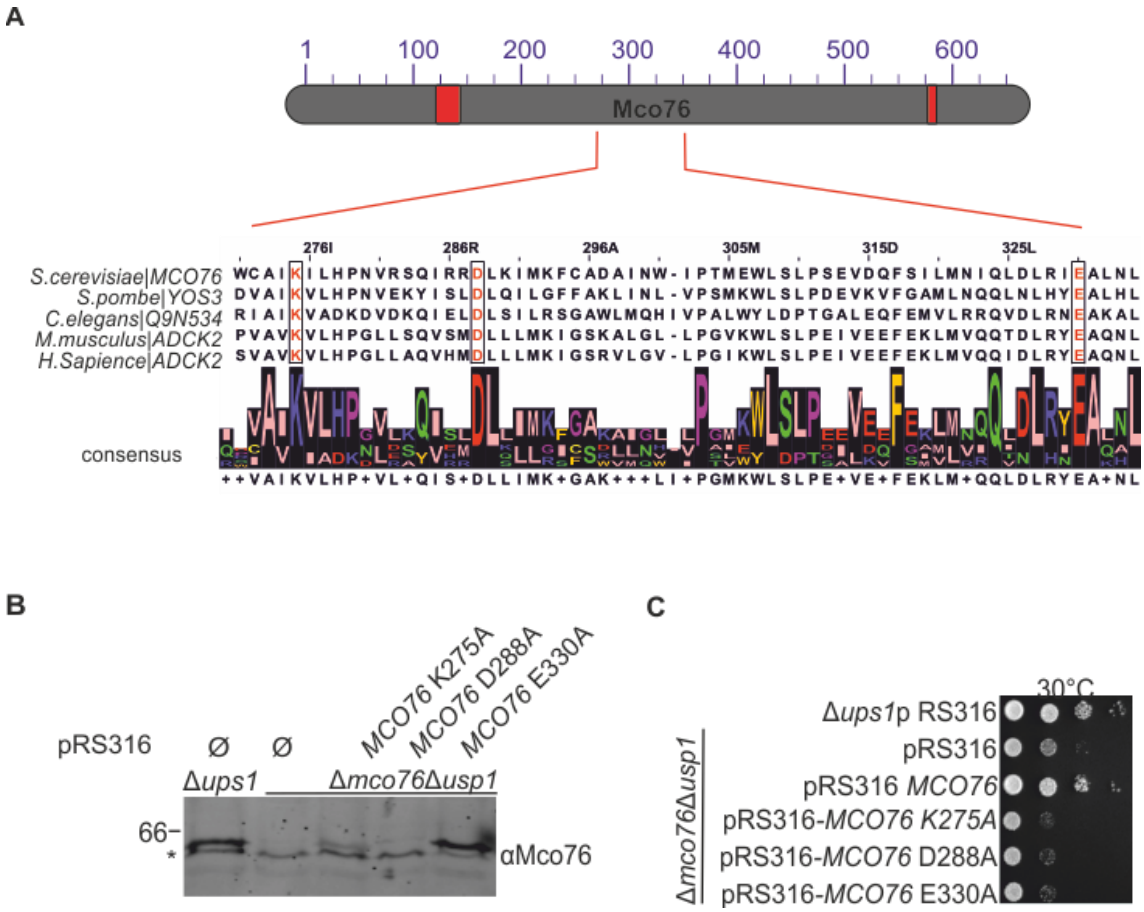

Figure 3.14 Glutamic acid 330, a conserved residue in the annotated kinase domain of Mco76 is crucial for its function.

A)Mco76 protein of *S. cerevisiae* was used as a query to search the available databases for homologs. The alignment shows a fragment of Mco76 and its homologs in different species. Mutated residues are squared and in red color.

B) Expression of wild type and mutant *MCO76* were analyzed by immunoblotting against Mco76.

C) Growth analysis of double deletion mutant Δ*mco76*Δ*ups1* expressing Mco76 and its mutated version. Asterisk indicates unspecific bands.

Since the insertion of point mutations in *MCO76* could lead to reduced protein expression or stability, the steady state levels of Mco76 in the various strains were analyzed. Therefore, crude mitochondria were isolated from cells expressing wild type and mutant versions of Mco76 and subjected to SDS-PAGE and immunoblotting. These analyses revealed that the steady state level of Mco76 D288A, as well as Mco76 K275A, were drastically below the level of the wild type protein (Figure 3.14 B). This indicates that residues D288 and K275 are essential for the stability of Mco76 in mitochondria. However, Mco76 E330A was present at similar levels as of the endogenous Mco76 allowing the desired functional comparison (Figure 3.14 B). Functional analysis of mutated versions of Mco76 has been achieved by testing the ability of mutated Mco76 in rescuing growth defect of double deletion Δ*mco76*Δ*ups1* strain. Expression of wild type *MCO76* in double deletion mutant Δ*mco76*Δ*ups1* is able to restore the growth defect of double deletion Δ*mco76*Δ*ups1* strain (Figure 3.14 C). However, Mco76 D330A does not restore the growth defect indicating the importance of this residue for the function of Mco76 (Figure 3.14 C).

3.13 Depletion of Ups1 and Mco76 leads to disturbed mitochondrial function.

Negative genetic interactions of *MCO76* with *UPS1* and *CRD1* led us to test whether mitochondrial functions of double deletion mutant Δ*mco76*Δ*ups1* are disturbed. It has been previously reported that defects in mitochondrial function can cause accumulation of Mdj1 precursor in the cytosol. Besides, it has been observed that the ratio of s-Mgm1 to l-Mgm1 isoforms is changed upon disruption of mitochondrial function (Osman et al., 2009; Sesaki et al., 2006). For instance, deletion of *PSD1* or *CRD1* leads to a change in the ratio of s-Mgm1 to l-Mgm1 isoforms by a dramatic reduction of PE and CL, respectively (Sesaki et al., 2006). Therefore, analysis of the proteins can reveal initial information on the shape of mitochondria. Thus, the accumulation of precursor of Mdj1 and ratio of s-Mgm1 to l-Mgm1 isoforms were analyzed by SDS-PAGE and Immunoblotting in wild type, Δ*mco76*, Δ*ups1*, and Δ*mco76Δups1* cells. Immunodecoration by specific antibodies against Mdj1 demonstrated that Mdj1 precursor accumulates in *Δups1* cells (Figure 3.15 A). Remarkably, the accumulation of Mdj1 precursor elevated significantly in *Δmco76Δups1* cells. It was shown previously that deletion of *UPS1* leads to a reduction in the ratio of Mgm1 short to long isoforms when cells are grown in fermenting media(Sesaki et al., 2006). I also observed that the ratio of Mgm1 short to long isoforms was decreased in *Δups1* cells. Strikingly, the reduction of Mgm1 short to long isoforms ratio is enhanced dramatically in

Δmco76Δups1 cells (Figure 3.15 B). These results indicate that mitochondrial function has been compromised in the double deletion *Δmco76Δups1* strain.

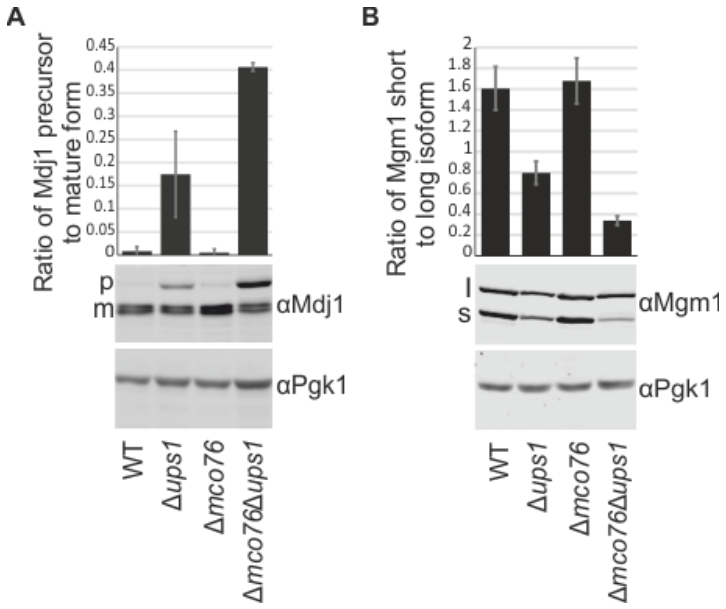

Figure 3.15 Deletion of *MCO76* aggravates the ratio of s-Mgm1 to l-Mgm1 isoforms and accumulation of precursor of Mdj1.

A)Changes in accumulation of Mdj1 precursor are demonstrated as the ratio of the signal of precursor to the total signal of mature and precursor of Mdj1 (m/m+p). Whole cell lysate was prepared from wild type cells and different mutant strains grown on SCD media. Cells were harvested in their logarithmic growth phase. Immunodecoration was performed by a specific antibody against Mdj1. Signal intensities were normalized to intensities of Pgk1 signal in wild type cells. P. precursor, M. Mature.

B) Proteolytic processing of Mgm1 is demonstrated as the ratio of short form to long isoforms of Mgm1. Immunodecoration was performed by specific antibody against Mgm1. Signal intensities are normalized to the signal intensity of Pgk1 in wild type cells. The signal intensity of the short isoform of Mgm1 was divided by the signal intensity of the long isoform of Mgm1. Error bars indicate the standard deviation of three independent experiments. Whole cell lysate was prepared similar to **A**.

3.14 Cells lacking Mco76 and Ups1 show altered mitochondria morphology.

Mitochondrial morphology is an intricate network regulated by fusion and fission machinery. It has been reported previously that deletion of *UPS1* leads to altered mitochondrial morphology (Osman et al., 2009; Sesaki et al., 2006). Based on the growth analysis of double deletion mutant *Δmco76Δups1* and the altered ratio of s-Mgm1 to l-Mgm1 isoforms, I hypothesized that the deletion of *MCO76* from cells lacking Ups1 affects the mitochondria morphology. To test this hypothesis, the morphology of

mitochondria in double deletion *Δmco76Δups1* cells was studied by fluorescence microscopy. Mitochondria were visualized by mKate2 fused to Su9(1–69), the mitochondrial presequence of subunit 9 of the F_1F_O-ATPase of Neurospora Crassa, under control of PGK1 promoter. Analysis of mitochondrial morphology by fluorescence microscopy revealed that wild type and Δmco76 show a tubular network of mitochondria in approximately 90% of cells (Figure 3.16). Previously, Sesaki et al. showed that deletion of *UPS1* decreases the number of cells having a tubular mitochondrial network (Sesaki et al., 2006). Consistently, I also observed that deletion of *UPS1* increases the percentage of cells harboring non-tubular network of mitochondria up to 42%. Interestingly, disruption of mitochondria morphology was enhanced when *MCO76* was deleted from cells lacking Ups1. 95% cells of double deletion mutant harbored non-tubular network of mitochondria (Figure 3.16). This result evidently supports the idea that Mco76 affects the mitochondria morphology while Ups1 is absent in the cell.

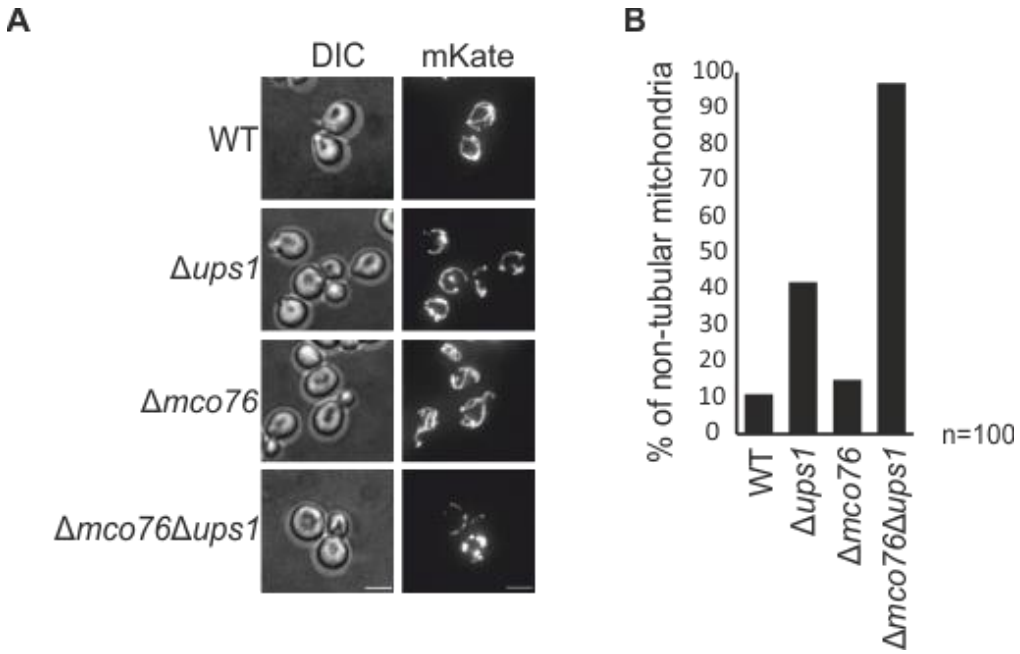

Figure 3.16 Deletion of *MCO76* affects mitochondrial morphology when Ups1 is depleted.

A) Mitochondria were visualized using mitochondria-targeted mKate (Su9-mKAte). Cells were growing YPD and then shifted to synthetic media containing glucose. Cells were harvested in their logarithmic growth phase and immobilized on slides covered with ConA. Fluorescence images of cells expressing Sue9-mKate of the indicated strains. Scale bar 4µ.

B) Quantification of the strains depicted in A. The percentages of non-tubular mitochondria were counted from 100 cells for each strain.

3.15 Deletion of *MCP2* restores growth defect of double deletion mutant *Δmco76 Δups1*.

Since Mcp2 and Mco76 belong to the UbiB protein family and in order to gain a better insight of functions of Mco76, genetic interaction of *MCO76* with *MCP2* was tested by growth analysis. Drop dilution assay revealed that deletion of *MCO76* and *MCP2* simultaneously does not affect cell growth. This indicates that *MCO76* does not have negative synthetic genetic interaction with *MCP2* (Figure 3.17 A).

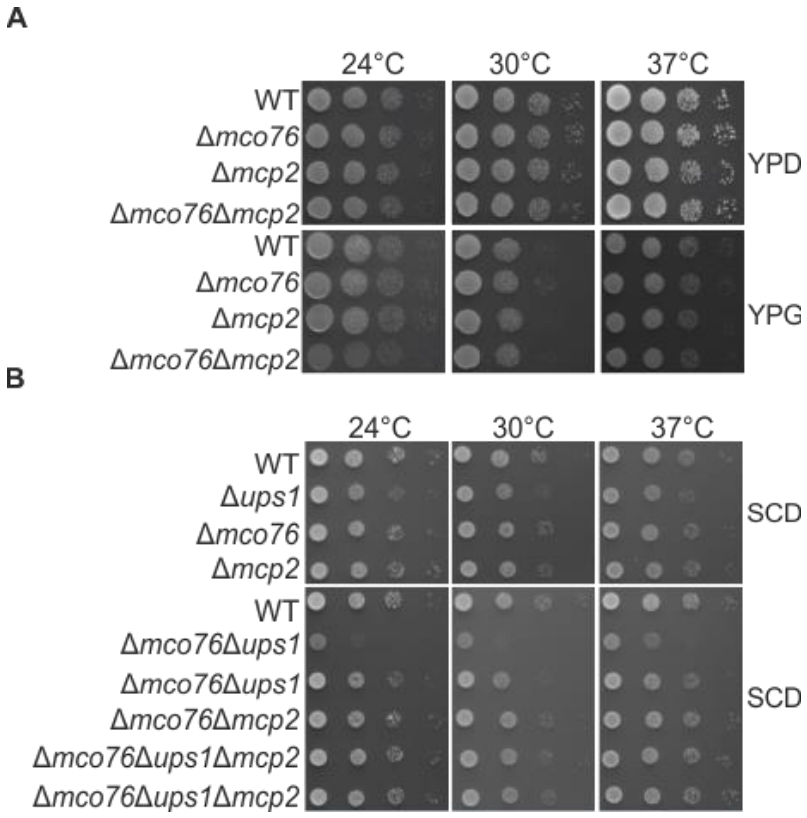

Figure 3.17 Deletion of *MCP2* restores the phenotypes of the double deletion mutant *Δmco76Δups1*.

A)Growth analysis of *Δmco76Δmcp2* double deletion mutant. Wild-type (WT), Δ*mco76*, Δ*mcp2*, and Δ*mo76*Δ*mcp2* cells were grown to logarithmic phase and spotted on either YPD or YPG plates in a 1:10 dilution series.

B) Growth analysis of *Δmco76Δups1Δmcp2* triple deletion mutant. Yeast wild type cells and cells of the indicated mutants were grown overnight on YPD. The cells were shifted to synthetic media containing glucose and cultured for a further 30h. cells were grown to logarithmic phase and spotted on either YPD or YPG plates in a 1:10 dilution series.

However, it has been reported that deletion of *MCP2* restores the growth phenotype of cells lacking Ups1 at high temperatures and in nonfermentable carbon sources (Odendall et al., 2019). So, it was tested whether deletion of *MCP2* from cells lacking Ups1 has any effect on cell growth in fermentable carbon sources. Cells were harvested in their logarithmic phase and serial dilution of cells were spotted on SCD plates. Growth analysis of double deletion mutant Δ*ups1*Δ*mcp2* demonstrates that deletion of *MCP2* in cells lacking Ups1 does not affect cell growth (Figure 3.17 B).

Next, I tested whether deletion of *MCP2* in double deletion strain *Δmco76Δups1* affects the cell growth. To do so, the growth of triple-deletion *Δups1Δmco76Δmcp2* strain was analyzed by drop dilution assay. Double deletion strain *Δmco76Δups1* showed a drastic growth defect, as it was shown before. Interestingly, the deletion of *MCP2* from double-deletion strain *Δmco76Δups1* restores its growth defects (Figure 3.17 B). Evidently, *MCP2* and *MCO76* have a genetic interaction when cell lack Ups1.

To test whether the rescuing of the growth defect in triple deletion mutant is due to restoration of mitochondrial function, I analyzed the accumulation of Mdj1 precursor and ratio of s-Mgm1 to l-Mgm1 isoforms in triple deletion mutant (Figure 3.18 A). Immunodecoration against Mdj1 showed that accumulation of Mdj1 precursor in the triple deletion strain is restored significantly (Figure 3.18 A). It implies mitochondria in triple deletion strain can import Mdj1 precursor more efficiently in comparison to mitochondria of double deletion mutant *Δmco76Δups1*. Additionally, the ratio of Mgm1 short to long isoforms of Mgm1 is retrieved back to its ratio in single deletion mutant Δ*ups1* (Figure 3.18 B). It indicates that the deletion of *MCP2* from double-deletion mutant *Δmco76Δups1* helps mitochondria retain their function.

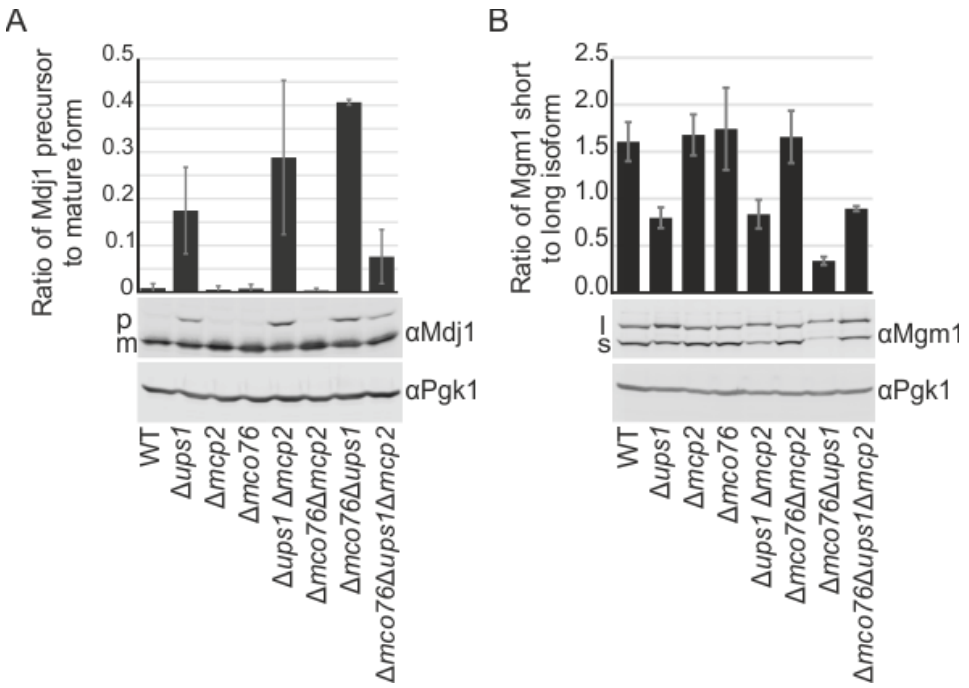

Figure 3.18 Deletion of *MCP2* reduces the accumulation of Mdj1 precursor and restores ratio of s-Mgm1 to l-Mgm1 isoforms.

A)Changes in accumulation of Mdj1 precursor are demonstrated as the ratio of the signal of precursor to the total signal of mature and precursor of Mdj1 (m/m+p). Cell lysate prepared according to the (Fig 3.13 A). Immunodecoration was performed by a specific antibody against Mdj1. Signal intensities were normalized to intensities of Pgk1 signal in wild type cells. P. precursor, M. Mature.

B) Proteolytic processing of Mgm1 is demonstrated as the ratio of short to long isoform of Mgm1. Immunodecoration was performed by a specific antibody against Mgm1. Signal intensities are normalized to the signal intensity of Pgk1 in wild type cells. Error bars indicate the standard deviation of three independent experiments.

3.16 Phosphatidic acid is reduced in mitochondria lacking Mco76.

Both *CRD1* and *UPS1* genes are involved in the synthesis of CL, and deletion of *CRD1* or *UPS1* alters the phospholipid composition of mitochondria (Chang et al., 1998; Tamura et al., 2009). In addition, the genetic interaction of *MCO76* with *UPS1* and *CRD1* led us to ask whether mitochondrial phospholipid composition of double deletion strain *Δmco76Δups1* has been altered. This could provide a potential hint that *MCO76* plays a role in mitochondrial phospholipid homeostasis. To address this question, phospholipid species of enriched mitochondrial fraction were quantified by mass spectrometry. To this end, crude isolated mitochondria from cells growing on SCG media were purified by sucrose density gradient to omit the other cellular organelles such as the nucleus, vacuole and, ER from mitochondrial fraction. The purity of

mitochondrial fractions from different mutant strains was tested by representative proteins of vacuolar and ER membranes. Immunodecoration against Vam3, vacuolar protein, showed that mitochondrial fraction was almost depleted from the membranes of the vacuole (Figure 3.19 A).

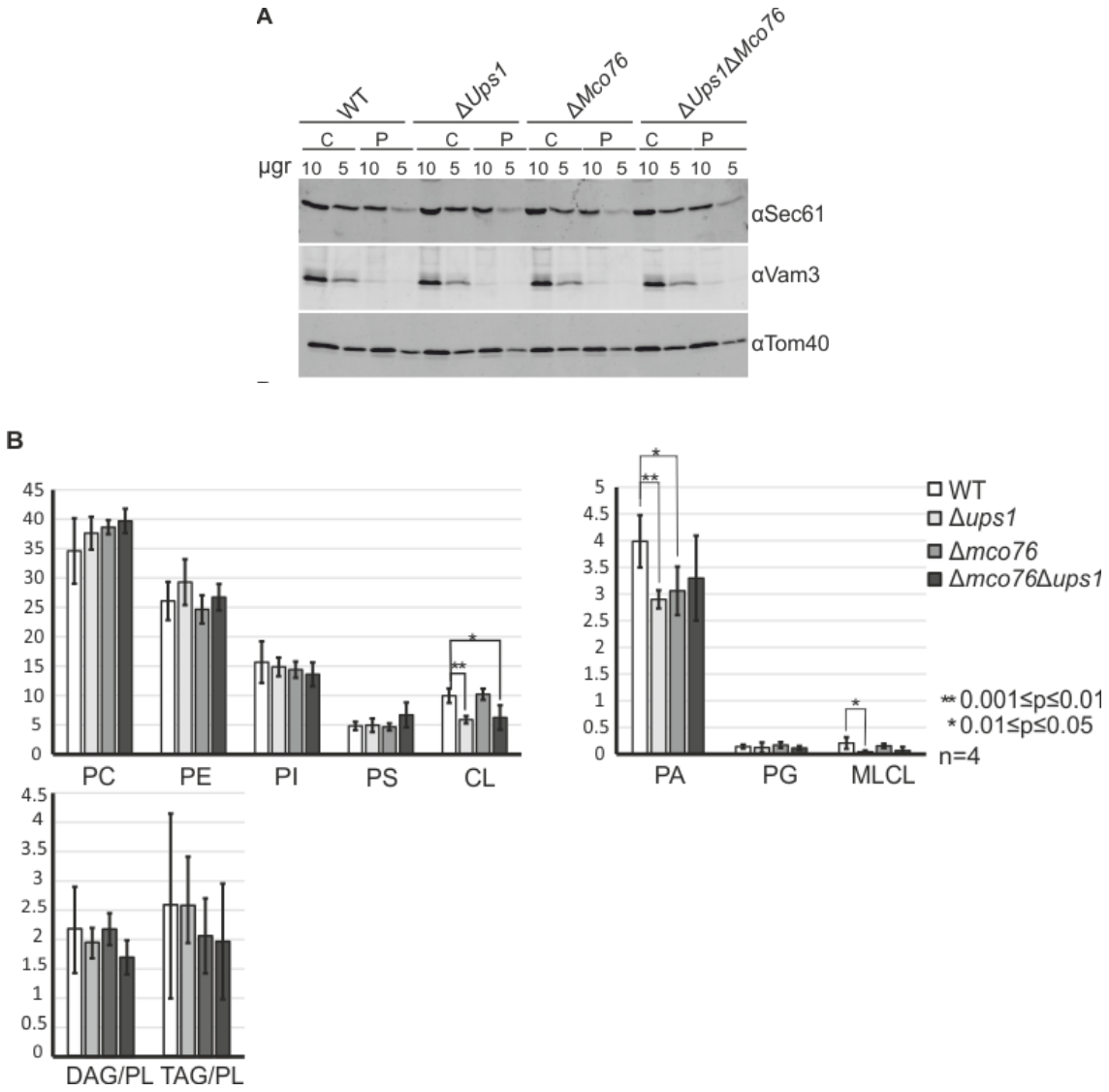

Figure 3.19 PA accumulation is impaired in mitochondrial fraction of cells lacking Mco76.

A)Purity of mitochondrial fractions were analyzed by crud mitochondrial fraction to pure mitochondrial fraction. Mitochondrial fraction was obtained from cells of different strains by succories gradient purification. Immunodecoration was achieved by using specific antibodies against Vam3, Sec61, and Tom40. C. crude mitochondria, P. pure mitochondria.

B)Lipids were extracted from mitochondrial fractions of wild type cells and different mutants then analyzed by mass spectrometry. The level of each phospholipid species is shown as a % of total PL in each strain. Bars indicate standard deviation from four independent

experiments (n=4). PC, phosphatidylcholine, PE, phosphatidylethanolamine, PS, Phosphatidylserine, PI, phosphatidylinositol, CL, cardiolipin, PG, phosphatidylglycerol, PA, phosphatidic acid, MLCL, monolysocardiolipin, Diacylglcerol (DAG), Threeacylglycerol (TAG).

However, mitochondrial fractions still contain a considerable amount of ER membranes as immunodecoration of Sec61, protein of ER, showed (Figure 3.19 B). Phospholipid species were extracted and quantified according to the material and methods (phospholipid extraction and mass spectrometry analysis were performed by Prof. Dr. Britta Brügger and coworkers, University of Heidelberg). Reduction of CL and PA were observed in deletion strain Δ*ups1* as different groups have previously reported it (Connerth et al., 2012; Osman et al., 2009; Sesaki et al., 2006; Tamura et al., 2009; Tamura et al., 2012). Deletion of *MCO76* does not significantly affect the relative phospholipid amount of CL, PG, PE, PI, PC, PA, and MLCL (Figure 3.19 B). However, PA has been reduced 20% in cells lacking Mco76 compared to wild type cells indicating deletion of *MCO76* affects the accumulation of PA independent of *UPS1* in mitochondria. Strikingly, Quantification of phospholipids by mass spectrometry showed no significant changes in the phospholipid composition of mitochondria in double deletion mutant *Δmco76Δups1* compared to the deletion strains Δ*ups1* or *Δmco76*. Of note, I did not detect a significant change in Diacylglycerol/phospholipid (DAG/PL) ratio and Triacylglycerol/phospholipid (TAG/PL) ratio (Figure 3.19 B).

4. Discussion

At the center of this study is an important question: What is the molecular function of the mitochondrial protein Mco76? To address this complex question, it was necessary to identify the genetic and physical interactions of Mco76. In this dissertation, a comprehensive study including biochemical, cell biological, and biophysical analyses have been performed to identify the physical and genetic interaction of *MCO76*.

Mco76 belongs to UbiB Kinase like proteins present in archaea, bacteria, and eukaryotes. The UbiB protein family belongs to the protein kinase like super family (PKL) (Leonard et al., 1998). However, there is no evidence showing Coq8, Mcp2, or Mco76 have any kinase activity. Coq8 is the best studied member of the UbiB protein family in *S. cerevisiae*. It has been shown that Coq8 is necessary for the biosynthesis of CoQ in *S. cerevisiae* (Bousquet et al., 1991; Poon et al., 2000). Additionally, It has been proposed that Mcp2 is involved in the phospholipid homeostasis of mitochondria and has genetic interaction with Ups1 (Odendall et al., 2019; Tan et al., 2013). However, the exact molecular functions of Coq8, Mcp2, and Mco76 are not known so far. In particular, regarding Mco76, our knowledge is minimal.

4.1 Mco76 forms a contact site between the outer and inner mitochondrial membranes.

The open reading frame (ORF) of *YPL109c* encodes for a protein that has been identified in high throughput studies as a mitochondrial protein (Morgenstern et al., 2017; Sickmann et al., 2003). The Ypl109c protein has been predicted to exhibit a size of 76 kD. Therefore, it has been named Mco76, which stands for Mitochondrial class one protein of 76kD. Recently, Kemmerer et al. have provided evidence that Mco76 is essential for the distribution of CoQ in the cell. They showed that the deletion of *CQD1* (*MCO76*) increases the resistance of cells to oxidative stress. So, they concluded that deletion of *CQD1* (*MCO76*) elevates the extra mitochondrial CoQ level. Therefore, it confers resistance to oxidative stress (Kemmerer et al., 2021). In addition, they provided evidence that the deletion of *MCO76* reduces the mitochondrial level of CoQ, indicating the role of *MCO76* in the CoQ biosynthesis and trafficking.

The first step to elucidate the function of Mco76 was to determine its topology in mitochondria. This study showed that Mco76 localizes to the IM while its C-terminus is present in the IMS (Figure 3.2). *In silico,* analysis of the amino acid sequence of

Mco76 showed that there are two hydrophobic regions in it (AA123-137 and AA574-582). To determine the correct topology of Mco76 in mitochondria, it is necessary to find out whether Mcoo76 spans the IM once or twice. Only the hydrophobic region close to the N-terminus of Mco76 is long enough (14 AA) to span the membrane (Figure 3.1). Hence, it is inferred that Mco76 spans the IM once by its hydrophobic region (AA123-137). Furthermore, mitochondria fractionation assay of cells expressing Mco76-3×HA supports the proposed topology for Mco76. My results are in line with the previous results showing Mcp2 and Coq8 are present in the IM. However, to analyze the precise localization of the N-terminus of Mco76, an N-terminally tagged version of Mco76 would be necessary. According to my experiments (not shown in this thesis), all N-terminally tagged versions of Mco76 generated were unstable, and my attempts failed to detect it by immunodecoration. This indicates that the N-terminus of Mco76 might have a critical role in its stability.

Mco76 behaves similar to subunits of MICOS complex in the fractionation assay (Figure 3.4). The presence of Mco76 in the intermediate density fractions indicates that it interacts with proteins present in the OM or Mco76, itself interacts peripherally with the OM. However, in this study, it was shown that Mco76 interacts with proteins of the OM. Therefore, it was concluded that interactions of Mco76 with proteins of the OM is the main reason for its presence in intermediate density fractions.

In addition, it has been shown that Mco76 forms protein complexes around 120 KDa, 440 KDa, and 640 KDa (Figure 3.5). Co-precipitation of Mco76-3×Myc with Mco76-3×HA showed that Mco76 can form homotypic interaction (Figure 3.5). Hence, these complexes are probably formed by the self-interaction of Mco76. Whether the homotypic interaction of Mco76 is essential for the function of Mco76 is not known so far, and would require further investigation. In order to get further hints for the molecular function of Mco76, I concentrated on the identification of the OM interaction partners.

The presence of Mco76 in fractions of intermediate density led us to speculate that the interacting partners of Mco76 are possibly located in the OM. Two highly abundant proteins meet these criteria, Om14 and Por1. Strikingly, the co-immunoprecipitation assay showed that Mco76 physically interacts with Om14 and Por1 (Figure 3.8). For the first time, a novel contact site between the IM and the OM was discovered in this study (Figure 3.8). Interestingly, the interactions of Por1 and Om14 with Mco76 were observed only when Por1-3xHA was immunoprecipitated (Figure 3.6). Immunoprecipitation of Mco76-3×HA did not lead to co-precipitation of Por1. The stoichiometry of Mco76 with Por1 and Om14 might explain this phenomenon. This is

plausible when several molecules of Mco76 (homo-oligomers of Mco76) interact with only one molecule of Por1. The other explanation could be that Por1 was not co-precipitated with Mco76-3×HA because the HA epitope disturbed this interaction. It is not unusual that tags interfere with protein-protein interactions. Importantly, Mco76-3xHA was clearly present in fractions of intermediate density, indicating that the tagged protein can still interact with its partners in the OM. The prime reason for this discrepancy might be the different conditions between the fractionation assay and the immunoprecipitation assay. Three HA tags in combination with conditions applied for immunoprecipitation, particularly detergent solubilization, might lead to loss of physical interaction in immunoprecipitation assays. However, no detergent was used in the fractionation assay. This could preserve the physical interactions of Mco76 in this assay. Apart from this minor inconsistency, my results strongly suggest that the presence of Mco76 in intermediate fractions is due to its interactions with Om14 and Por1.

In the last decade, several contact sites have been identified between the IM and the OM. The most prominent contact sites are formed by Mic60, which interacts with various OM proteins and complexes such as the TOB/SAM complex(Bohnert et al., 2012; Darshi et al., 2011; Harner et al., 2011), and the TOM complex (von der Malsburg et al., 2011). Since Mco76 is present in fractions of intermediate density like subunits of the MICOS complex, I hypothesized that the interaction of Mco76 is dependent on the presence of the MICOS. To test this idea, I analyzed the interaction of Om14 with Mco76 in the absence of Mic60 (and consequently disassociated MICOS) (Figure 3.6). Contrary to my initial hypothesis, my results showed that deletion of *MIC60* does not disturb the interaction of Mco76 with Om14. This means that the interaction of Mco76 with Om14 is independent of MICOS complex formation. Therefore, it was concluded that the novel contact site composed of Mco76, Por1, Om14 forms independent of the MICOS complex.

Proteins forming contact sites between the IM and the OM such as Mgm1 and Mic60 play essential roles in mitochondrial form and functions. Since Mco76 is a contact site forming protein, it was investigated if Mco76 affects the formation or maintenance of the ultrastructure of mitochondria. Depleting Mco76 did not affect mitochondria morphology and the formation of protein complexes which are essential for the formation and maintenance of the mitochondria ultrastructure. This indicates that Mco76 is not essential for maintaining and formation of mitochondrial ultrastructure (Figure 3.10, Figure 3.11). In contrast, electron microscopy analysis of cells overexpressing *MCO76* showed that the ultrastructure of mitochondria is severely altered (Figure 3.11). In addition, evidence was obtained that overexpression of

MCO76 affects the mitochondrial morphology. In line with this result, it was observed that the formation or stability of the MICOS complex and F_1F_O ATP-synthase were significantly affected when *MCO76* was overexpressed (Figure 3.12). These results suggest that alteration of mitochondrial ultrastructure might be due to disruption of the MICOS complex and F_1F_O ATP-synthase. More precisely, it was shown that defined levels of Mco76 are essential for mitochondrial architecture and morphology.

My co-immunoprecipitation assays suggest that Mco76 is not a subunit of the MICOS complex (Figure 3.6). In addition, no changes were observed in the steady state level of the MICOS subunits upon overexpression of *MCO76*. Therefore, I conclude that disruption of the MICOS complex and F_1F_O ATP-synthase are a secondary effect of overexpression of *MCO76*. How overexpression of *MCO76* leads to this phenotype is not clear. However, there are some indications that Mco76 is involved in lipid metabolism (Chapter 4.2). Therefore, I speculate that massive overexpression of *MCO76* leads to significant changes in the phospholipid composition of the IM. In consequence, the lipid environment for the formation of the MICOS complex and the ATP synthase is disturbed, and consequently, this leads to the alteration of mitochondrial ultrastructure.

Taken together, a Novel contact site between the IM and the OM was discovered in this study. Por1, OM14, Om45 from the OM, and Mco76 integrated into the IM, form a protein complex to shape this contact site. Strikingly, it has been reported that poring proteins are involved in the phospholipid metabolism of mitochondria (Miyata et al., 2018). So this data opens the possibility that the identified CS composing of Mco76, Por1, Om14, and Om45 is also involved in lipid metabolism. Therefore, the role of *MCO76* in lipid metabolism was investigated more in detail.

4.2 Mco76 and lipid homeostasis of mitochondria.

Genetic interactions of *MCO76* were investigated to unravel the function of the contact site composed of Mco76, Por1, Om45, and Om14 in mitochondria. Growth analysis of double deletion mutants showed that deletion of *MCO76* simultaneously with *UPS1* or *CRD1* reduces the growth of double deletion mutants (Figure 3.13). This was concomitant with the impairment of mitochondrial morphology, the accumulation of Mdj1 precursor, and the changes in the ratio of s-Mgm1 to l-Mgm1 isoforms. Based on the genetic interactions of MCO76, I hypothesized that the function of Mco76 is related to phospholipid homeostasis. Observed phenotypes of *Δups1Δ*cells are common phenotypes in deletion strains in which biosynthesis of CL and PE are disturbed. For instance, It has been shown that deletion of genes such as *CRD1*, *PSD1*, and *UPS1*

leads to accumulation of Mdj1 precursor and changes in the ratio of s-Mgm1 to l-Mgm1 isoforms (Osman et al., 2009; Sesaki et al., 2006; Tamura et al., 2009). In addition, it has been suggested that Por1 which is also present with Mco76 in the newly identified contact site is involved in the biogenesis of CL (Miyata et al., 2018). These results support the hypothesis that *MCO76* is involved in the lipid homeostasis of mitochondria.

Since it has been shown that simultaneous reduction of PE and CL in the cells affects cell growth, I hypothesized that deletion of *MCO76* might reduce the levels of CL or PE (Gohil et al., 2005). We measured the relative abundance of phospholipids using mass spectrometry to test this hypothesis. Mass spectrometry is a powerful technique to measure phospholipids quantitatively. The results of this analysis did not support my initial hypothesis since no statistically significant changes in PE levels of mitochondria of *Δmco76Δups1* cells were observed. However, surprisingly, the level of PA was reduced by 20% in Δ*mco76* mutant strain compared to wild type. For the first time, we showed that the deletion of *MCO76* leads to reducing the PA level in the mitochondria. This result strengthens the hypothesis that Mco76 plays a role in mitochondria lipid homeostasis. The reduction of PA in the Δ*mco76* deletion mutant could indicate that Mco76 plays a role in the phosphorylation of DAG and the synthesis of PA in mitochondria. Assuming this role for Mco76, it would be expected that the level of DAG is elevated in the mitochondria of Δ*mco76* cells. However, no changes were observed in the relative abundance of DAG in the Δ*mco76* single deletion mutant.

Although no significant changes in the phospholipid composition of the double deletion mutant were observed, I cannot rule out that the contamination of ER membranes in the enriched mitochondrial fraction led to this observation. ER membrane has a very different phospholipid compositing than mitochondria, so the ER membrane's contamination in the samples can mask the slight difference of relative phospholipid amounts among different samples. Besides, this might explain the relatively high standard deviation in the quantitative phospholipid analyses that preventing us from detecting statistically significant differences among the samples.

The double deletion mutants of *MCO76* with *UPS1* or *CRD1* grow slower on fermentable carbon sources implying that mitochondria’s loss of respiration capacity is not the primary reason for the slow growth of double deletion mutants. However, elevated accumulation of precursor of Mdj1 in the Δ*ups*1Δ*mco76* cells indicates that the import of mitochondrial proteins is compromised. Therefore, I conjectured that the mitochondrial membrane potential (Δψ) which is necessary for the protein import is reduced in double deletion mutants. This is in line with previous reports that the deletion of *UPS1* leads to reducing the membrane potential and the protein import.

Therefore, I conclude that the additional reduction of membrane potential (Δψ) and the impaired protein import in *Δups1Δmco76* cells lead to the observed growth phenotype. However, more detailed studies are necessary to elucidate how deletion of *MCO76* from cells lacking Ups1 might reduce mitochondrial membrane potential. I speculate that the deletion of *MCO76* and *UPS1* simultaneously affects the mitochondrial membranes' integrity to an extend that disturbs vital mitochondrial functions such as protein imports. Interestingly, Kemmerer et al. recently proposed that Cqd1 (Mco76) and Cqd2 (Mcp2) regulate the level of CoQ in the IM (Kemmerer et al., 2021). Besides, they provided evidence that the level of CoQ in the IM is reduced when *CQD1* (*MCO76*) is deleted from the cells. Therefore, it is tempting to speculate that due to the CoQ reduction in the IM, protein complexes of the mitochondrial electron transport chain cannot produce gradient proton across the IM. Hence, the membrane potential is additionally reduced in the cell cells lacking Ups1 and Mco76.

In this study, it was observed that *MCP2* has genetic interaction with *MCO76* while *UPS1* is deleted (Figure 3.17). It suggests that *MCP2* and *MCO76* function in opposing manners in mitochondria. In line with this, it was shown that deletion of *MCP2* from *Δmco76Δups1* cells recovers the changes in the ratio of s-Mgm1 to l-Mgm1 isoforms and the accumulation of precursor of Mdj1 (Figure 3.17). These results are consistent with the reports showed that extra mitochondrial CoQ levels are elevated when *MCO76* is deleted (Kemmerer et al., 2021). On contrary they observed that the level of extra mitochondrial CoQ is reduced upon deletion of *MCP2*. Considering all these observations, it is tempting to conclude that a concerted equilibrium between Mcp2 and Mco76 is essential in cells. Disruption of mitochondria morphology and ultrastructure, which is observed upon overexpression of *MCO76,* might occur due to the changes in equilibrium of *MCO76* and *MCP2*.

Here, biochemical study of Mco76 strengthens the idea that the ADCK-like (ATPase) domain of Mco76 is essential for its function. This study revealed that the E330 amino acid residue of Mco76, which is present in the ADCK-like domain (ATPase) of Mco76 and homologs residue of Glu256 in Mcp2, is necessary for restoring the growth defect of Δmco76Δups1 double deletion strain (Figure 3.14). This is consistent with the observation that three amino acids (Lys210, Asp223, and Glu256) of Mcp2 are crucial for its function (Odendall et al., 2019). Coq8, Mcp2, and Mco76 belong to the PKL super family, and it has been predicted that they possess ADCK–like (ATPase) domain. It has been shown previously that introducing mutations in ADCK-like (ATPase) domain of Coq8 and Mcp2 disturb their function. However, there is no evidence showing kinase activity of members of the UbiB protein family in *S. cerevisiae*. Glu330 of Mco76 is a highly conserved residue from yeast to humans and is present in ADCK2, the closest

homolog of Mco76 in humans (Figure 3.14). This also indicates the importance of this residue for the function of Mco76.

4.3 Model

Based on data available in literature and evidence provided in this study, I propose a model of function for the Mco76 forming a novel contact site composed of Por1, Om14, and Om15. Mco76, with the help of its interacting partners, facilitates the transport of lipids between the IM and the OM (Figure 4.1). Mco76 is most likely involved in the transport of lipids from the OM to the IM. Kemmerer et al. has shown that deletion of *CQD1* (*MCO76*) increases the level of extra mitochondrial CoQ while its deletion reduces the level of mitochondrial CoQ (Kemmerer et al., 2021). Therefore, it is tempting to conclude that Mco76 is involved in transporting extra mitochondrial CoQ from the OM to the IM. Concrete evidence provided by Kemmerer et al. implicating that Mco76 involved in the transport of CoQ. However, the genetic interactions of *MCO76* and *MCP2* with genes that are involved in the phospholipid metabolism indicate that Mco76 and Mcp2 influence lipid transport and homeostasis more broadly (Odendall et al., 2019).

Two scenarios are possible for the function Mco76. First possible scenario is that Mco76 extracts its cargo alone from the OM. Then it transfers the cargo from the OM to the IM. In the first scenario, Por1, Om14, and Om45 interact with Mco76, and they provide an anchor solely for Mco76 to facilitate the extraction of the cargo from the OM by Mco76. The second scenario is that Por1, Om14, and Om45 extract the cargo from the OM and hand it over to the Mco76 and then Mco76 transfers it to the IM. Although there is no structural data available for Mco76, due to its similarity with Coq8 it is tempting to speculate that Mco76 extracts the phospholipid from the lipid membranes by hydrolyzing ATP like Coq8 (Reidenbach et al., 2018; Stefely et al., 2015). If Mco76 mechanistically functions similar to Coq8, it is possible that Mco76 extracts its cargo (possibly CoQ and phospholipid) without the help of Por1, Om14, and Om45.

Although no interacting protein has been reported for Mcp2, due to similarities between Mcp2 and Mco76, Mcp2 might form a contact site between the IM and the OM. Regarding evidence provided by Kemmerer et al., it is possible that Mcp2 functions in a similar mode, Like Mco76, but transporting lipids in the opposite direction from the IM to the OM. However, further investigation is needed to provide evidence of how Mcp2 transfers the lipids between the IM and OM.

At first, this model seems to contradict the phospholipid analysis of different mutant strains in this study. Since no significant changes were observed in the relative abundance of phospholipids of mitochondria among different mutant strains. However, this is only true if Mco76 transports precursor lipids necessary for the biogenesis of other phospholipids, such as CL and PE. Consequently, it would be logical to assume that deletion of *MCO76* leads to a reduction or accumulation of one or other phospholipid due to lack of a precursor for biogenesis of that phospholipid. If Mco76 transports lipids between the IM and the OM, which are not used as a precursor for the biogenesis of other phospholipids, in that case, deletion of *MCO76* does not change the phospholipid composition of mitochondria. For instance, Mco76 might transport CL, PE, between the IM and the OM, and as a consequence, its deletion would not alter the whole phospholipid composition of mitochondria. So, deletion of Mco76 only affects the phospholipid composition of the IM and the OM without altering the phospholipid composition of whole mitochondria.

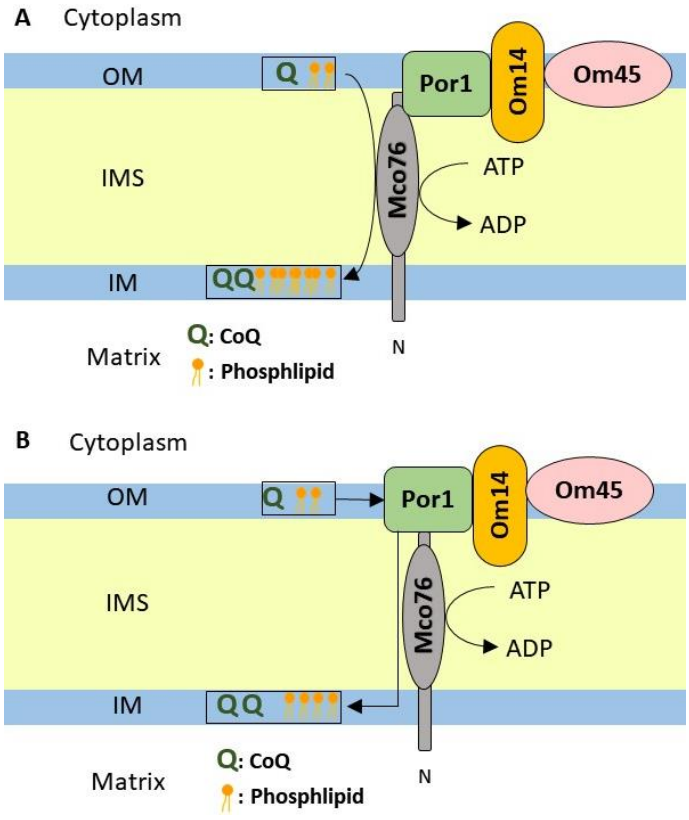

Figure 4.1 schematic model for transport of lipids between the OM and the IM by Mco76.

A)In the First scenario, Mco76 extract the cargo (CoQ and Phospholipids) from the OM and transfer it to the IM. Hydrolyzing ATP provide the energy for the extraction of the lipids

from the OM. the interactions of Mco76 with Por, Om14, and Om45 solely provide the correct position for the Mco76.

B) In the Second scenario, Mco76 receives the cargo (CoQ and Phospholipids) from the complex composed of Por1, Om14, and Om45. Then Mco76 transfers the cargo to the IM by hydrolyzing the ATP.

CoQ is present in all biological membranes, but it is preliminarily synthesized in mitochondria (Hatefi et al., 1962; Jones, 1980). It is interesting to understand how CoQ is transported from mitochondria to other organelles. CoQ is not able to diffuse freely to other organelles since CoQ is not water-soluble. Hence, the cell should deploy different mechanisms to control the transport of CoQ from mitochondria to other organelles. One of the most promising candidates that might facilitate the transport of CoQ from the OM to the ER is the ERMES complex. Consistent with this idea, it has been reported that mitochondrial CoQ domains localize adjacent to the ER-mitochondria contact sites (Subramanian et al., 2019). However, it has been claimed that disruption of Mdm34, a subunit of the ERMES complex, did not affect the oxidative stress resistance of cells lacking Mco76 (Kemmerer et al., 2021). This means that ERMES complex might not be involved in the transport of CoQ from mitochondria to the ER. However, it is important to investigate if the other subunits of ERMES complex, such as Mmm1, Mdm12, and Mdm10, are involved in the transfer of CoQ from mitochondria to the ER.

The other promising candidate is Por1 since it has been reported that Por1 interacts with Mmm1 and Spf1 that is present in the ER too (Kornmann et al., 2011). Therefore, Por1 might be a promising candidate for the transport of CoQ between ER and mitochondria. Investigating the role of Por1 and Om14 in the transport of CoQ and phospholipids between the mitochondria and the ER will shed new light on the mechanisms that cells use to control CoQ distribution among different organelles.

Mutations in the genes encoding CoQ biosynthesis proteins, such *COQ8A/B* cause CoQ deficiency. CoQ deficiency is linked to many human diseases disrupting many organs system in humans. CoQ deficiency commonly affects the brain (encephalopathy) heart, and kidney. Understanding the function of proteins involved in CoQ biosynthesis and distribution will have a tremendous potential to enhance the treatment of numerous human diseases. Overall, this study revealed a new molecular mechanism of Mco76, which is involved in the transport of CoQ. In addition, the results of this study can provide potential hints of how Mcp2 and other proteins, such as Por1 and Om14, are involved in the transport of CoQ and the other phospholipids.

5. Conclusions and future perspectives

My work demonstrates that Mco76 resides in the IM of mitochondria. Furthermore, I provided evidence that deletion of *MCO76* reduces the relative abundance of PA in mitochondria. I discovered that *MCO76* is a negative genetic interactor of *UPS1* and *CRD1*. The hallmark of this study is discovering a novel contact site formed by the interaction of Mco76 with Por1, Om45 and Om14 proteins. Based on this evidence and the recent report on the function of Mco76, I proposed that Mco76 is involved in the homeostasis of phospholipid and CoQ by transporting these lipids between the IM and the OM.

In spite of these new findings, several questions remain to be answered. Among them, does Mco76 interact with phospholipids or CoQ directly? Answering this question could support my model that Mco76 transports phospholipid and/or CoQ between the IM and the OM. To address this question, it is necessary to purify recombinant Mco76. Then it is possible to study Mco76 interaction with different lipids using approaches such as a liposome co-floatation assay. Besides, my efforts to purify Mco76 recombinantly, did not lead to purification of Mco76 (results are not shown in this study). In addition, Kemmerer et al. has also reported that Mco76 is recalcitrant to recombinant protein purification (Kemmerer et al., 2020). However, new techniques such as cell-free protein synthesis and the use of soluble nanoscale lipid bilayers might be a promising approach to tackle this problem.

Another important question is how deletion of *MCO76* changes the relative phospholipid composition between the IM and the OM? In other words, Mco76 is involved in the transfer of what type of phospholipid? Answering this question can provide concrete evidence showing that Mco76 is directly involved in the transport of phospholipids. To tackle this question, purification of the OM membrane with minimum contamination from ER and the IM is necessary. One possible solution to minimize the ER contamination is the assay suggested by Forner et al. for the purification of mitochondria. In this method, Crude isolated mitochondria are treated with trypsin under mild proteolysis conditions (Forner et al., 2006). In Consequence, all potential contact sites between mitochondria and the ER are degraded which lowers the ER contamination in mitochondrial fraction. Purification of the OM makes it possible to analyze the phospholipid composition of the OM quantitatively by MS. Therefore, it is possible to investigate the specific changes of phospholipids in cells lacking Mco76.

It will be interesting to investigate how Por1 and Om14 are involved in the transport of CoQ to mitochondria. It has been shown that deletion of *MCO76* in cells lacking Gpx1, Gpx2, and Gpx3 makes the cells more resistant to oxidative stress (Kemmerer et al., 2021). A compelling question would be whether deletion of *POR1* also increases the resistance of *ΔGPX1ΔGPX2ΔGPX3* cells to oxidative stress indicating an increase in the level of extra mitochondrial CoQ. Answering this question would help determine whether Por1 affects the export of CoQ from mitochondria.

It is also not clear how Mcp2 is involved in the process of transporting CoQ. Finding proteins interacting with Mcp2 elucidates the precise function of Mcp2 in transporting lipid inside the mitochondria. Finally, it aids us in understanding how cells distribute CoQ and phospholipids among different organelles.

6. Abbreviations

AAC – ATP-ADP carrier

APS – ammonium peroxide disulphate

ADP – adenosine diphosphate

ATP – adenosine triphosphate

BN-PAGE – blue native polyacrylamide gel electrophoresis

BSA – bovine serum albumin

CDP – Cytidine diphosphate

Da – Dalton

DMSO – dimethyl sulfoxide

DAG – diacylglycerol

DNA – desoxyribonucleic acid

DTT – dithiothreitol

E. coli – Escherichia coli

ECL – electrochemical luminescence

EDTA – ethylenedinitrilotetraacetic acid (also Triplex III)

F1ß – ß-subunit of ATP synthase

GTP – guanosine triphosphate

His – histidine

HEPES – 2-[4-(2-hydroxyethyl) piperazin-1-yl] ethanesulfonic acid

HRP – horseradish peroxidase

IM – Inner mitochondrial membrae

IMS – intermembrane space

kDa – kilo Dalton

LB – Luria-Bertani

LMU – Ludwig-Maximilians-Universität München

MIA – mitochondrial intermembrane space import and assembly (machinery)

min – minute

mRNA – messenger ribonucleic acid

mtDNA – mitochondrial desoxyribonucleic acid

MS – mass spectrometry

NTP – nucleoside triphosphate

OM – outer mitochondrial membrane

PA – Phosphatidic acids

PAGE – polyacrylamide gel electrophoresis

PE – phosphatidylethanolamines

PG – phosphatidylglycerol

PGP – phosphatidylglycerolphosphate

pH – potential of hydrogen

PMSF – phenylmethylsulfonylfluoride

PVDF – polyvinylidene fluoride

RNA – ribonucleic acid

RNase – ribonuclease

RT – room temperature

SAM – sorting and assembly machinery

SDS – sodiumdodecylsulfate

SDS-PAGE – sodiumdodecylsulfate polyacrylamide gel electrophoresis

Su9 - subunit 9 of Fo-ATPase from *Neurospora crassa*

TAG –

TBS – Tris buffered saline

TCA – trichloracetic acid

TEMED - N, N, N“, N“-Tetramethylethylendiamine

TIM – translocase of the inner (mitochondrial) membrane

7. References

Aaltonen, M.J., Friedman, J.R., Osman, C., Salin, B., di Rago, J.P., Nunnari, J., Langer, T., and Tatsuta, T. (2016). MICOS and phospholipid transfer by Ups2-Mdm35 organize membrane lipid synthesis in mitochondria. J Cell Biol *213*, 525-534.

Acehan, D., Malhotra, A., Xu, Y., Ren, M., Stokes, D.L., and Schlame, M. (2011). Cardiolipin affects the supramolecular organization of ATP synthase in mitochondria. Biophys J *100*, 2184-2192.

Achleitner, G., Zweytick, D., Trotter, P.J., Voelker, D.R., and Daum, G. (1995). Synthesis and intracellular transport of aminoglycerophospholipids in permeabilized cells of the yeast, Saccharomyces cerevisiae. J Biol Chem *270*, 29836-29842.

Adachi, Y., Itoh, K., Yamada, T., Cerveny, K.L., Suzuki, T.L., Macdonald, P., Frohman, M.A., Ramachandran, R., Iijima, M., and Sesaki, H. (2016). Coincident Phosphatidic Acid Interaction Restrains Drp1 in Mitochondrial Division. Mol Cell *63*, 1034-1043.

Alkhaja, A.K., Jans, D.C., Nikolov, M., Vukotic, M., Lytovchenko, O., Ludewig, F., Schliebs, W., Riedel, D., Urlaub, H., Jakobs, S.*, et al.* (2012). MINOS1 is a conserved component of mitofilin complexes and required for mitochondrial function and cristae organization. Mol Biol Cell *23*, 247-257.

Anderson, S., Bankier, A.T., Barrell, B.G., de Bruijn, M.H., Coulson, A.R., Drouin, J., Eperon, I.C., Nierlich, D.P., Roe, B.A., Sanger, F.*, et al.* (1981). Sequence and organization of the human mitochondrial genome. Nature *290*, 457-465.

Appelhans, T., and Busch, K.B. (2017). Dynamic imaging of mitochondrial membrane proteins in specific sub-organelle membrane locations. Biophys Rev *9*, 345-352.

Arnold, I., Pfeiffer, K., Neupert, W., Stuart, R.A., and Schägger, H. (1998). Yeast mitochondrial F1F0-ATP synthase exists as a dimer: identification of three dimer-specific subunits. Embo j *17*, 7170-7178.

Awad, A.M., Bradley, M.C., Fernández-Del-Río, L., Nag, A., Tsui, H.S., and Clarke, C.F. (2018). Coenzyme Q(10) deficiencies: pathways in yeast and humans. Essays Biochem *62*, 361-376.

Basu Ball, W., Neff, J.K., and Gohil, V.M. (2018). The role of nonbilayer phospholipids in mitochondrial structure and function. FEBS Lett *592*, 1273-1290.

Bauer, C., Herzog, V., and Bauer, M.F. (2001). Improved Technique for Electron Microscope Visualization of Yeast Membrane Structure. Microsc Microanal *7*, 530-534.

Bereiter-Hahn, J., and Vöth, M. (1994). Dynamics of mitochondria in living cells: shape changes, dislocations, fusion, and fission of mitochondria. Microsc Res Tech *27*, 198-219.

Bleazard, W., McCaffery, J.M., King, E.J., Bale, S., Mozdy, A., Tieu, Q., Nunnari, J., and Shaw, J.M. (1999). The dynamin-related GTPase Dnm1 regulates mitochondrial fission in yeast. Nat Cell Biol *1*, 298-304.

Bohnert, M., Wenz, L.S., Zerbes, R.M., Horvath, S.E., Stroud, D.A., von der Malsburg, K., Müller, J.M., Oeljeklaus, S., Perschil, I., Warscheid, B.*, et al.* (2012). Role of mitochondrial inner membrane organizing system in protein biogenesis of the mitochondrial outer membrane. Mol Biol Cell *23*, 3948-3956.

Bohnert, M., Zerbes, R.M., Davies, K.M., Mühleip, A.W., Rampelt, H., Horvath, S.E., Boenke, T., Kram, A., Perschil, I., Veenhuis, M.*, et al.* (2015). Central role of Mic10 in the mitochondrial contact site and cristae organizing system. Cell Metab *21*, 747-755.

Böttinger, L., Horvath, S.E., Kleinschroth, T., Hunte, C., Daum, G., Pfanner, N., and Becker, T. (2012). Phosphatidylethanolamine and cardiolipin differentially affect the stability of mitochondrial respiratory chain supercomplexes. J Mol Biol *423*, 677-686.

Bousquet, I., Dujardin, G., and Slonimski, P.P. (1991). ABC1, a novel yeast nuclear gene has a dual function in mitochondria: it suppresses a cytochrome b mRNA translation defect and is essential for the electron transfer in the bc 1 complex. Embo j *10*, 2023-2031.

Bradford, M.M. (1976). A rapid and sensitive method for the quantitation of microgram quantities of protein utilizing the principle of protein-dye binding. Anal Biochem *72*, 248-254.

Burger, G., Gray, M.W., and Lang, B.F. (2003). Mitochondrial genomes: anything goes. Trends Genet *19*, 709-716.

Bürgermeister, M., Birner-Grünberger, R., Nebauer, R., and Daum, G. (2004). Contribution of different pathways to the supply of phosphatidylethanolamine and phosphatidylcholine to mitochondrial membranes of the yeast Saccharomyces cerevisiae. Biochim Biophys Acta *1686*, 161-168.

Chandel, N.S. (2014). Mitochondria as signaling organelles. BMC Biol *12*, 34.

Chang, S.C., Heacock, P.N., Mileykovskaya, E., Voelker, D.R., and Dowhan, W. (1998). Isolation and characterization of the gene (CLS1) encoding cardiolipin synthase in Saccharomyces cerevisiae. J Biol Chem *273*, 14933-14941.

Chowdhury, A., Aich, A., Jain, G., Wozny, K., Lüchtenborg, C., Hartmann, M., Bernhard, O., Balleiniger, M., Alfar, E.A., Zieseniss, A.*, et al.* (2018). Defective Mitochondrial Cardiolipin Remodeling Dampens HIF-1α Expression in Hypoxia. Cell Rep *25*, 561-570.e566.

Cipolat, S., Martins de Brito, O., Dal Zilio, B., and Scorrano, L. (2004). OPA1 requires mitofusin 1 to promote mitochondrial fusion. Proc Natl Acad Sci U S A *101*, 15927-15932.

Connerth, M., Tatsuta, T., Haag, M., Klecker, T., Westermann, B., and Langer, T. (2012). Intramitochondrial transport of phosphatidic acid in yeast by a lipid transfer protein. Science *338*, 815-818.

Daems, W.T., and Wisse, E. (1966). Shape and attachment of the cristae mitochondriales in mouse hepatic cell mitochondria. J Ultrastruct Res *16*, 123-140.

Darshi, M., Mendiola, V.L., Mackey, M.R., Murphy, A.N., Koller, A., Perkins, G.A., Ellisman, M.H., and Taylor, S.S. (2011). ChChd3, an inner mitochondrial membrane protein, is essential for maintaining crista integrity and mitochondrial function. J Biol Chem *286*, 2918-2932.

Davies, K.M., Anselmi, C., Wittig, I., Faraldo-Gómez, J.D., and Kühlbrandt, W. (2012). Structure of the yeast F1Fo-ATP synthase dimer and its role in shaping the mitochondrial cristae. Proc Natl Acad Sci U S A *109*, 13602-13607.

de Kroon, A.I., Dolis, D., Mayer, A., Lill, R., and de Kruijff, B. (1997). Phospholipid composition of highly purified mitochondrial outer membranes of rat liver and Neurospora crassa. Is cardiolipin present in the mitochondrial outer membrane? Biochim Biophys Acta *1325*, 108-116.

Detmer, S.A., and Chan, D.C. (2007). Functions and dysfunctions of mitochondrial dynamics. Nat Rev Mol Cell Biol *8*, 870-879.

Dowhan, W. (1997). Molecular basis for membrane phospholipid diversity: why are there so many lipids? Annu Rev Biochem *66*, 199-232.

Ejsing, C.S., Sampaio, J.L., Surendranath, V., Duchoslav, E., Ekroos, K., Klemm, R.W., Simons, K., and Shevchenko, A. (2009). Global analysis of the yeast lipidome by quantitative shotgun mass spectrometry. Proc Natl Acad Sci U S A *106*, 2136-2141.

Elbaz-Alon, Y., Eisenberg-Bord, M., Shinder, V., Stiller, S.B., Shimoni, E., Wiedemann, N., Geiger, T., and Schuldiner, M. (2015). Lam6 Regulates the Extent of Contacts between Organelles. Cell Rep *12*, 7-14.

Elbaz-Alon, Y., Rosenfeld-Gur, E., Shinder, V., Futerman, A.H., Geiger, T., and Schuldiner, M. (2014). A dynamic interface between vacuoles and mitochondria in yeast. Dev Cell *30*, 95-102.

Fawcet, D.W. (1981). The cell (W. B. Saunders company).

Forner, F., Arriaga, E.A., and Mann, M. (2006). Mild protease treatment as a small-scale biochemical method for mitochondria purification and proteomic mapping of cytoplasm-exposed mitochondrial proteins. J Proteome Res *5*, 3277-3287.

Foury, F., Roganti, T., Lecrenier, N., and Purnelle, B. (1998). The complete sequence of the mitochondrial genome of Saccharomyces cerevisiae. FEBS Lett *440*, 325-331.

Frey, T.G., Renken, C.W., and Perkins, G.A. (2002). Insight into mitochondrial structure and function from electron tomography. Biochim Biophys Acta *1555*, 196-203.

Friedman, J.R., Kannan, M., Toulmay, A., Jan, C.H., Weissman, J.S., Prinz, W.A., and Nunnari, J. (2018). Lipid Homeostasis Is Maintained by Dual Targeting of the Mitochondrial PE Biosynthesis Enzyme to the ER. Dev Cell *44*, 261-270.e266.

Fujiki, Y., Hubbard, A.L., Fowler, S., and Lazarow, P.B. (1982). Isolation of intracellular membranes by means of sodium carbonate treatment: application to endoplasmic reticulum. J Cell Biol *93*, 97-102.

Fukasawa, Y., Tsuji, J., Fu, S.C., Tomii, K., Horton, P., and Imai, K. (2015). MitoFates: improved prediction of mitochondrial targeting sequences and their cleavage sites. Mol Cell Proteomics *14*, 1113-1126.

Gatta, A.T., Wong, L.H., Sere, Y.Y., Calderón-Noreña, D.M., Cockcroft, S., Menon, A.K., and Levine, T.P. (2015). A new family of StART domain proteins at membrane contact sites has a role in ER-PM sterol transport. Elife *4*.

Gebert, N., Joshi, A.S., Kutik, S., Becker, T., McKenzie, M., Guan, X.L., Mooga, V.P., Stroud, D.A., Kulkarni, G., Wenk, M.R.*, et al.* (2009). Mitochondrial cardiolipin involved in outer-membrane protein biogenesis: implications for Barth syndrome. Curr Biol *19*, 2133-2139.

Gilkerson, R.W., Selker, J.M., and Capaldi, R.A. (2003). The cristal membrane of mitochondria is the principal site of oxidative phosphorylation. FEBS Lett *546*, 355-358.

Gohil, V.M., Thompson, M.N., and Greenberg, M.L. (2005). Synthetic lethal interaction of the mitochondrial phosphatidylethanolamine and cardiolipin biosynthetic pathways in Saccharomyces cerevisiae. J Biol Chem *280*, 35410-35416.

González Montoro, A., Auffarth, K., Hönscher, C., Bohnert, M., Becker, T., Warscheid, B., Reggiori, F., van der Laan, M., Fröhlich, F., and Ungermann, C. (2018). Vps39 Interacts with Tom40 to Establish One of Two Functionally Distinct Vacuole-Mitochondria Contact Sites. Dev Cell *45*, 621-636.e627.

Gray, M.W. (1992). The endosymbiont hypothesis revisited. Int Rev Cytol *141*, 233-357.

Griffin, E.E., Graumann, J., and Chan, D.C. (2005). The WD40 protein Caf4p is a component of the mitochondrial fission machinery and recruits Dnm1p to mitochondria. J Cell Biol *170*, 237-248.

Grillitsch, K., and Daum, G. (2011). Triacylglycerol lipases of the yeast. Frontiers in Biology *6*, 219-230.

Gulshan, K., Shahi, P., and Moye-Rowley, W.S. (2010). Compartment-specific synthesis of phosphatidylethanolamine is required for normal heavy metal resistance. Mol Biol Cell *21*, 443-455.

Hackenbrock, C.R. (1966). Ultrastructural bases for metabolically linked mechanical activity in mitochondria. I. Reversible ultrastructural changes with change in metabolic steady state in isolated liver mitochondria. J Cell Biol *30*, 269-297.

Hackenbrock, C.R. (1968). Chemical and physical fixation of isolated mitochondria in low-energy and high-energy states. Proc Natl Acad Sci U S A *61*, 598-605.

Hales, K.G., and Fuller, M.T. (1997). Developmentally regulated mitochondrial fusion mediated by a conserved, novel, predicted GTPase. Cell *90*, 121-129.

Ham, H.J., Rho, H.J., Shin, S.K., and Yoon, H.J. (2010). The TGL2 gene of Saccharomyces cerevisiae encodes an active acylglycerol lipase located in the mitochondria. J Biol Chem *285*, 3005-3013.

Harner, M., Körner, C., Walther, D., Mokranjac, D., Kaesmacher, J., Welsch, U., Griffith, J., Mann, M., Reggiori, F., and Neupert, W. (2011). The mitochondrial contact site complex, a determinant of mitochondrial architecture. EMBO J *30*, 4356-4370.

Harner, M.E., Unger, A.K., Geerts, W.J., Mari, M., Izawa, T., Stenger, M., Geimer, S., Reggiori, F., Westermann, B., and Neupert, W. (2016). An evidence based hypothesis on the existence of two pathways of mitochondrial crista formation. Elife *5*.

Hatefi, Y., Haavik, A.G., Fowler, L.R., and Griffiths, D.E. (1962). Studies on the electron transfer system. XLII. Reconstitution of the electron transfer system. J Biol Chem *237*, 2661-2669.

Herlan, M., Vogel, F., Bornhovd, C., Neupert, W., and Reichert, A.S. (2003). Processing of Mgm1 by the rhomboid-type protease Pcp1 is required for maintenance of mitochondrial morphology and of mitochondrial DNA. J Biol Chem *278*, 27781-27788.

Hermann, G.J., Thatcher, J.W., Mills, J.P., Hales, K.G., Fuller, M.T., Nunnari, J., and Shaw, J.M. (1998). Mitochondrial fusion in yeast requires the transmembrane GTPase Fzo1p. J Cell Biol *143*, 359-373.

Hönscher, C., Mari, M., Auffarth, K., Bohnert, M., Griffith, J., Geerts, W., van der Laan, M., Cabrera, M., Reggiori, F., and Ungermann, C. (2014). Cellular metabolism regulates contact sites between vacuoles and mitochondria. Dev Cell *30*, 86-94.

Hoppins, S., Collins, S.R., Cassidy-Stone, A., Hummel, E., Devay, R.M., Lackner, L.L., Westermann, B., Schuldiner, M., Weissman, J.S., and Nunnari, J. (2011). A mitochondrial-focused genetic interaction map reveals a scaffold-like complex required for inner membrane organization in mitochondria. J Cell Biol *195*, 323-340.

Hoppins, S., Lackner, L., and Nunnari, J. (2007). The machines that divide and fuse mitochondria. Annu Rev Biochem *76*, 751-780.

Horvath, S.E., and Daum, G. (2013). Lipids of mitochondria. Prog Lipid Res *52*, 590-614.

Iadarola, D.M., Basu Ball, W., Trivedi, P.P., Fu, G., Nan, B., and Gohil, V.M. (2020). Vps39 is required for ethanolamine-stimulated elevation in mitochondrial phosphatidylethanolamine. Biochim Biophys Acta Mol Cell Biol Lipids *1865*, 158655.

Ingerman, E., Perkins, E.M., Marino, M., Mears, J.A., McCaffery, J.M., Hinshaw, J.E., and Nunnari, J. (2005). Dnm1 forms spirals that are structurally tailored to fit mitochondria. J Cell Biol *170*, 1021-1027.

Ishihara, N., Eura, Y., and Mihara, K. (2004). Mitofusin 1 and 2 play distinct roles in mitochondrial fusion reactions via GTPase activity. J Cell Sci *117*, 6535-6546.

Jakubke, C., Roussou, R., Maiser, A., Schug, C., Thoma, F., Bunk, D., Hörl, D., Leonhardt, H., Walter, P., Klecker, T.*, et al.* (2021). Cristae-dependent quality control of the mitochondrial genome. Sci Adv *7*, eabi8886.

Janke, C., Magiera, M.M., Rathfelder, N., Taxis, C., Reber, S., Maekawa, H., Moreno-Borchart, A., Doenges, G., Schwob, E., Schiebel, E.*, et al.* (2004). A versatile toolbox for PCR-based tagging of yeast genes: new fluorescent proteins, more markers and promoter substitution cassettes. Yeast *21*, 947-962.

Jones, B.A., and Fangman, W.L. (1992). Mitochondrial DNA maintenance in yeast requires a protein containing a region related to the GTP-binding domain of dynamin. Genes Dev *6*, 380-389.

Jones, M.E. (1980). Pyrimidine nucleotide biosynthesis in animals: genes, enzymes, and regulation of UMP biosynthesis. Annu Rev Biochem *49*, 253-279.

Kannan, N., Taylor, S.S., Zhai, Y., Venter, J.C., and Manning, G. (2007). Structural and functional diversity of the microbial kinome. PLoS Biol *5*, e17.

Kawano, S., Tamura, Y., Kojima, R., Bala, S., Asai, E., Michel, A.H., Kornmann, B., Riezman, I., Riezman, H., Sakae, Y.*, et al.* (2018). Structure-function insights into direct lipid transfer between membranes by Mmm1-Mdm12 of ERMES. J Cell Biol *217*, 959-974.

Kemmerer, Z.A., Robinson, K.P., Schmitz, J.M., Manicki, M., Paulson, B.R., Jochem, A., Hutchins, P.D., Coon, J.J., and Pagliarini, D.J. (2021). UbiB proteins regulate cellular CoQ distribution in Saccharomyces cerevisiae. Nat Commun *12*, 4769.

Kemmerer, Z.A., Robinson, K.P., Schmitz, J.M., Paulson, B.R., Jochem, A., Hutchins, P.D., Coon, J.J., and Pagliarini, D.J. (2020). UbiB proteins regulate cellular CoQ distribution. bioRxiv, 2020.2012.2009.418202.

Khosravi, S., and Harner, M.E. (2020). The MICOS complex, a structural element of mitochondria with versatile functions. Biol Chem *401*, 765-778.

Kodaki, T., and Yamashita, S. (1987). Yeast phosphatidylethanolamine methylation pathway. Cloning and characterization of two distinct methyltransferase genes. J Biol Chem *262*, 15428-15435.

Kojima, R., Endo, T., and Tamura, Y. (2016). A phospholipid transfer function of ER-mitochondria encounter structure revealed in vitro. Sci Rep *6*, 30777.

Kojima, R., Kakimoto, Y., Furuta, S., Itoh, K., Sesaki, H., Endo, T., and Tamura, Y. (2019). Maintenance of Cardiolipin and Crista Structure Requires Cooperative Functions of Mitochondrial Dynamics and Phospholipid Transport. Cell Rep *26*, 518-528.e516.

Körner, C., Barrera, M., Dukanovic, J., Eydt, K., Harner, M., Rabl, R., Vogel, F., Rapaport, D., Neupert, W., and Reichert, A.S. (2012). The C-terminal domain of Fcj1 is required for formation of crista junctions and interacts with the TOB/SAM complex in mitochondria. Mol Biol Cell *23*, 2143-2155.

Kornmann, B., Currie, E., Collins, S.R., Schuldiner, M., Nunnari, J., Weissman, J.S., and Walter, P. (2009). An ER-mitochondria tethering complex revealed by a synthetic biology screen. Science *325*, 477-481.

Kornmann, B., Osman, C., and Walter, P. (2011). The conserved GTPase Gem1 regulates endoplasmic reticulum-mitochondria connections. Proc Natl Acad Sci U S A *108*, 14151-14156.

Koshiba, T., Detmer, S.A., Kaiser, J.T., Chen, H., McCaffery, J.M., and Chan, D.C. (2004). Structural basis of mitochondrial tethering by mitofusin complexes. Science *305*, 858-862.

Labbé, K., Murley, A., and Nunnari, J. (2014). Determinants and functions of mitochondrial behavior. Annu Rev Cell Dev Biol *30*, 357-391.

Lauffer, S., Mäbert, K., Czupalla, C., Pursche, T., Hoflack, B., Rödel, G., and Krause-Buchholz, U. (2012). Saccharomyces cerevisiae porin pore forms complexes with

mitochondrial outer membrane proteins Om14p and Om45p. J Biol Chem *287*, 17447-17458.

Leonard, C.J., Aravind, L., and Koonin, E.V. (1998). Novel families of putative protein kinases in bacteria and archaea: evolution of the "eukaryotic" protein kinase superfamily. Genome Res *8*, 1038-1047.

Longtine, M.S., McKenzie, A., 3rd, Demarini, D.J., Shah, N.G., Wach, A., Brachat, A., Philippsen, P., and Pringle, J.R. (1998). Additional modules for versatile and economical PCR-based gene deletion and modification in Saccharomyces cerevisiae. Yeast *14*, 953-961.

Malhotra, K., Modak, A., Nangia, S., Daman, T.H., Gunsel, U., Robinson, V.L., Mokranjac, D., May, E.R., and Alder, N.N. (2017). Cardiolipin mediates membrane and channel interactions of the mitochondrial TIM23 protein import complex receptor Tim50. Sci Adv *3*, e1700532.

Mannella, C.A., Pfeiffer, D.R., Bradshaw, P.C., Moraru, II, Slepchenko, B., Loew, L.M., Hsieh, C.E., Buttle, K., and Marko, M. (2001). Topology of the mitochondrial inner membrane: dynamics and bioenergetic implications. IUBMB Life *52*, 93-100.

Manning, G., Whyte, D.B., Martinez, R., Hunter, T., and Sudarsanam, S. (2002). The protein kinase complement of the human genome. Science *298*, 1912-1934.

Margulis, L. (1971). Symbiosis and evolution. Sci Am *225*, 48-57.

Martin, W. (2010). Evolutionary origins of metabolic compartmentalization in eukaryotes. Philos Trans R Soc Lond B Biol Sci *365*, 847-855.

Matyash, V., Liebisch, G., Kurzchalia, T.V., Shevchenko, A., and Schwudke, D. (2008). Lipid extraction by methyl-tert-butyl ether for high-throughput lipidomics. J Lipid Res *49*, 1137-1146.

McBride, H.M., Neuspiel, M., and Wasiak, S. (2006). Mitochondria: more than just a powerhouse. Curr Biol *16*, R551-560.

Meeusen, S., DeVay, R., Block, J., Cassidy-Stone, A., Wayson, S., McCaffery, J.M., and Nunnari, J. (2006). Mitochondrial inner-membrane fusion and crista maintenance requires the dynamin-related GTPase Mgm1. Cell *127*, 383-395.

Meeusen, S., McCaffery, J.M., and Nunnari, J. (2004). Mitochondrial fusion intermediates revealed in vitro. Science *305*, 1747-1752.

Mitchell, P. (1975). Protonmotive redox mechanism of the cytochrome b-c1 complex in the respiratory chain: protonmotive ubiquinone cycle. FEBS Lett *56*, 1-6.

Miyata, N., Fujii, S., and Kuge, O. (2018). Porin proteins have critical functions in mitochondrial phospholipid metabolism in yeast. J Biol Chem *293*, 17593-17605.

Miyata, N., Goda, N., Matsuo, K., Hoketsu, T., and Kuge, O. (2017). Cooperative function of Fmp30, Mdm31, and Mdm32 in Ups1-independent cardiolipin accumulation in the yeast Saccharomyces cerevisiae. Sci Rep *7*, 16447.

Miyata, N., Watanabe, Y., Tamura, Y., Endo, T., and Kuge, O. (2016). Phosphatidylserine transport by Ups2-Mdm35 in respiration-active mitochondria. J Cell Biol *214*, 77-88.

Modi, S., López-Doménech, G., Halff, E.F., Covill-Cooke, C., Ivankovic, D., Melandri, D., Arancibia-Cárcamo, I.L., Burden, J.J., Lowe, A.R., and Kittler, J.T. (2019). Miro clusters regulate ER-mitochondria contact sites and link cristae organization to the mitochondrial transport machinery. Nat Commun *10*, 4399.

Mokranjac, D., and Neupert, W. (2009). Thirty years of protein translocation into mitochondria: unexpectedly complex and still puzzling. Biochim Biophys Acta *1793*, 33-41.

Morgenstern, M., Stiller, S.B., Lübbert, P., Peikert, C.D., Dannenmaier, S., Drepper, F., Weill, U., Höß, P., Feuerstein, R., Gebert, M.*, et al.* (2017). Definition of a High-Confidence Mitochondrial Proteome at Quantitative Scale. Cell Rep *19*, 2836-2852.

Mozdy, A.D., McCaffery, J.M., and Shaw, J.M. (2000). Dnm1p GTPase-mediated mitochondrial fission is a multi-step process requiring the novel integral membrane component Fis1p. J Cell Biol *151*, 367-380.

Murley, A., Yamada, J., Niles, B.J., Toulmay, A., Prinz, W.A., Powers, T., and Nunnari, J. (2017). Sterol transporters at membrane contact sites regulate TORC1 and TORC2 signaling. J Cell Biol *216*, 2679-2689.

Naylor, K., Ingerman, E., Okreglak, V., Marino, M., Hinshaw, J.E., and Nunnari, J. (2006). Mdv1 interacts with assembled dnm1 to promote mitochondrial division. J Biol Chem *281*, 2177-2183.

Nunnari, J., Marshall, W.F., Straight, A., Murray, A., Sedat, J.W., and Walter, P. (1997). Mitochondrial transmission during mating in Saccharomyces cerevisiae is determined by mitochondrial fusion and fission and the intramitochondrial segregation of mitochondrial DNA. Mol Biol Cell *8*, 1233-1242.

Odendall, F., Backes, S., Tatsuta, T., Weill, U., Schuldiner, M., Langer, T., Herrmann, J.M., Rapaport, D., and Dimmer, K.S. (2019). The mitochondrial intermembrane space-facing proteins Mcp2 and Tgl2 are involved in yeast lipid metabolism. Mol Biol Cell *30*, 2681-2694.

Osman, C., Haag, M., Potting, C., Rodenfels, J., Dip, P.V., Wieland, F.T., Brügger, B., Westermann, B., and Langer, T. (2009). The genetic interactome of prohibitins: coordinated control of cardiolipin and phosphatidylethanolamine by conserved regulators in mitochondria. J Cell Biol *184*, 583-596.

Osman, C., Voelker, D.R., and Langer, T. (2011). Making heads or tails of phospholipids in mitochondria. J Cell Biol *192*, 7-16.

Otsuga, D., Keegan, B.R., Brisch, E., Thatcher, J.W., Hermann, G.J., Bleazard, W., and Shaw, J.M. (1998). The dynamin-related GTPase, Dnm1p, controls mitochondrial morphology in yeast. J Cell Biol *143*, 333-349.

Özbalci, C., Sachsenheimer, T., and Brügger, B. (2013). Quantitative analysis of cellular lipids by nano-electrospray ionization mass spectrometry. Methods Mol Biol *1033*, 3-20.

Palade, G.E. (1952). The fine structure of mitochondria. Anat Rec *114*, 427-451.

Palade, G.E. (1953). An electron microscope study of the mitochondrial structure. J Histochem Cytochem *1*, 188-211.

Papagiannidis, D., Bircham, P.W., Lüchtenborg, C., Pajonk, O., Ruffini, G., Brügger, B., and Schuck, S. (2021). Ice2 promotes ER membrane biogenesis in yeast by inhibiting the conserved lipin phosphatase complex. Embo j *40*, e107958.

Paumard, P., Arselin, G., Vaillier, J., Chaignepain, S., Bathany, K., Schmitter, J.M., Brèthes, D., and Velours, J. (2002a). Two ATP synthases can be linked through subunits i in the inner mitochondrial membrane of Saccharomyces cerevisiae. Biochemistry *41*, 10390-10396.

Paumard, P., Vaillier, J., Coulary, B., Schaeffer, J., Soubannier, V., Mueller, D.M., Brèthes, D., di Rago, J.P., and Velours, J. (2002b). The ATP synthase is involved in generating mitochondrial cristae morphology. Embo j *21*, 221-230.

Perkins, G., Renken, C., Martone, M.E., Young, S.J., Ellisman, M., and Frey, T. (1997). Electron tomography of neuronal mitochondria: three-dimensional structure and organization of cristae and membrane contacts. J Struct Biol *119*, 260-272.

Perrone, M., Caroccia, N., Genovese, I., Missiroli, S., Modesti, L., Pedriali, G., Vezzani, B., Vitto, V.A.M., Antenori, M., Lebiedzinska-Arciszewska, M.*, et al.* (2020). The role of mitochondria-associated membranes in cellular homeostasis and diseases. Int Rev Cell Mol Biol *350*, 119-196.

Pon, L., Moll, T., Vestweber, D., Marshallsay, B., and Schatz, G. (1989). Protein import into mitochondria: ATP-dependent protein translocation activity in a submitochondrial fraction enriched in membrane contact sites and specific proteins. J Cell Biol *109*, 2603-2616.

Poon, W.W., Davis, D.E., Ha, H.T., Jonassen, T., Rather, P.N., and Clarke, C.F. (2000). Identification of Escherichia coli ubiB, a gene required for the first monooxygenase step in ubiquinone biosynthesis. J Bacteriol *182*, 5139-5146.

Rabl, R., Soubannier, V., Scholz, R., Vogel, F., Mendl, N., Vasiljev-Neumeyer, A., Körner, C., Jagasia, R., Keil, T., Baumeister, W.*, et al.* (2009). Formation of cristae and crista junctions in mitochondria depends on antagonism between Fcj1 and Su e/g. J Cell Biol *185*, 1047-1063.

Rapaport, D., Brunner, M., Neupert, W., and Westermann, B. (1998). Fzo1p is a mitochondrial outer membrane protein essential for the biogenesis of functional mitochondria in Saccharomyces cerevisiae. J Biol Chem *273*, 20150-20155.

Rasmussen, N. (1995). Mitochondrial structure and the practice of cell biology in the 1950s. J Hist Biol *28*, 381-429.

Reidenbach, A.G., Kemmerer, Z.A., Aydin, D., Jochem, A., McDevitt, M.T., Hutchins, P.D., Stark, J.L., Stefely, J.A., Reddy, T., Hebert, A.S.*, et al.* (2018). Conserved Lipid and Small-Molecule Modulation of COQ8 Reveals Regulation of the Ancient Kinase-like UbiB Family. Cell Chem Biol *25*, 154-165.e111.

Rubinstein, J.L., Walker, J.E., and Henderson, R. (2003). Structure of the mitochondrial ATP synthase by electron cryomicroscopy. Embo j *22*, 6182-6192.

Sagan, L. (1993). On the origin of mitosing cells. 1967. J NIH Res *5*, 65-72.

Schülke, N., Sepuri, N.B., and Pain, D. (1997). In vivo zippering of inner and outer mitochondrial membranes by a stable translocation intermediate. Proc Natl Acad Sci U S A *94*, 7314-7319.

Sesaki, H., Dunn, C.D., Iijima, M., Shepard, K.A., Yaffe, M.P., Machamer, C.E., and Jensen, R.E. (2006). Ups1p, a conserved intermembrane space protein, regulates mitochondrial shape and alternative topogenesis of Mgm1p. J Cell Biol *173*, 651-658.

Sesaki, H., and Jensen, R.E. (1999). Division versus fusion: Dnm1p and Fzo1p antagonistically regulate mitochondrial shape. J Cell Biol *147*, 699-706.

Sesaki, H., and Jensen, R.E. (2001). UGO1 encodes an outer membrane protein required for mitochondrial fusion. J Cell Biol *152*, 1123-1134.

Sesaki, H., Southard, S.M., Yaffe, M.P., and Jensen, R.E. (2003). Mgm1p, a dynamin-related GTPase, is essential for fusion of the mitochondrial outer membrane. Mol Biol Cell *14*, 2342-2356.

Shiao, Y.J., Balcerzak, B., and Vance, J.E. (1998). A mitochondrial membrane protein is required for translocation of phosphatidylserine from mitochondria-associated membranes to mitochondria. Biochem J *331 (Pt 1)*, 217-223.

Sickmann, A., Reinders, J., Wagner, Y., Joppich, C., Zahedi, R., Meyer, H.E., Schönfisch, B., Perschil, I., Chacinska, A., Guiard, B.*, et al.* (2003). The proteome of Saccharomyces cerevisiae mitochondria. Proc Natl Acad Sci U S A *100*, 13207-13212.

Sikorski, R.S., and Hieter, P. (1989). A system of shuttle vectors and yeast host strains designed for efficient manipulation of DNA in Saccharomyces cerevisiae. Genetics *122*, 19-27.

Smirnova, E., Griparic, L., Shurland, D.L., and van der Bliek, A.M. (2001). Dynamin-related protein Drp1 is required for mitochondrial division in mammalian cells. Mol Biol Cell *12*, 2245-2256.

Song, Z., Ghochani, M., McCaffery, J.M., Frey, T.G., and Chan, D.C. (2009). Mitofusins and OPA1 mediate sequential steps in mitochondrial membrane fusion. Mol Biol Cell *20*, 3525-3532.

Stefely, J.A., Reidenbach, A.G., Ulbrich, A., Oruganty, K., Floyd, B.J., Jochem, A., Saunders, J.M., Johnson, I.E., Minogue, C.E., Wrobel, R.L.*, et al.* (2015). Mitochondrial ADCK3 employs an atypical protein kinase-like fold to enable coenzyme Q biosynthesis. Mol Cell *57*, 83-94.

Stroud, D.A., Oeljeklaus, S., Wiese, S., Bohnert, M., Lewandrowski, U., Sickmann, A., Guiard, B., van der Laan, M., Warscheid, B., and Wiedemann, N. (2011). Composition and topology of the endoplasmic reticulum-mitochondria encounter structure. J Mol Biol *413*, 743-750.

Subramanian, K., Jochem, A., Le Vasseur, M., Lewis, S., Paulson, B.R., Reddy, T.R., Russell, J.D., Coon, J.J., Pagliarini, D.J., and Nunnari, J. (2019). Coenzyme Q biosynthetic proteins assemble in a substrate-dependent manner into domains at ER-mitochondria contacts. J Cell Biol *218*, 1353-1369.

Tamura, Y., Endo, T., Iijima, M., and Sesaki, H. (2009). Ups1p and Ups2p antagonistically regulate cardiolipin metabolism in mitochondria. J Cell Biol *185*, 1029-1045.

Tamura, Y., Kawano, S., and Endo, T. (2019a). Organelle contact zones as sites for lipid transfer. J Biochem *165*, 115-123.

Tamura, Y., Kawano, S., and Endo, T. (2020). Lipid homeostasis in mitochondria. Biol Chem *401*, 821-833.

Tamura, Y., Kojima, R., and Endo, T. (2019b). Advanced In Vitro Assay System to Measure Phosphatidylserine and Phosphatidylethanolamine Transport at ER/Mitochondria Interface. Methods Mol Biol *1949*, 57-67.

Tamura, Y., Onguka, O., Hobbs, A.E., Jensen, R.E., Iijima, M., Claypool, S.M., and Sesaki, H. (2012). Role for two conserved intermembrane space proteins, Ups1p and Ups2p, [corrected] in intra-mitochondrial phospholipid trafficking. J Biol Chem *287*, 15205-15218.

Tan, T., Ozbalci, C., Brügger, B., Rapaport, D., and Dimmer, K.S. (2013). Mcp1 and Mcp2, two novel proteins involved in mitochondrial lipid homeostasis. J Cell Sci *126*, 3563-3574.

Tarasenko, D., Barbot, M., Jans, D.C., Kroppen, B., Sadowski, B., Heim, G., Möbius, W., Jakobs, S., and Meinecke, M. (2017). The MICOS component Mic60 displays a conserved membrane-bending activity that is necessary for normal cristae morphology. J Cell Biol *216*, 889-899.

Tieu, Q., and Nunnari, J. (2000). Mdv1p is a WD repeat protein that interacts with the dynamin-related GTPase, Dnm1p, to trigger mitochondrial division. J Cell Biol *151*, 353-366.

Trotter, P.J., and Voelker, D.R. (1995). Identification of a non-mitochondrial phosphatidylserine decarboxylase activity (PSD2) in the yeast Saccharomyces cerevisiae. J Biol Chem *270*, 6062-6070.

Unger, A.K., Geimer, S., Harner, M., Neupert, W., and Westermann, B. (2017). Analysis of Yeast Mitochondria by Electron Microscopy. Methods Mol Biol *1567*, 293-314.

van den Brink-van der Laan, E., Killian, J.A., and de Kruijff, B. (2004). Nonbilayer lipids affect peripheral and integral membrane proteins via changes in the lateral pressure profile. Biochim Biophys Acta *1666*, 275-288.

van Meer, G., Voelker, D.R., and Feigenson, G.W. (2008). Membrane lipids: where they are and how they behave. Nat Rev Mol Cell Biol *9*, 112-124.

Velours, J., and Arselin, G. (2000). The Saccharomyces cerevisiae ATP synthase. J Bioenerg Biomembr *32*, 383-390.

Vogel, F., Bornhövd, C., Neupert, W., and Reichert, A.S. (2006). Dynamic subcompartmentalization of the mitochondrial inner membrane. J Cell Biol *175*, 237-247.

von der Malsburg, K., Müller, J.M., Bohnert, M., Oeljeklaus, S., Kwiatkowska, P., Becker, T., Loniewska-Lwowska, A., Wiese, S., Rao, S., Milenkovic, D.*, et al.* (2011). Dual role of mitofilin in mitochondrial membrane organization and protein biogenesis. Dev Cell *21*, 694-707.

Voutilainen, R., and Kahri, A.I. (1979). Functional and ultrastructural changes during ACTH-induced early differentiation of cortical cells of human fetal adrenals in primary cultures. J Ultrastruct Res *69*, 98-108.

Wallin, I.E. (1927). Symbionticism and the origin of species. Williams and Wilkins.

Wittig, I., Braun, H.P., and Schägger, H. (2006). Blue native PAGE. Nat Protoc *1*, 418-428.

Wong, E.D., Wagner, J.A., Gorsich, S.W., McCaffery, J.M., Shaw, J.M., and Nunnari, J. (2000). The dynamin-related GTPase, Mgm1p, is an intermembrane space protein required for maintenance of fusion competent mitochondria. J Cell Biol *151*, 341-352.

Wurm, C.A., and Jakobs, S. (2006). Differential protein distributions define two sub-compartments of the mitochondrial inner membrane in yeast. FEBS Lett *580*, 5628-5634.

Xie, J., Marusich, M.F., Souda, P., Whitelegge, J., and Capaldi, R.A. (2007). The mitochondrial inner membrane protein mitofilin exists as a complex with SAM50, metaxins 1 and 2, coiled-coil-helix coiled-coil-helix domain-containing protein 3 and 6 and DnaJC11. FEBS Lett *581*, 3545-3549.

Zerbes, R.M., Bohnert, M., Stroud, D.A., von der Malsburg, K., Kram, A., Oeljeklaus, S., Warscheid, B., Becker, T., Wiedemann, N., Veenhuis, M.*, et al.* (2012). Role of MINOS in mitochondrial membrane architecture: cristae morphology and outer membrane interactions differentially depend on mitofilin domains. J Mol Biol *422*, 183-191.

Zhao, J., Lendahl, U., and Nistér, M. (2013). Regulation of mitochondrial dynamics: convergences and divergences between yeast and vertebrates. Cell Mol Life Sci *70*, 951-976.

Zick, M., Duvezin-Caubet, S., Schäfer, A., Vogel, F., Neupert, W., and Reichert, A.S. (2009). Distinct roles of the two isoforms of the dynamin-like GTPase Mgm1 in mitochondrial fusion. FEBS Lett *583*, 2237-2243.

Zinser, E., and Daum, G. (1995). Isolation and biochemical characterization of organelles from the yeast, Saccharomyces cerevisiae. Yeast *11*, 493-536.

Zung, N., and Schuldiner, M. (2020). New horizons in mitochondrial contact site research. Biol Chem *401*, 793-809.

Acknowledgement

Throughout the writing of this dissertation, I have received a great deal of support and assistance. First, I would like to thank my supervisor Prof Walter Neupert, and Dr. Max E. Harner, whose expertise was invaluable in formulating the research questions and methodology. Your insightful feedback pushed me to sharpen my thinking and brought my work to a higher level.

I should thank Prof. Barbara Conradt, Dr. Dejana Makronjak, and Prof. Christoph Osman for their valuable guidance throughout my studies. You provided me with the insight and ideas to choose the right direction and successfully complete my dissertation.

I want to thank my colleagues, Dr. Toshiaki Izawa and Johanna Frickel for their excellent collaboration and support. I would particularly like to single out Dr. Till Kleckel and Prof. Dr. Britta Brügger for their valuable collaboration.

In addition, let me convey my gratitude to my parents for their wise counsel and sympathetic ear during these years. Finally, I could not have completed this dissertation without the support of my wife, Asal Amraei. She always supported me with love and happy distractions to rest my mind outside of my research. You were always there for me.